博士論文（要約）

Ubiquitous wireless power transfer in three-dimensional spaces

（三次元空間におけるユビキタスな無線電力伝送）

笹谷　拓也
Takuya Sasatani
The University of Tokyo

This thesis is submitted for the degree of
Ph.D. in Information Science and Technology

Abstract

Wireless power transfer has the promise to eliminate power cords and radically change how we interact with technologies involving electricity. However, existing approaches fail to embody this vision because achieving "high-power" and "wide-range" all at once in wireless power is challenging; microwave-based methods have limited power-levels due to safety concerns, and inductive systems using coils suffer from the narrow powering range.

In this thesis, I explore the fundamental physics, system design, and deployment of cavity-inspired, magnetoquasistatic wireless power technologies for drastically extending the powering range of inductive approaches, which are known to be capable of safely delivering higher power-levels. Unlike previous coil-based methods, the presented techniques leverage the widely distributed currents on conductive surfaces around the target volume for generating widely distributed 3-D magnetic field patterns while confining the troublesome electrical field within embedded circuit components. The presented approaches enable high-power, high-efficiency, and safe wireless power transfer over large areas, which would unlock device modalities that were previously inaccessible owing to limitations in power supply technologies.

Chapter 1 introduces the vision I aim to embody, describes the confronting challenges, and defines the scope of this thesis. Then, I provide a brief survey of relevant topics and research in chapter 2 to motivate the technologies developed in this thesis.

Chapter 3 presents an approach termed multimode quasistatic cavity resonance for enabling efficient wireless power throughout the full room-volume. This approach drastically extends the powering range of previous quasistatic cavity resonators, which could only cover half of the room volume, by introducing "multimode" features. By appropriately arranging conductive surfaces around the empowered volume and leveraging the nature that surface conductors can accommodate multi-directional and widely distributed current, this approach generates multiple, mutually unique, widely distributed 3-D magnetic field patterns within the room-volume. These modes used together achieved a power delivery efficiency exceeding 37.1% throughout the constructed test room (with dimensions of 3 m $\times$ 3 m $\times$ 2 m), and power exceeding 50 W could be delivered to mobile receivers, in accordance with safety guidelines.

Chapter 4 empowers IoT nodes by utilizing the room-wide channel for wireless power and low-power communication. This work reuses the room-wide wireless power transfer system as a communication channel, where nodes communicate with a centralized reader and each other via load-modulation. Because this communication system works in the near-field regimes where the source and the nodes intensely interact, and the communication signals and power inputs coexist, the incoming signals have a large dynamic range. To overcome this challenge, I develop a hardware/software-combined decoding circuit to normalize the incoming signals and read out the embedded data bits without distortion. Furthermore, I provide a theoretical analysis of the channel, followed by performance evaluations of communication and power transfer to validate this analysis. The proposed system shows that ten receiver nodes fully-equipped with custom-designed front-ends and power management units can be safely and efficiently wirelessly charged through analysis and experiments. The end node to end node communication rate can achieve from 1 kbps without occurring any errors, up to 5 kbps with a 6% bit error rate (BER), while the end node to the central unit can achieve 10 kbps without occurring any errors.

Chapter 5 tackles the challenge for powering pebble-scale (*i.e.*, a few cm) devices via room-scale transmitters. Such significantly asymmetric transmitter/receiver links suffer from a $1/\alpha^4$ degradation with increasing transmitter/receiver size ratio α; thereby, room-scale power transfer systems can barely empower pebble-scale devices. Inspired by optical lenses, I present a concept termed hierarchical resonance, which efficiently bridges significantly asymmetric transmitter/receiver links by focusing the ambient magnetic field using relay modules. General large-scale inductive transmitters can introduce this hierarchical link by placing low-cost, low-power, maintenance-free relay modules within the powering range. This approach offers a much more robust and efficient link than straightforward methods, which directly couple large transmitters with small receivers. I demonstrated the proposed concept and show that the hierarchical link increases the power efficiency by more than ten times compared to direct power transfer. Furthermore, I demonstrate a 500 mW power supply to pebble-sized (20 mm) devices, enabling driving microcontrollers and various sensing sub-systems without batteries.

Finally, chapter 6 concludes this thesis and raises future research directions.

Acknowledgements

Firstly I would like to thank Professor Yoshihiro Kawahara for giving me a fantastic opportunity to complete my Ph.D. thesis under his supervision. His friendly guidance and expert advice have been invaluable throughout my graduate studies. The opportunities and chances he gave me have greatly broadened my horizons as a researcher.

I would also like to offer my special thanks to Professor Alanson P. Sample, who supervised me during my internship in Disney Research Pittsburgh and dedicatedly supported my research life even after then. Also, I would like to express gratitude to Professor Tohru Asami and Dr. Yoshiaki Narusure, who guided me in the early years of my research life and gave me many encouraging pieces of advice thereafter. I would also like to thank Dr. Chouchang Jack Yang and Dr. Matthew J. Chabalko, who helped me in this thesis's research projects. They were great senior collaborators and astonished me with outstanding engineering skills and deep insights into science. I would also like to acknowledge the committee members of this thesis, Professor Shuichi Sakai, Professor Kaoru Sezaki, Professor Takeshi Naemura, Professor Shinya Sugiura, and Professor Tohru Asami, for improving this thesis through insightful feedback.

I would also like to thank my (ex-)colleagues and our research group's administrative staff. Dr. Koya Narumi, Takashi Ikeuchi, Tatsuya Iizuka were generally a great help throughout my graduate studies and always motivated me to work harder. Ryo Takahashi, Ken Takaki, Kazunobu Sumiya, Yuki Nishizawa, Hiromasa Hayashi, Masahiro Morita, Weiwei Jiang, and Yuta Hirai gave me many inspirations through the numerous research projects we conducted together. I appreciate the many exciting discussions with Dr. Fuminori Okuya, Matthew Ishige, Kota Suzuki, Takahiro Hashizume, Natsuki Ikeda, Dr. Masaru Takagi, Dr. Tung Duc Ta, Dr. Ryo Shigeta, and Dr. Takefumi Hiraki. Also, I am immensely grateful for the administrative support given by Kenji Tsushio, Noriko Mizuno, Saiko Akabane, Dr. Isamu Amir, Meiko Fujita, Hideyuki Kanai, Tsugami Tetsuya, Miki Domen, and Kozue Misawa; without their help, I could not have had a fun research life and succeed in the numerous outreach opportunities. Furthermore, it was an invaluable opportunity working in the same group with Professor Kazuya Saito, Professor Takuya Umedachi, Hisato Ogata,

Ken Nakagaki, Dr. Yang Zhang, and Professor Makoto Takamiya who gave me precious advice regarding my research and carrier.

Lastly, I would like to express my most profound appreciation to my family for their moral support and warm encouragement.

Table of contents

List of figures

List of tables

Chapter 1

Introduction

Electronic devices, such as mobiles, sensor nodes, and robots, are widely used in industrial and personal living spaces. However, these devices are primarily powered via wired connections or disposable batteries, which require manual maintenance and may adversely affect the environment [1]. The benefits of untethering these devices have been widely acknowledged, as evidenced by the recent commercialization of wireless communication technologies, which also promote emerging computational paradigms such as the Internet of Things [2, 3].

Wireless power transfer technologies, capable of safe power transfer to numerous devices scattered over large 3-D volumes, could overcome the limitations of tethered devices. Beyond embodying this grand challenge, users would never have to care about battery capacity, sensor systems would work forever without maintenance, and power outlets would no longer constrain the layout of equipment. Furthermore, thinking speculatively, this vision has the promise for completely changing the modality of electronics; if battery-less, despite active electronics gain ground, highly functional devices with non-constrained form-factors would appear, and they will actively operate in domains where wired power supply is difficult (*e.g.* mid-air, underwater, in biological tissue, within solids). However, the current form of wireless power transfer, such as charging pads (figure 1.1(a)) and RFID systems, lacks utility and does not offer such autonomous charging experiences.

This thesis explores "ubiquitous" wireless power transfer, which can enable safe, autonomous, and unaided powering of distributed devices within large 3-D volumes (figure 1.1(b)). To attain this, I explore the fundamental physics and system design of cavity-inspired, magnetoquasistatic wireless power technologies for drastically extending the powering range of inductive approaches, which are known to be capable of safely delivering higher power-levels. Unlike previous coil-based methods, the presented techniques leverage the widely distributed currents on conductive surfaces around the target volume for generating

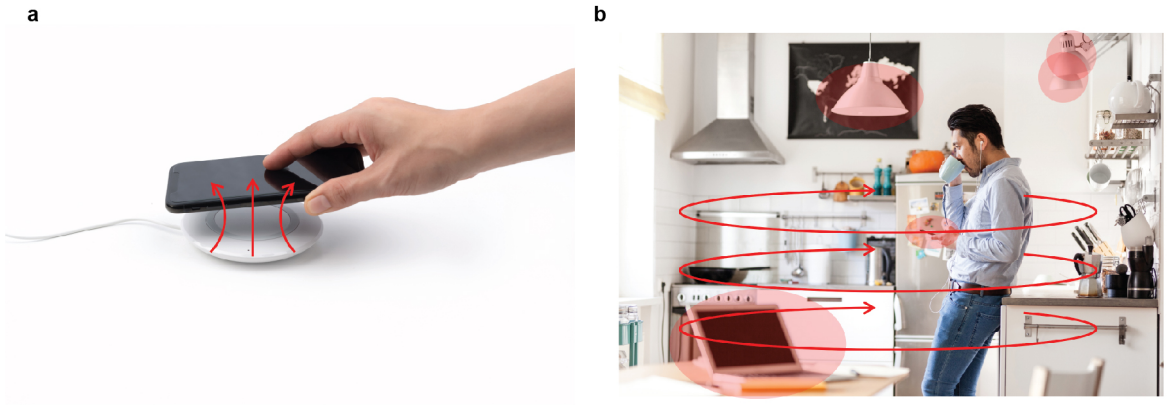

Figure 1.1 The (a) current and (b) envisioned form of wireless power transfer, which is capable of delivering several Watts of power.

widely distributed 3-D magnetic field patterns while confining the troublesome electrical field within embedded circuit components. The presented technologies offer a qualitative leap towards high-power, high-efficiency, and safe wireless power throughout large volumes. In the rest of this chapter, I explain the confronting challenges toward embodying the vision of ubiquitous wireless power, define the thesis's scope, and explain how I organized this thesis.

1.1 Challenges of ubiquitous wireless power transfer

The actual, ongoing wireless power transfer technology is far from the experience we conjure up when we hear the term "wireless power transfer." This gap owes to the trade-off between "the deliverable power-levels" and "the power transfer range," which have longly hindered the utility of wireless power technologies (see figure 1.2). **Considering the power demand and mobility of distributed electronic devices, several to ten Watts power delivery at room-scales or larger would be a key enabler of various physical computing paradigms and would significantly enhance consumer electronics' utility.** However, this domain, shown as "Ubiquitous wireless power transfer (WPT)" in figure 1.2 is still inaccessible.

Early attempts of wireless power transfer were mainly based on electromagnetic radiation (*i.e.*, microwaves) [4–6]. Although modern beamforming techniques enable efficient power delivery over a certain distance, such approaches require large rectenna arrays and complicated continuous tracking mechanisms. Moreover, safety concerns arise because exposed electrical fields, which are necessary for wave propagation, are a significant factor of tissue heating [7, 8].

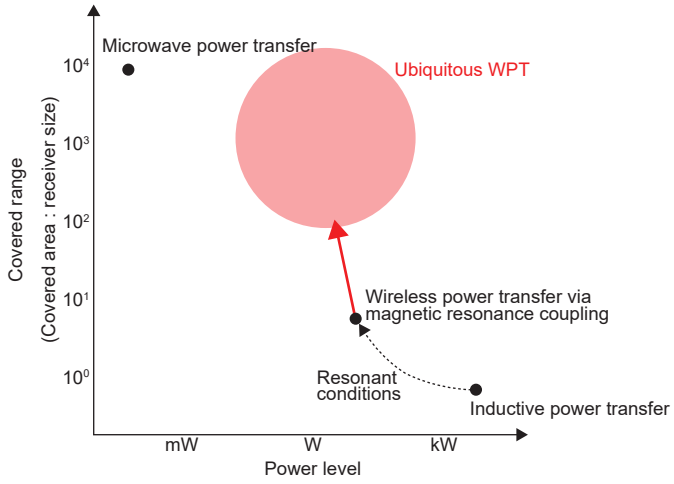

Figure 1.2 The ubiquitous wireless power transfer I envision and relevant approaches. (WPT: wireless power transfer)

For transmitting higher power levels without harming people, magnetic resonance coupling, which transmits power between a pair of coil-based resonators, has been explored [9–18]. We can understand this method as a subset of inductive power transfer adopted in the Qi-standard, which is the most commercially successful wireless charging standard up-to-date. Typically, these coil-based approaches require strong coupling between the transmitter/receiver pair for efficient power delivery, *i.e.*, a large portion of magnetic flux generated by the transmitter coil needs to interlink with the receiver coil, as shown in figure 1.3(a). Thus, the rapid decrease in field intensity with increasing distances limits the power transfer range of this approach to approximately the coils' diameter; furthermore, asymmetric systems, such as those comprising a large transmitter and a small receiver, exhibit low efficiency owing to insufficient coupling [16].

Returning to the intended vision, a technology that can safely deliver several to tens of Watts throughout large volumes is needed. This domain is plotted on figure 1.2 as "Ubiquitous wireless power transfer (WPT)". This technical domain is fundamentally useful, despite apparently above the trade-off curve. Thus, many previous works attempted to extend the powering range of safer inductive approaches, which typically lack utility due to range limitations. Next, I briefly explain the factors dominating the powering range of wireless power transfer via magnetic resonant coupling and explain how previous research attempted to extend the operation range.

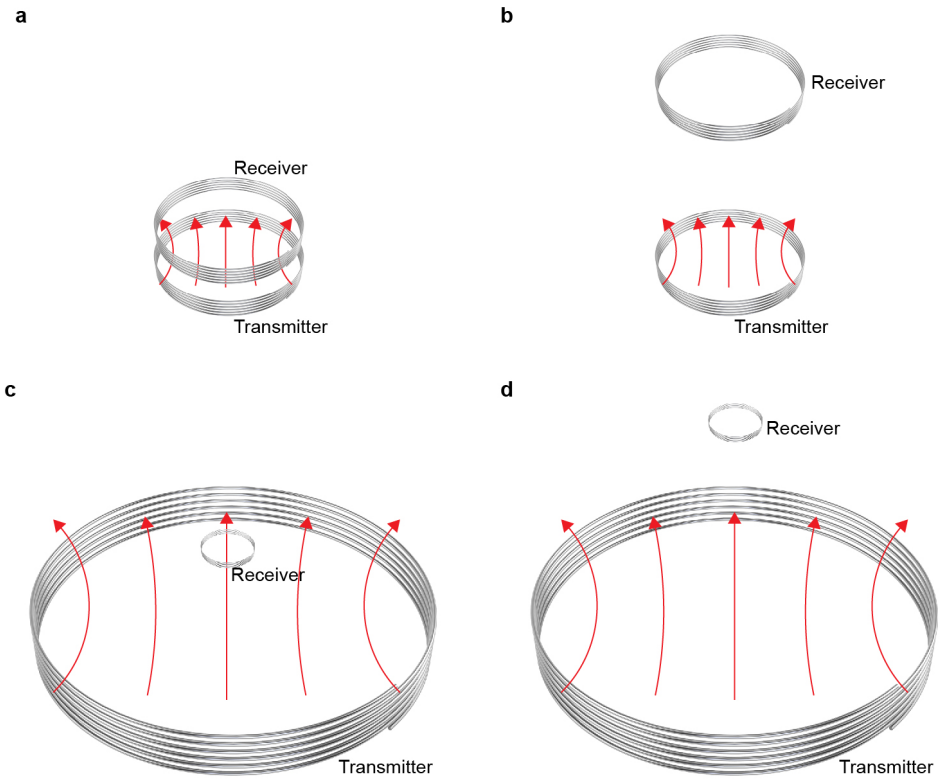

Figure 1.3 The range limitation of wireless power transfer technologies using the magnetic field. (a) Setups with short transfer distances and similar transmitter/receiver size can attain high power transfer efficiency. (b) Longer transfer distance leads to lower power transfer efficiency. (c) Asymmetric transmitter/receiver size ratios lead to lower power transfer efficiency. (d) Setups with long transfer distance and asymmetric transmitter/receiver size ratios result in very low power transfer efficiency.

1.2 Efficiency of wireless power transfer via magnetic resonant coupling

Analysis in previous work revealed that two critical factors determine the power transfer efficiency of systems based on magnetic resonant coupling; (i) the coupling coefficient (k) and (ii) the quality factor (Q) [19]. Using these two parameters further described in the following paragraphs, the kQ product, *i.e.*, $k_{\mathrm{TX,RX}}\sqrt{Q_{\mathrm{TX}}Q_{\mathrm{RX}}}$, is the figure-of-merit for power transfer efficiency in such systems (TX: transmitter, RX: receiver).

The coupling coefficient k in these technologies is *the ratio of the magnetic flux captured by the receiver coil to the total flux generated by the transmitter*. Thereby k is high when similar sized transmitter/receiver pairs are placed close to each other (figure 1.3(a)) However, coupling

typically decreases with (i) the increasing distance (figure 1.3(b)) and (ii) the increasing transmitter/receiver size ratios (figure 1.3(c)); not to mention, it significantly falls when the transmitter has to cover a wide volume, which suffers from both factors (figure 1.3(d)). As ubiquitous power transfer typically requires a broader charging range, it usually suffers from low-k conditions. Because the discussed figure-of-merit is the product of coupling coefficient k and quality factor Q, some may think that enhancing Q would enable efficient power delivery in wide-ranges. Thereby, I next proceed to describe the quality factor, Q.

Coil resonators, composed of air-core coils and lumped capacitors, can be abstracted as general oscillators. The energy oscillates between the coil's inductive energy and the electrical energy confined within the lumped capacitor. Borrowing the definition in general physics, quality factor Q is the ratio of the peak energy stored in the resonator in a cycle of oscillation to the energy lost per radian of the cycle. Meanwhile, from the electrical engineering perspective, the Q factor of a typical coil resonator can be denoted as $\omega L/r$ (ω: angular resonant frequency, L: inductance of the coil, r: copper loss). This expression shows that large inductance and small loss leads to high-Q. More coil-turns increase L in low frequencies; however, in higher frequencies, increasing turns will make the stray capacitance dominant, limiting the rise of inductance. Besides, using better conductors can attain lower losses. However, copper, commonly used for building coil resonators, is excellent in this aspect; therefore, this direction can not expect drastic improvements. Even with these extensive efforts to enhance coupling and quality factor, the domain where wireless power transfer via magnetic resonant coupling covers remain in the region shown in figure 1.2.

1.3 My contributions in this area

Extending powering ranges can be translated into holding a high kQ-product within a wide operating range from the above observations. For attaining this goal, previous works have explored the following two directions:

a. Cooperatively operating transmitter elements forming a two-dimensional array to cover surfaces. This approach enhances the coupling coefficient k by punctuating wide surfaces into small areas that a single transmitter can efficiently cover. Figure 1.4(a).

b. Covering large volumes with a single transmitter. This approach can cover three-dimensional volumes; however, it needs schemes to enhance quality factor Q for efficient powering. Figure 1.4(b).

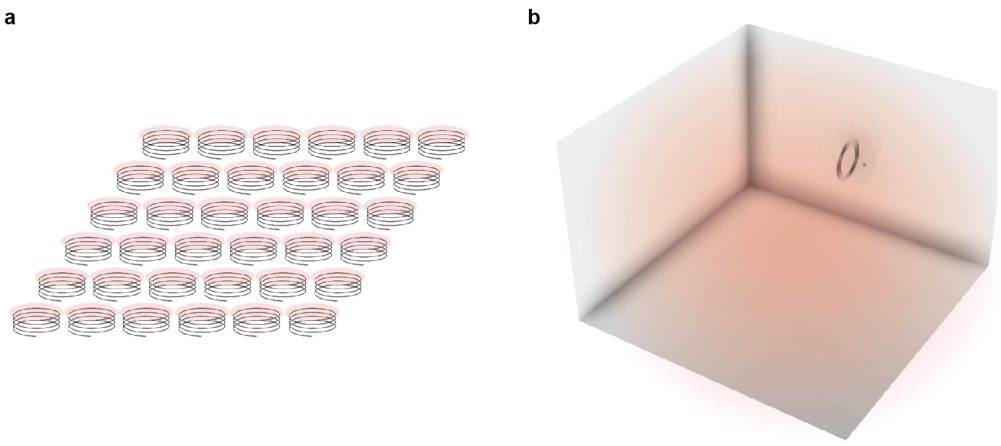

Figure 1.4 Techniques for extending the coverage range of inductive approaches. (a) Cooperatively operating transmitter elements forming a two-dimensional array to cover surfaces. (b) A room-scale high-Q transmitter covering large volumes.)

However, these approaches still have critical challenges as an enabler for the vision of ubiquitous wireless power transfer. I will describe the confronting challenges and my contributions in the following:

Facilitating the deployment of 2-D wireless charging systems

The 2-D transmitter arrays are natural ways to empower devices since we frequently place such devices on surfaces surrounding daily life, such as desks, floors, walls, etc. This approach has been explored for over ten years, and the physical aspect has mostly been revealed. Thereby, we intend that we need more comprehensive explorations for further advancement. From this aspect, this approach becomes effective as more familiar surfaces are retro-fitted into wireless charging surfaces; therefore, a critical yet overlooked aspect is lowering the barriers for deploying these systems into various surfaces.

Thus, I developed easily deployable wireless charging surfaces (figure 1.5). Several instances of this project intend to build “ready-made” frameworks that non-expert users can easily augment daily surfaces into wireless powering surfaces. This series of research introduced familiar metaphors in the deployment process of wireless charging surfaces, such as cut & pasting a large functional sheet (wallpaper) [P11], and laying ready-made tile-shaped modules (tile carpets) [P10]. These projects facilitated the deployment process of such wireless charging sheets that only existed in laboratory setups. I also discovered that the boundaries between transmitter elements occur “dead-zones”, where transmitters can deliver almost no

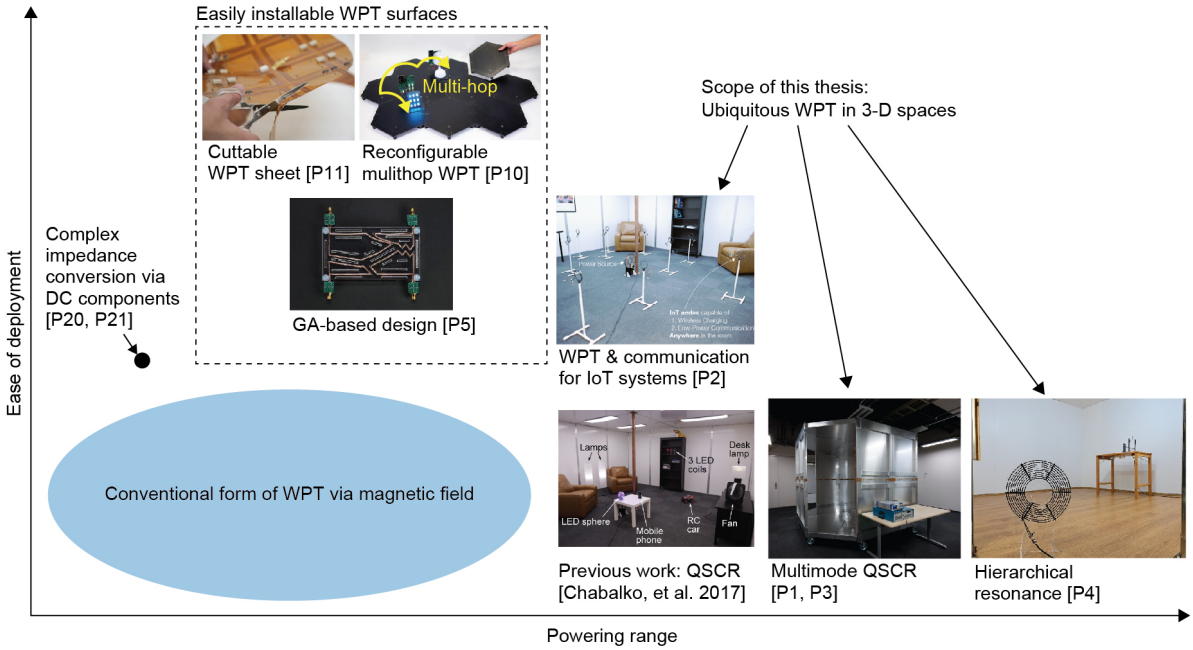

Figure 1.5 My research projects for embodying the vision of ubiquitous wireless power transfer. The reference number corresponds to the publication list at the end of this dissertation. (WPT: Wireless power transfer, QSCR: Quasistatic cavity resonance.)

power. I leveraged meta-heuristics to develop a resonator design method for enhancing these worst-case scenarios, which, in contrast to improving best-case scenarios, reveals significant complexities due to the need to consider numerous possible placements [P5, P23]. **I note that I excluded these portions of research from the scope of this thesis.**

Scope of this thesis: ubiquitous wireless power transfer in 3-D spaces

The direction of covering large volumes with a single transmitter has a clear advantage that it has the promise for covering "volumes" instead of the proximity of surfaces. This research direction is rather treated as grand challenges. It will lead to more ideal usage scenarios such as powering mobiles stuffed in pockets, empowering spatially distributed sensor networks, and powering implants.

As described in Section 1.2, this approach is physically difficult and intuitively contradicts the rules that govern efficiency in these systems. Thereby, most studies set aside efficiency and tried to send small amounts of power using wide-range yet inefficient systems. Meanwhile, in 2017, a technology termed quasistatic cavity resonance (QSCR) demonstrated efficient power delivery within large portions of the room volume by developing cavity-inspired

structures [20]. However, this technology is emerging; thereby, critical challenges exist. It can only efficiently power *half* of the room volume, the uncertain surface current makes the technology difficult to handle, communication channels for power negotiation is not explored, and QSCRs can barely charge small scale devices (*i.e.*, smaller than 50 mm).

The intention and scope of this thesis are to overcome these confronting challenges and pioneer the field of ubiquitous wireless power transfer in three-dimensional spaces. I explore the fundamental physics, system design, and deployment of cavity-inspired, magnetoquasistatic wireless power technologies for drastically extending the powering range of inductive approaches.

1.4 Thesis organization

I provide a brief survey of relevant topics and research in chapter 2 to motivate the technologies developed in this thesis.

Chapter 3 presents an approach termed multimode quasistatic cavity resonance (multimode QSCR) for enabling efficient wireless power throughout the full room-volume. This approach drastically extends the powering range of previous quasistatic cavity resonators, which could only cover half of the room volume, by introducing "multimode" features. By appropriately arranging conductive surfaces around the empowered volume and leveraging the nature that surface conductors can accommodate multi-directional and widely distributed current, this approach generates multiple, mutually unique, widely distributed 3-D magnetic field patterns within the room-volume. These modes used together achieved a power delivery efficiency exceeding 37.1% throughout the constructed test room (with dimensions of 3 m $\times$ 3 m $\times$ 2 m), and power exceeding 50 W could be delivered to mobile receivers, in accordance with safety guidelines.

Chapter 4 empowers IoT nodes by utilizing the room-wide channel for wireless power and low-power communication. This work reuses the room-wide wireless power transfer system as a communication channel, where nodes communicate with a centralized reader and each other via load-modulation. Because this communication system works in the near-field regimes where the source and the nodes intensely interact, and the communication signals and power inputs coexist, the incoming signals have a large dynamic range. To overcome this challenge, I develop a hardware/software-combined decoding circuit to normalize the incoming signals and read out the embedded data bits without distortion. Furthermore, I provide a theoretical analysis of the channel, followed by performance evaluations of communication and power transfer to validate this analysis. The proposed system shows that ten receiver

nodes fully-equipped with custom-designed front-ends and power management units can be safely and efficiently wirelessly charged through analysis and experiments. The end node to end node communication rate can achieve from 1 kbps without occurring any errors, up to 5 kbps with a 6% bit error rate (BER), while the end node to the central unit can achieve 10 kbps without occurring any errors.

Chapter 5 tackles the challenge for powering pebble-scale (*i.e.*, a few cm) devices via room-scale transmitters. Such significantly asymmetric transmitter/receiver links suffer from a $1/\alpha^4$ degradation with increasing transmitter/receiver size ratio α; thereby, room-scale power transfer systems can barely empower pebble-scale devices. Inspired by optical lenses, I present a concept termed hierarchical resonance, which efficiently bridges significantly asymmetric transmitter/receiver by focusing the ambient magnetic field using relay modules. General large-scale inductive transmitters can introduce this hierarchical link by placing low-cost, low-power, maintenance-free relay modules within the powering range. This approach offers a much more robust and efficient link than straightforward methods, which directly couple large transmitters with small receivers. I demonstrated the proposed concept and show that the hierarchical link increases the power efficiency by more than ten times compared to direct power transfer. Furthermore, I demonstrate a 500 mW power supply to pebble-sized (20 mm) devices, enabling driving microcontrollers and various sensing sub-systems without batteries.

Finally, chapter 6 concludes this thesis and raises future research directions.

Chapter 2

Related works

In this chapter, I pick up several research domains relevant to the scope of this thesis to clarify my contribution and motivate the technologies developed in this thesis. Note that previous work particularly related to each chapter are covered later in each chapter.

2.1 Modern approaches of wireless power transfer

The concept of wireless power was introduced by Tesla at the beginning of the 20th century [4]. This concept has become more noticeable as relevant fields of electrical engineering, such as semiconductor technology and integrated circuits (ICs), developed. It is even commercialized in some domains, such as RFIDs and Qi charging pads. Thereby, a large body of technology, developed through various theoretical, numerical, and experimental investigations, exists in wireless power transfer. However, because these methods have various trade-offs, no approach can effectively cover all situations; thus, it is essential to look at the field's big picture and review the strengths and weaknesses of typical methods. Here, I will cover the previous attempts and relevant topics for embodying the concept of ubiquitous wireless power transfer.

Microwave power transfer

Wireless power transfer using far-field electromagnetic waves is one of the most longly and intensely studied approaches [4, 5]. In the context of IoT, this approach is typically aiming for powering ultra-low-power devices such as RFIDs and primitive sensor nodes [21–23].

The fundamental physics governing this technology is analogous to radiowaves used in typical wireless communication systems (*i.e.*, cellular, Wi-Fi, Bluetooth, etc.); the transmitter antenna radiates microwaves, whereas the receiver antennas receive this. Thereby, RF energy

harvesting, which instead of using dedicated power sources, harvests power from existing microwaves such as TV broadcasts and Wi-Fi, is also widely studied [24]. However, the power level of these systems is limited to several microwatts because the ambient microwave signals, and conversion efficiencies are inherently small [24].

Microwave power transfer technology shows a different type of development outside the context of IoT, leveraging the long-range nature of radiative electromagnetic waves. Theoretically, this approach can attain high efficiency in long-range by introducing extensive facilities such as large rectenna arrays (*i.e.,* receivers), beam-focusing mechanisms, and continuous tracking mechanisms. Therefore, different directions of engineering would lead to applications such as space solar power stations (SSPS) and wirelessly powered aircraft, which have been intensely explored [5].

Because the typical frequencies used in this approach is around a GHz, a significant drawback of this approach is that it significantly interferes with daily objects (*i.e.*, biological tissue, water, soil, biological tissue). Considering ubiquitous setups, this is critical because this prevents efficient propagation through typical indoor environments. Furthermore, the deliverable power-levels within regulatory guidelines become very small due to safety concerns [7].

Mid-field

Some research reports that using electromagnetic fields in the intermediate regions between far-field and near-field enhances the power transfer efficiency in specific setups [25]. Example applications of these technologies are power delivery to deep tissue micro-implants using a phased surface [26] and self-tracking power delivery within a small cavity [27].

While these approaches enable significant miniaturization of the receiver size, the need to design the system considering the surrounding dielectrics narrows the usage scenario, making it non-available in most IoT applications. Moreover, the transferable power levels are still low (below milli-Watts) because they have to use frequency bands that significantly interact with biological tissue.

Acoustic waves

The use of acoustic waves for power delivery has also been explored [28, 29]. The main application of this approach is networking underwater or implant devices because electromagnetic waves can not efficiently propagate through these domains [30]. This approach typically uses ultrasound frequencies, and the acoustic waves are generated and received using

piezoelectric devices [28]. Acoustic waves at ultrasound frequencies have smaller wavelengths than typically used microwaves; therefore, the receiver dimensions can be smaller. However, the low conversion efficiency and low channel efficiency makes the power delivery inefficient and heating issues will arise for powering mobiles. Besides, this method's intense directivity requires line-of-sight; significant reflection occurs at boundaries of different mediums. These factors make this infeasible in many applications.

Laser

Optical approaches, which transfer energy via laser beams, is another method that is gaining attention [31]. The smart dust project, which implemented a tiny networked device, used optical approaches to harvest power and communicate with the central computer [32]. Laser beams are a subset of electromagnetic waves in which the wavelength are magnitudes smaller (∼a micrometer) than microwaves (∼around a few hundred millimeters).

This approach often uses Laser-diodes and photo-diodes as the transmitters and receivers. This ultra-small wavelength enables highly directive radiation, which can favor the extension of operation range and miniaturization of receivers; however, this guarantees the use of this approach to line-of-sight configurations [33]. Besides, due to the short wavelength of light, the energy easily gets absorbed in biological tissue and damages the eyes, leading to severe health problems. Also, the low conversion efficiency of photovoltaic cells (∼20% [31]) leads to low system efficiency and causes non-trivial thermal issues. Thereby, the receiver dimensions typically become large for thermal requirements, even if the short wavelength can miniaturize the power receiving elements.

Magnetic resonant coupling

Introduced by MIT in 2007, magnetic resonant coupling-based wireless power transfer is a method that transfers energy via the inductive link between the transmitting and receiving resonators. This method offers the promise for *high-efficiency* and *safe* power delivery in mid-range distances (*i.e.*, approximately, the size of the resonators) [34, 13, 10]. From the circuit theory perspective, the magnetic resonant coupling is an extension of inductive power transfer; inductive power transfer is a method that enables high-efficiency power delivery between short distances and is used in Qi standards [10]. The difference between the two methods is that inductive power transfer uses a pair of ordinary coils. Magnetic resonant coupling uses a pair of high-Q LC resonators; this high-Q resonance successfully enhances the power delivery range.

Albeit the high efficiency of magnetic resonant coupling-based wireless power transfer, the limited power delivery range and the degradation of efficiency in asymmetrical (*i.e.*, receiver is much smaller than the transmitter) systems still confront as critical challenges for use in ubiquitous wireless power transfer. Some studies attempt to extend the power delivery range by using 2-D resonator arrays as transmitters [35]; this makes a 2-D area of power delivery range, although the extension of this range to a 3-D volume remains a big challenge. Near-field 2-D phased array techniques, which aim to enhance power delivery range by making a constructive interference at the receiver, are also considered [36, 37]. Although these methods show a substantial advantage when the receiver's angle is misaligned, it doesn't offer a significant difference in long-distance configurations, which is necessary for 3-D wireless power transfer [38].

Cavity resonators

Cavity resonators, which are the ancestor of the later explained quasistatic cavity resonance (QSCR), are well known for generating 3-D near-field electromagnetic field patterns (*i.e.*, resonant modes) in a metallic cavity. There were many attempts to directly apply cavity resonators for 3-D wireless power transfer because they naturally withhold a 3-D power supply range [39–41].

However, they suffered from two fundamental challenges: (i) the co-existence of the intense electrical and magnetic field and (ii) the resonant frequency uniquely fixed by the cavity dimensions. While magnetic fields are less affected by everyday objects, electric fields intensely interfere with dielectrics (*e.g.*, human body, water, pieces of wood, etc.). This interference leads to safety issues and the distortion of the resonant modes, which hinders robust power delivery. Besides, if structure dimensions strictly define the resonant frequency, it is hard to comply with regulatory guidelines as rooms-sizes are not uniform. These limitations may be acceptable in specific industrial applications; however, it is a barrier to adopting practical systems from both technical and regulatory aspects.

Quasistatic cavity resonators (QSCR)

Quasistatic cavity resonators (QSCR), initially presented in 2017, are a recently developed technology that has the promise of ubiquitous power delivery in large 3-D volumes [20]. QSCR is a technique that compensates for the disadvantages of cavity resonators (*i.e.*, interference with dielectric, resonant frequency fixed by geometry, etc.) while preserving the 3-D nature. This technique uses enclosed metallic cavities containing a central conductive pole with

discrete capacitors inserted in a gap in the pole. This addition makes one of the resonant modes of the cavity enter quasistatic operation, allowing the magnetic fields to permeate the interior of the cavity while confining electric fields to the discrete capacitors. These features should be ideal for ubiquitous wireless power transfer because the magnetic field less interacts with daily objects and biological tissue. Besides, the quasistatic operation allows tuning the resonant frequency of the structure independently with geometry via the lumped capacitors' value. This approach demonstrated high efficiency (>50%) power transfer within large portions of the room-sized (4.9 m × 4.9 m × 2.3 m) volume [20]. Moreover, the dominant magnetic field enables the delivery of over tens of Watts to mobile devices [20].

Although this approach is promising, it is still an emerging technique with many drawbacks. For instance, it can only cover around half of the room volume efficiently; this technology can hardly power small (below 50 mm) devices; previous work only explored the abstract forms of physical analysis; thus, they still lack utility. This thesis's scope is to advance this emerging direction to deliver a genuinely ubiquitous powering experience, unravel the physics governing this approach, and investigate new system architectures that effectively support this emerging technology.

2.2 Safety of wireless power transfer systems

Generally speaking, excessive exposure to a time-varying electromagnetic field could cause biological effects and harm nearby people. Various non-ideal effects appear on tissues depending on the field's frequency, power-level, compositions (*i.e.,* electric, magnetic), etc.; thus, the operating frequency of systems exposing electromagnetic fields need to be carefully considered. Based on the knowledge delivered by various dedicated research, practical wireless systems (*i.e.,* wireless communication, wireless power transfer, wireless sensing) usually use the frequency range where tissue heating is the only significant effect. Furthermore, the inductive field in the range of around 100 kHz to 10 MHz, which the technologies developed in this thesis rides on, is known to have small effects on biological tissue even among the frequency bands that other wireless systems use [7].

Wireless power transfer approaches leveraging the oscillating electromagnetic field over 100 kHz (including the inductive approaches explored in this thesis) often assesses safety based on the guidelines adopted by the FCC and the Institute of Electrical and Electronics Engineers (IEEE) [42]. These guidelines primarily focus on preventing localized heat stress and full-body heating. Therefore, restrictions are imposed based on the specific absorption rate (SAR), which is a measure of the amount of power absorbed by biological tissue [8, 43].

For uncontrolled exposure of the general public, these restrictions limit the average SAR of the entire body to 0.08 W/kg and the localized SAR, defined as the average power absorbed by a 1 g tissue sample, to 1.6 W/kg.

In practical wireless power systems operating in the near-field, SAR significantly varies depending on the operating conditions (*e.g.,* input power, power transfer efficiency) [20, 43]. Thereby, safety can not be generally defined based on just the core components of wireless power. The peripherals, total system architecture, and usage scenario need to be collectively understood in practicality. Following the SAR evaluations conducted for many commercial electronics, the safety evaluations in this thesis assess the maximum power levels compliant with regulatory guidelines in many typical example cases.

2.3 Communication via backscatter/load-modulation

Typical wireless power transfer systems require communication links for covering broader needs. Example usages of these links are feeding-back power demands, bidding power within multiple receivers, collecting sensor data, and sending control packets. Sharing the wireless power channel for communication is often used [44–46, 24, 21]. This approach exposes benefits such as reducing hardware cost because it can share the antennas and front-end circuits; furthermore, it can leverage backscatter/load-modulation techniques, which don't require equipping active radio transmitters in the distributed nodes. Besides, as it shares the same channel, it is guaranteed that the link is available whenever wireless power is; this prevents situations in which the power supply can not start because the communication link is not established.

Backscatter and load-modulation enable nodes to communicate in a "semi-passive" manner. In a backscatter/load-modulation-based communication system, an external source generates the carrier, and the data transmitter modulates this carrier by changing the phase/amplitude of the reflection. The term backscatter is used for far-field systems, and load-modulation is used for near-field systems. We can understand this process as the external source is "off-loading" the energy-hungry, carrier generation routine from the distributed node devices with limited power. This off-loading allows each node to communicate with minimum energy consumption, expanding the battery lifetime of nodes; it is essential to effectively use energy because they tend to have tight battery capacity limitations.

This technology is practically used in passive RFIDs and NFC tags. Compared to active radio transmitters (*i.e.,* Bluetooth, Wi-Fi, Zigbee, etc.) which use local oscillators for generating the carrier, backscatter/load-modulation techniques have the promise for

magnitudes of lower energy consumption. I should also remark that these schemes reuse the spectrum when configured on the wireless power transfer frequency band. I consider these two factors essential for future IoT systems because the power consumption is vital and the general depletion of the spectrum.

2.4 Internet of things (IoT)

Internet of Things (IoT) is a computing paradigm, which distributes cooperated computation devices for seamlessly and adaptively assisting real-world activities via computation technology. Beyond this vision, computation devices would assimilate with the environment and become indistinguishable from everyday objects, leading to a world in which computation naturally permeates various physical spaces without the users noticing [2].

IoT systems work by collecting data via numerous distributed sensors, aggregating these data using the networked computers, and collectively offering feedback via distributed end effectors. By linking various real-world contexts via the digital domain in such a manner, these systems promise to make industrial systems more efficient and provide people a more natural way to interact with computing systems [47].

As IoT systems develop, the number of connected computation devices working as interfaces, sensors, and actuators will increase. These devices are typically driven by small batteries, which need manual maintenance and strictly limits the computation burden it can handle. Although battery technologies and low-power circuit technologies are advancing, computation and communication demands are also increasing. Besides, many fundamentally energy-hungry functions such as actuation and high-precision sensing still exist. Furthermore, physical prototyping tools (*e.g.,* Arduino, Raspberry Pi), which consumes extra power for enhancing usability, proved to be useful for long-tale development. Thus, the need to remotely empower the distributed computation devices is rising, and the IoT paradigm's development strongly motivates my vision of ubiquitous wireless power transfer.

Chapter 3

Multimode quasistatic cavity resonators for wireless power transfer

For transmitting high power levels without harming people, magnetic resonance coupling, which transmits power between a pair of coil-based resonators, has been explored [9–12, 14–18] (figure 3.1(a)). However, the rapid decrease in field intensity with increasing distances limits the power transfer range of this approach to approximately the coils' diameter; furthermore, asymmetric systems, such as those comprising a large transmitter and a small receiver, exhibit low efficiency owing to insufficient coupling [16]. In contrast, instead of using coil-based resonators, quasistatic cavity resonance (QSCR) uses a room-scale cavity with a central pole and inserted lumped capacitors [20, P2]. This generates a 3-D magnetic field distribution via the widely distributed surface current (figure 3.1(b)). Unlike ordinary cavity resonators [39, 40], the electric field, which mainly interferes with biological tissue, is confined within the lumped capacitors. However, the field distribution of QSCR is non-uniform and drops in a large area within the room; consequently, there are large portions of the volume where power delivery is inefficient.

3.1 The concept of multimode quasistatic cavity resonance

In this chapter, I reveal that efficient power transfer over a larger volume could be achieved by extending QSCR to multimode structures. Furthermore, I show that, by leveraging multi-directional surface current, two unique and widely distributed magnetic field patterns can be generated, which sufficiently cover the entire volume when used together. Using these field patterns, power could be efficiently delivered throughout a constructed test room with dimensions of 3 m $\times$ 3 m $\times$ 2 m. This approach, termed multimode quasistatic cavity

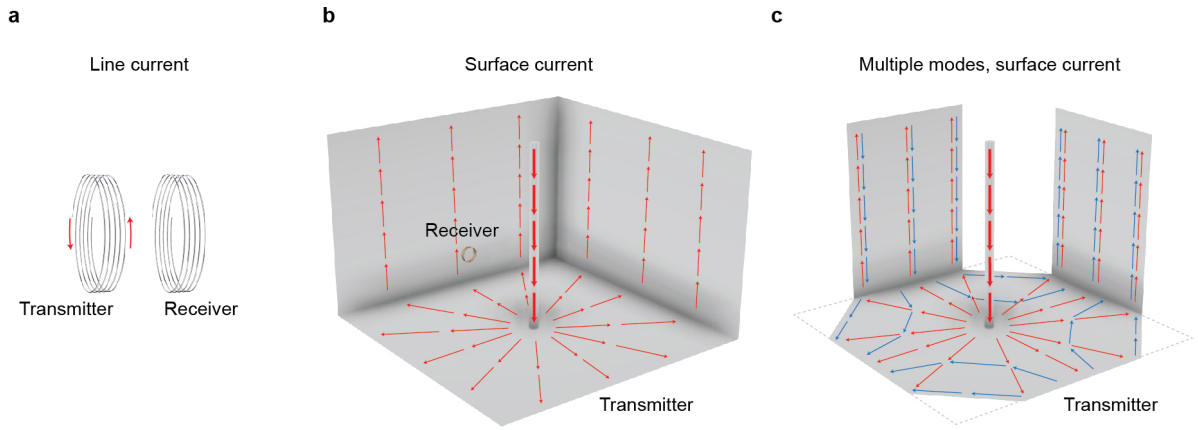

Figure 3.1 Overview of the concept of multimode quasistatic cavity resonance (multimode QSCR). (a) Conceptual diagrams of wireless power transfer via typical coil-based resonators, which exhibit low efficiency in asymmetric systems (such as those with a large transmitter and a small receiver); (b) quasistatic cavity resonance, which involves areas where efficient power transfer does not occur; and (c) multimode-quasistatic cavity resonance, which enables highly efficient and safe wireless transfer of high amounts of power through large volumes by utilizing the generated multiple magnetic field patterns. I omitted the conductive sheets at the front in (b) and (c) for visibility.

resonance (multimode QSCR), uses a resonant structure composed of conductive surfaces and lumped capacitors to accommodate multiple resonant modes with mutually unique patterns of the oscillating surface current (figure 3.1(c)). This differentiates our approach from previous magnetoquasistatic methods, which only support a single current and magnetic field distribution (figure 3.1(a) and (b)).

The proposed approach can selectively generate magnetic field patterns based on the input tone of the external drive coil, which is inductively coupled with the transmitter resonator. Thereafter, the receivers positioned within the range of the generated magnetic field are powered (figure 3.2). As the generated field patterns complement the null zones of each other, the entire volume can be covered efficiently. This cannot be achieved by using either mode alone. Moreover, simulations show that our room-scale resonator can safely deliver over 50 W of power to devices as small as 1/5000 of the powering range (see Methods A for details regarding range and scaling). Furthermore, I show that by leveraging the repertoire of existing resonant modes, the obstructive central conductive pole, which was necessary for the previous QSCR, can be omitted, while still maintaining a large power delivery range. Finally, stand lights, fans, and smartphones were wirelessly powered in a furnished room to demonstrate the feasibility of the proposed technology in typical living spaces.

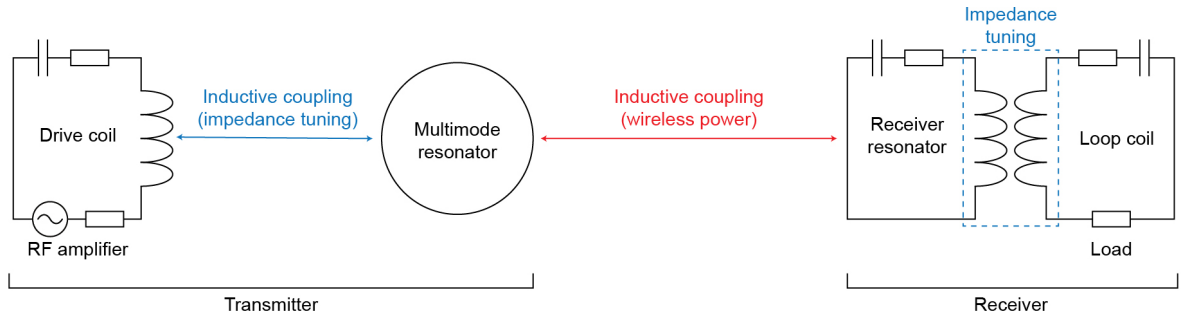

Figure 3.2 Fundamental system diagram of the studied wireless power transfer system. the room-wide multimode QSCR was stimulated via an external drive coil (figure 3.4(b)). The receiver used in the latter experiments is composed of a high-Q receiver coil and a loop coil for impedance adjustment connected to the load (see figure 3.4(a)).

3.2 Structure of the room-scale resonator

Surface conductors such as aluminum sheets naturally support current distributions along various directions. However, methods of accommodating multiple high-quality (Q) factor resonant modes, where each mode generates a magnetic field pattern that covers mutually different large portions of the volume, remain unclear. As the proposed approach is based on magnetoquasistatic fields, resonance can be understood as the condition under which magnetic energy, possessed by the widely distributed current, and electrical energy, confined in the lumped capacitors, are balanced. Therefore, the arrangement of the conductive surfaces that generate the widely distributed magnetic field patterns and the effective insertion of the lumped capacitors within the assumed current loops are primary criteria for designing the structure.

Accordingly, I designed a room-scale resonant structure that accommodates the two widely distributed current patterns shown in figure 3.1(c). One current pattern is mainly distributed near the center of the room (*i.e.*, at the pole), whereas the other is distributed near the edges (*i.e.*, the walls of the structure); I assumed that this distribution would compose unique magnetic field patterns that would cover the null zones of each other. An overview of the designed room-scale resonator that enables these current flows and a photograph of the constructed wireless power transfer system are shown in figure 3.3(a) and (b). Refer to Methods A for the covered powering range and the construction details. This room-scale resonant structure is composed of (i) an aluminium box with the corners cut off and capacitive lumped elements inserted at the center of each wall, and (ii) a conductive pole with an inserted capacitive element. This structure accommodates two resonant modes that possess unique current distribution and magnetic field patterns, as shown in figure 3.5(c–f). I termed these two modes

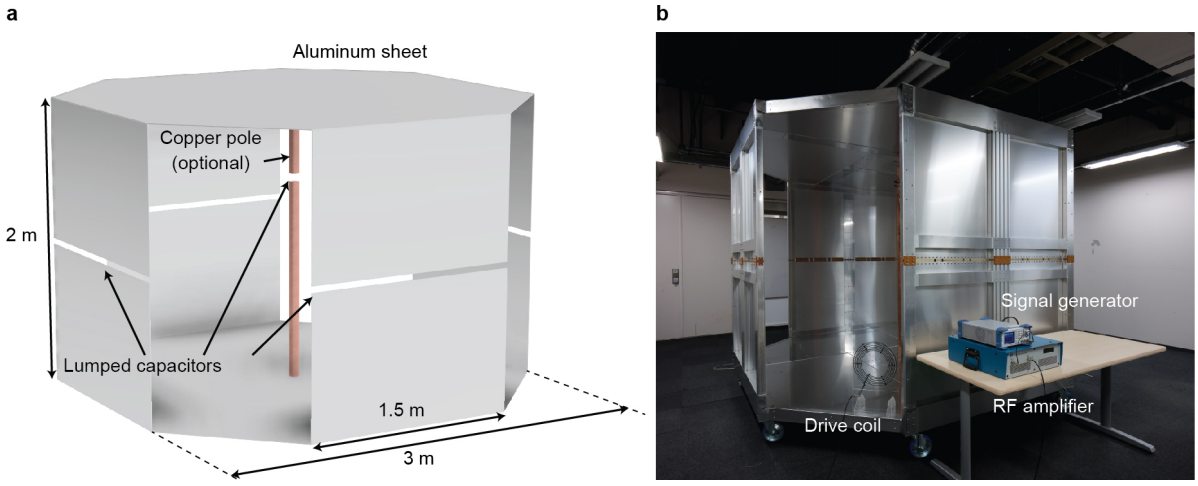

Figure 3.3 The structure and construction of the room-scale resonator. (a) Structure overview and (b) implementation of the room-scale wireless power transfer system based on multimode QSCR (see Methods A for construction details).

as the pole independent (PI) mode and the pole dependent (PD) mode based on the following observations. When the PI mode is excited, current only flows through the walls, ceiling, and floor and generates an intense magnetic field distribution near the walls. Conversely, the PD mode induces a current that flows through the central pole, which generates a magnetic field that circulates around the pole and is most intense near the central pole. These two modes yield magnetic field distributions that cover the weak areas of each mode. Therefore, by multiplexing these resonant modes, an intense magnetic field permeating a larger volume than that covered by either mode alone can be achieved; thus, high-efficiency power delivery throughout the volume can be achieved. For the PI mode, the current and magnetic field intensity decrease to zero near the center of the room. Therefore, the presence of the central pole does not affect this mode. Consequently, wireless power transfer over a large portion of the volume is enabled even when the central conductive pole is omitted.

3.3 Analyses and tuning of resonant frequencies

Although the resonant frequency of typical *LC* resonators can be tuned using lumped capacitors, the widely used expression for the resonant frequency of an *LC* tank is not directly applicable to the multimode QSCR. For the proposed resonator, it is difficult to define the inductance L because the current is widely distributed over the surfaces without converging to a single port and four independent current loops that do not intersect exist within each

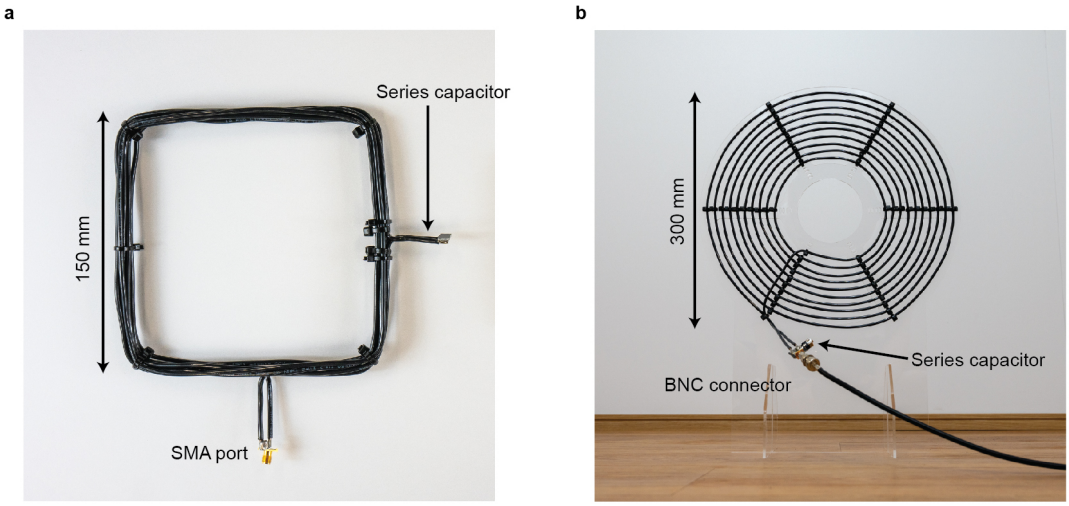

Figure 3.4 Coil resonators used in the measurements, (a) receiver coil and (b) drive coil.

current distribution (figure 3.5 and figure 3.6). Furthermore, relevant regulations regarding the safety of wireless power transfer, such as the Federal Communications Commission' s (FCC' s) regulations, restrict the frequency of exposed electromagnetic fields and the operating frequencies of such systems. Therefore, the following analysis is performed to independently tune each resonant frequency of the structure to predefined values. For tuning the resonant frequency of each mode, ω_{PI} and ω_{PD}, the structure is assumed to have an equivalent inductance L_{eq}. Thus, the resonant frequency is determined using the conventional expression for an LC tank, *i.e.*, $\omega_0 = 1/\sqrt{LC}$, whereas the capacitance C is set by using discrete capacitors with known values. Analytical expressions for the remaining parameter, equivalent inductance L_{eq}, are difficult to derive, as mentioned above. Hence, to subvert manual calculation, I developed an approach based on the finite element method (FEM) for computing the inductance of a structure with a fixed geometry.

Under both modes, the surface current, J_{S}, does not cross the $J_{\mathrm{S}} = 0$ boundaries shown in figure 3.5(a) and (c). Therefore, the total current can be analyzed as a combination of four independent current loops flowing through the unit cells shown in figure 3.6, which are coupled with each other. Thus, owing to the symmetry of the structure, the magnetic energy corresponding to a unit current loop, ω_{unit}, should be equal to a quarter of the total energy in the entire volume. If we solve the eigenmodes using FEM simulations involving known capacitance values and a fixed structure, we can then use the software to evaluate the current in a unit loop, I_{unit}, and the total magnetic energy of the structure, α. On dividing α by four, we can obtain ω_{unit}.

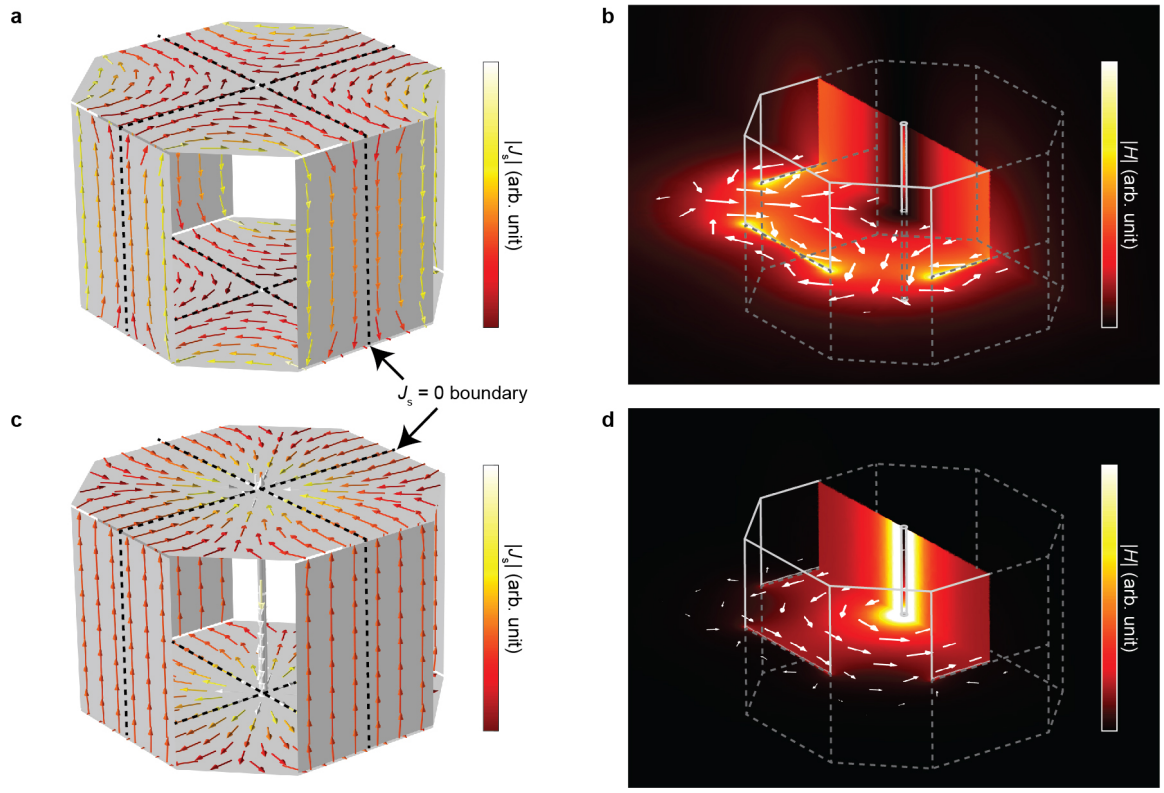

Figure 3.5 Magnetic field and current of the multimode-quasistatic cavity resonator. (a) and (b) show the current distribution and magnetic field distribution of the pole independent (PI) mode. (c) and (d) show the current distribution and magnetic field distribution of the pole dependent (PD) mode, respectively. The $J_S = 0$ boundary, where current never flows through, is overlaid for later analysis.

Finally, I determined the equivalent inductance by noting that the energy stored in an inductor (a unit cell) is $\alpha/4 = \omega_{\text{unit}} = L_{\text{eq}} I_{\text{unit}}^2/2$, where α and I_{unit} are obtained from the simulations. After computing L_{eq}, the desired resonant frequency can be determined by calculating the discrete capacitance, C, from the following expression:

$$\omega_0 = \frac{1}{\sqrt{L_{\text{eq}} C}} = \frac{1}{\sqrt{\frac{\alpha}{2I_{\text{unit}}} \cdot C}} \tag{3.1}$$

Considering the capacitor positions and current paths shown in figure 3.3 and figure 3.5, the capacitance inserted in the unit current loops of the PD and PI modes can be calculated as

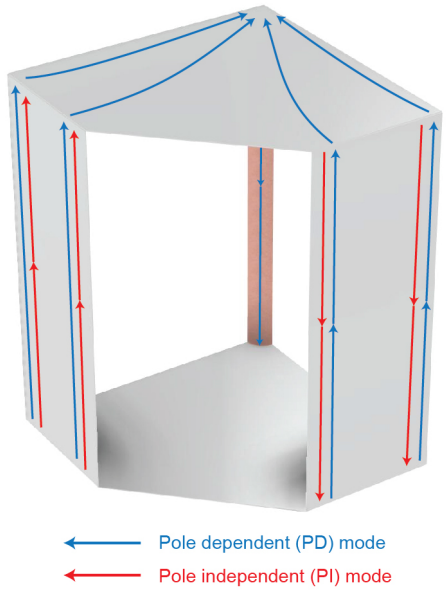

Figure 3.6 Unit structure (*i.e.*, unit current loop) used for the analysis of the resonant frequency. This image is a quarter of the whole structure.

shown below by applying fundamental circuit analysis:

$$C_{\mathrm{PD}} = \frac{C_1 C_2}{2C_1 + 4C_2} \tag{3.2}$$

$$C_{\mathrm{PI}} = \frac{C_2}{8} \tag{3.3}$$

Using these expressions together with equation 3.1, the two resonant frequencies can be tuned independently. The resonant frequencies of the PD mode, f_{PD}, and the PI mode, f_{PI}, are set to 1.20 MHz and 1.34 MHz, respectively, through the process described above. The quality factors of each mode, measured via previous methods [48], were 1230 (PD mode) and 615 (PI mode).

3.4 Evaluation of power transfer efficiency

Next, I determine the power transfer efficiency between the 3 m × 3 m × 2 m room-scale resonator and the 150 mm × 150 mm receiver through simulations and measurements. The receiver is as small as 1/5000 of the powering range (see Methods A for details regarding the range and scaling); this can be considered as a highly asymmetric configuration (such as one

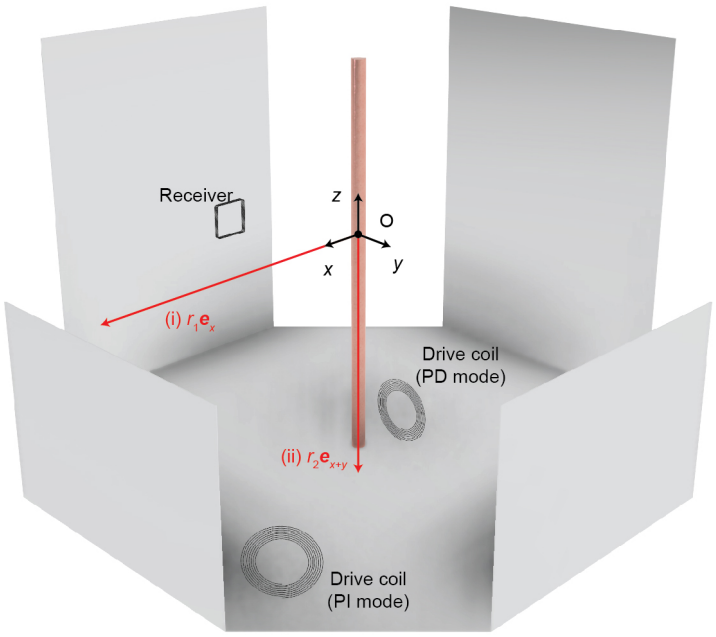

Figure 3.7 The setup and coordinates used for evaluating the power transfer efficiency. I partially omitted the conductor sheets for visibility. I altered the drive coil positions depending on the excited resonant mode. The parameters r_1 and r_2 indicate the distance from the center of the room. $\vec{e}_x$ and $\vec{e}_{x+y}$ are the unit vectors along the $+x$ direction and $x + y$ direction, respectively.

involving a large transmitter and a small receiver) used in typical coil-based wireless power transfer systems (figure 3.1(a)), which suffer from insufficient coupling. The power transfer efficiency throughout the volume was determined based on the coupled mode theory by using the measured Q factors and the simulated coupling coefficients [20, 39, 49] (see Methods C for details). In addition, to confirm these results, efficiency measurements based on the measured S-parameters were conducted at the extracted positions [50] (see Methods D for details). For the receiver, I used a six-turn, 150 mm × 150 mm square coil with a series capacitor connected to tune the resonance frequency, as shown in figure 3.4(a). The Q factor of this receiver was 236. In the measurements, an external drive coil, shown in figure 3.4(b), was used to stimulate the resonant modes of the room-scale resonator. In both the coupled mode theory-based evaluations and the S-parameter-based evaluations, the value of load impedance is assumed to be one that maximises the power transfer efficiency; this is a reasonable and typical assumption considering the development of maximum efficiency point tracking methods [18]. Evaluations based on the coupled mode theory revealed that the proposed approach achieved an efficiency

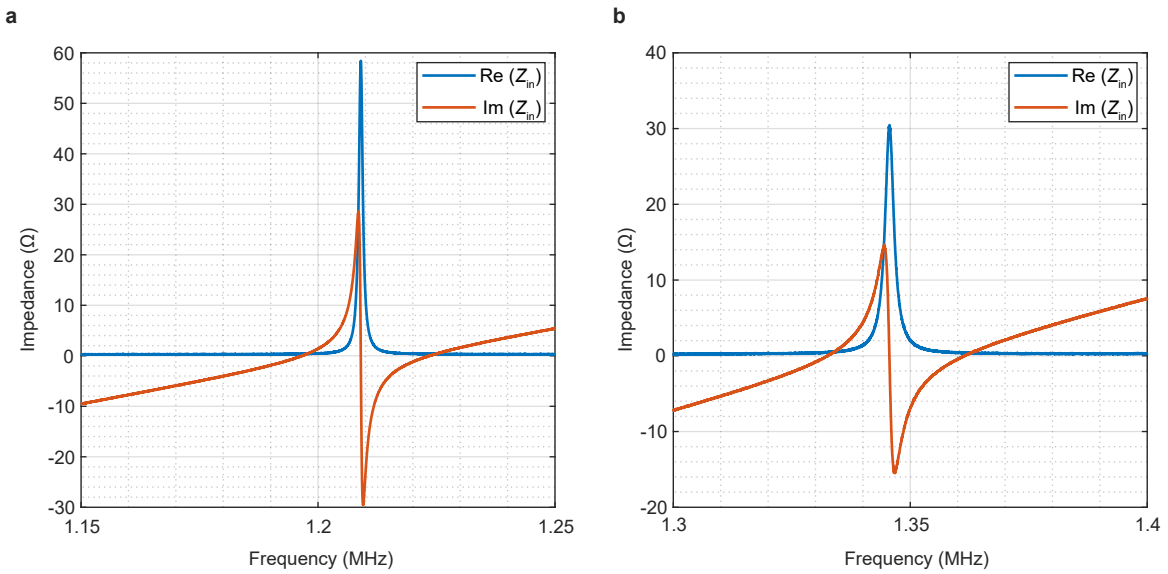

Figure 3.8 The input impedance of the drive coil. (a) PD mode and (b) PI mode.

exceeding 50% in 98.0% of the room volume by multiplexing the PI and PD modes based on the receiver position. Moreover, power transfer efficiency was greater than 37.1% at any position within the room volume. This analysis also revealed that the PD mode alone, which closely resembles the mode in the previous QSCR [P3], can achieve an efficiency exceeding 50% in only 57.5% of the room volume, and its efficiency decreases to 1% near the walls. These results show that the proposed approach covers the entire volume of the room, even though the PD mode alone (resembling the previous method) only covers approximately half of the room (considering positions where the efficiency exceeds 50%). Figure 3.9(a)-(e) show the simulated efficiencies along the $z = 0$ and $y = 0$ planes. When only the PI mode is used (*i.e.*, when the central conductive pole is omitted), an efficiency exceeding 50% could be obtained in 52.4% of the room volume. Overall, these results indicate the following: (i) by leveraging multiple resonant modes (*i.e.*, magnetic field patterns), a significantly larger portion of the volume could be covered, as compared to that covered by either mode alone; (ii) the power transfer range successively forms a 3-D volume, and the transfer efficiency has a limited dependence on z-coordinates; and (iii) the resonant modes' repertoire allows omission of the central pole, which was essential for previous approaches, while still covering a large portion of the room.

Lastly, I measured the power transfer efficiency at extracted positions within the room volume to confirm these results based on the coupled mode theory; this measurement was based on the S-parameters obtained by two-port measurements using a vector network analyser

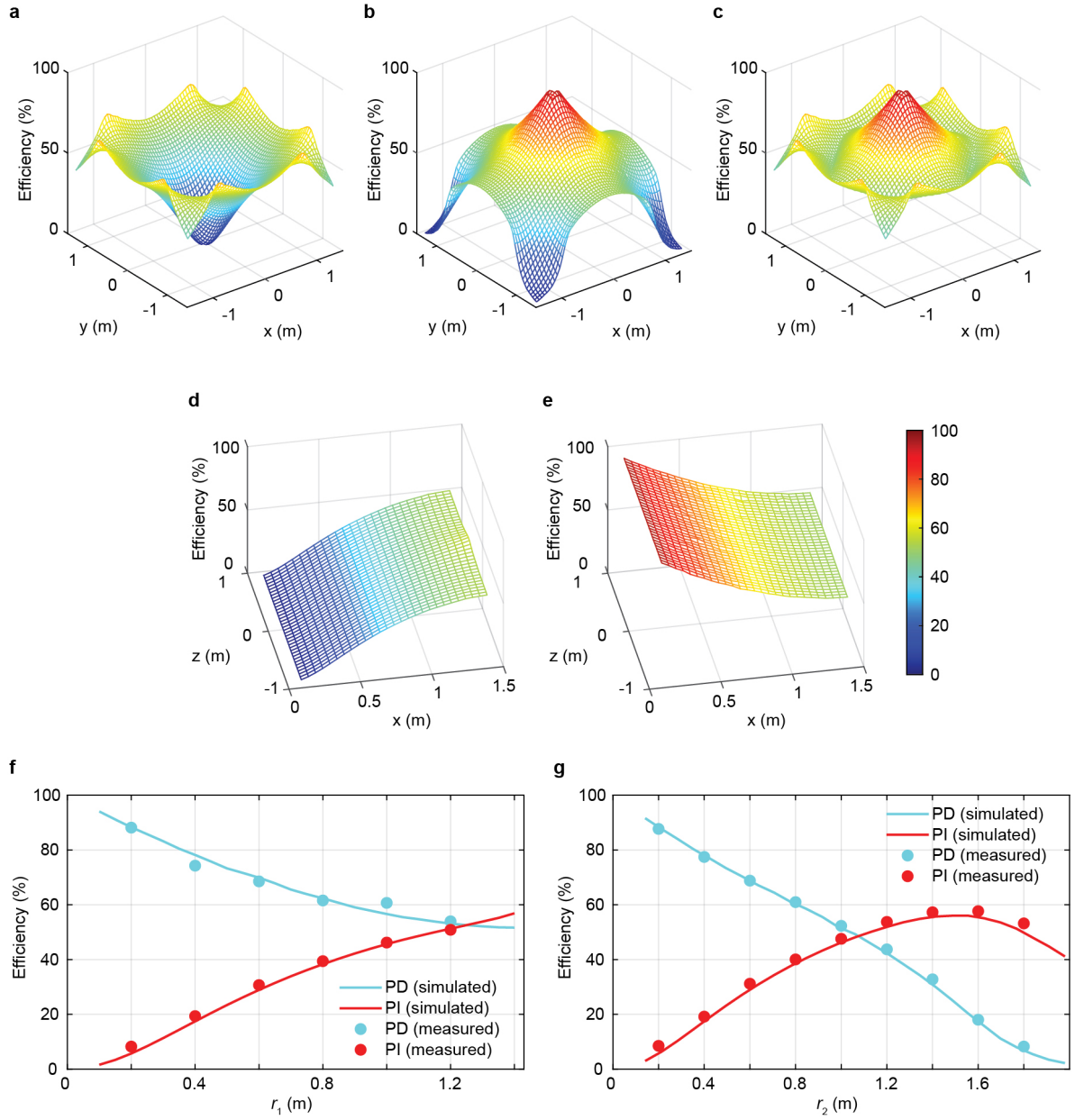

Figure 3.9 Evaluation of the power transfer efficiency. Efficiencies when I placed the receiver on the $z = 0$ plane (see figure 3.7) using the (a) pole independent (PI) mode, (b) pole dependent (PD) mode, and (c) both modes. The power transfer efficiencies when I placed the receiver on the $y = 0$ plane using the (d) PI mode and (e) PD mode. (f) shows the simulated and measured power transfer efficiency when I placed the receiver on line (i) (see figure 3.7). (g) shows the simulated and measured efficiencies when I placed the receiver on line (ii) (see figure 3.7).

Table 3.1 The simulated transfer efficiency over the entire volume.

	PD mode	PI mode	Dual mode
Maximum efficiency	94.3 %	76.5%	94.3%
Minimum efficiency	1.0 %	1.7%	37.1%
Average efficiency	50.4%	46.7%	60.6%
Positions with over 50% efficiency	57.5%	52.4%	98.0%

(VNA). Line (i) and line (ii) in figure 3.7 depict the positions where the receiver was located for this measurement. As shown in figure 3.7, the drive coil was placed such that it efficiently coupled with the magnetic field patterns of the corresponding resonant mode. Figure 3.8 shows the input impedance seen from these drive coils. Figure 3.9(f) and (g) presents a comparison of the power transfer efficiency determined using the measured S-parameters and that determined based on the coupled mode theory. The validity of the coupled mode theory-based analysis conducted across the entire room volume was proved by the good agreement between these results. I note as a limitation that in this initial work, the receiver coil needs to be orientated orthogonally with the ambient magnetic field to obtain the maximum efficiency at each point; as a simple countermeasure, receiver coils can gain orientation insensitivity by combining multiple orthogonal coils [51, 52].

3.5 Modeling the magnetic field

As explained in Methods C, the computation of coupling coefficients require (i) the volume integral of the magnetic field energy confined, and (ii) the surface integral of the magnetic flux captured by the receiver. Because electromagnetic field calculation using finite element methods require a large computation burden, I offer an approximate, yet analytic model of the magnetic field in the following (see Methods E for details for field extraction and current modeling):

$$H_{\mathrm{PD}}(\vec{r}) = \begin{pmatrix} H_{\mathrm{pole},x}(\vec{r}) + H_{\mathrm{wall},x,1}(\vec{r}) + H_{\mathrm{wall},x,2}(\vec{r}) \\ H_{\mathrm{pole},y}(\vec{r}) + H_{\mathrm{wall},y,1}(\vec{r}) + H_{\mathrm{wall},y,2}(\vec{r}) \\ 0 \end{pmatrix} \tag{3.4}$$

$$H_{\mathrm{PI}}(\vec{r}) = \begin{pmatrix} -H_{\mathrm{wall},x,1}(\vec{r}) + H_{\mathrm{wall},x,2}(\vec{r}) \\ H_{\mathrm{wall},y,1}(\vec{r}) - H_{\mathrm{wall},y,2}(\vec{r}) \\ 0 \end{pmatrix}, \tag{3.5}$$

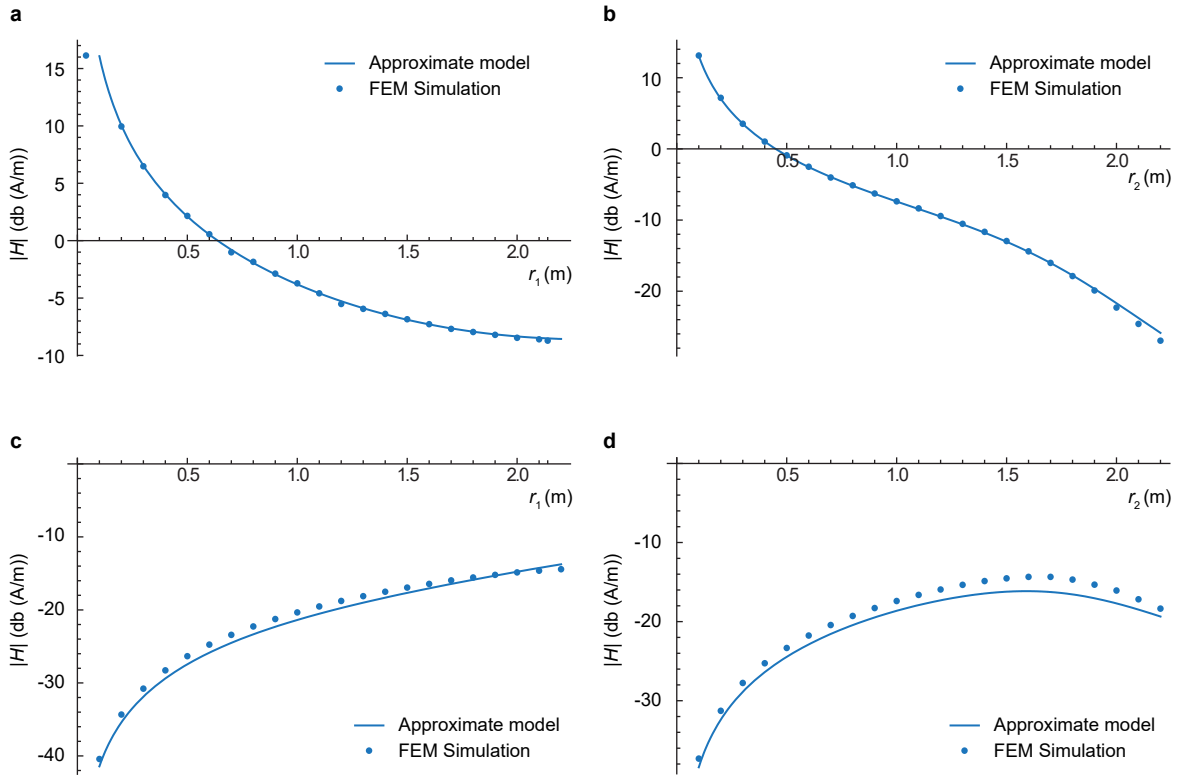

Figure 3.10 Validation of the approximate magnetic field model. These figures show the analytical model and the FEM simulation values of magnetic field intensity on the lines (i) and (ii) shown in figure 3.7. (a) shows the magnetic field amplitude of the PD mode on line (i). (b) shows the magnetic field amplitude of the PD mode on line (ii). (c) shows the magnetic field amplitude of the PI mode on line (i). (d) shows the magnetic field amplitude of the PI mode on line (ii).

using the following expressions:

$$H_{\text{wall},x,1}(\vec{r}) = \frac{\mathrm{d}I_0}{4\pi} \cdot 2 \cdot \sum_{m=0}^{1} \sum_{n=0}^{1} \left((-1)^{m+1} \cdot \arctan\left[\frac{x + \frac{(-1)^m pw}{2}}{y + \frac{(-1)^n w}{2}} \right] \right) \tag{3.6}$$

$$H_{\text{wall},x,2}(\vec{r}) = \frac{\mathrm{d}I_0}{4\pi} \sum_{m=0}^{1} \left((-1)^m \log\left[1 + \frac{(-1)^{m+1} 8pwy}{4\left(x^2+y^2\right) + (-1)^m 4w(x+py) + \left(1+p^2\right)w^2} \right] \right) \tag{3.7}$$

$$H_{\text{pole},x}(\vec{r}) = \frac{\mathrm{d}I_0}{4\pi} \cdot \frac{8pwy}{x^2+y^2} \tag{3.8}$$

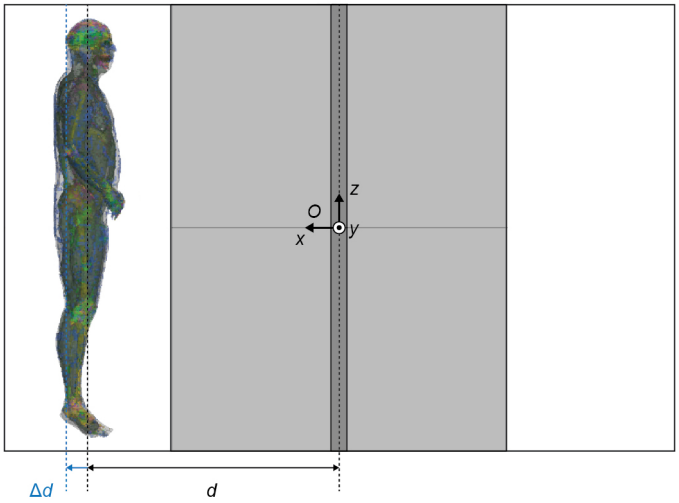

Figure 3.11 Simulation setup for evaluating safety based on specific absorption rate (SAR). This image shows the side view of the human anatomical model used in SAR evaluations and its placement within the room-scale transmitter resonator. I moved the human model along the x-axis in the evaluations.

$$H_{\text{wall},y,1}(\vec{r}) = \frac{\mathrm{d}I_0}{4\pi} \cdot 2 \cdot \sum_{m=0}^{1} \sum_{n=0}^{1} \left((-1)^m \cdot \arctan\left[\frac{y + \frac{(-1)^m pw}{2}}{x + \frac{(-1)^n w}{2}} \right] \right) \tag{3.9}$$

$$H_{\text{wall},y,2}(\vec{r}) = \frac{\mathrm{d}I_0}{4\pi} \sum_{m=0}^{1} \left((-1)^m \log\left[1 + \frac{(-1)^m 8pwx}{4\left(x^2+y^2\right) + (-1)^m 4w(y-px) + \left(1+p^2\right)w^2} \right] \right) \tag{3.10}$$

$$H_{\text{pole},x}(\vec{r}) = \frac{\mathrm{d}I_0}{4\pi} \cdot \frac{8pwy}{x^2+y^2} \tag{3.11}$$

$$H_{\text{pole},y}(\vec{r}) = \frac{\mathrm{d}I_0}{4\pi} \cdot \frac{8pwx}{x^2+y^2} \tag{3.12}$$

Figure 3.10 compares these derived formulas with FEM-simulation values, which indicates that the fields are successfully modeled with small errors. By using these equations, the integral in equation 3.19 and 3.20 can be calculated with small computation burden, which enables the quick estimation of coupling coefficient κ.

3.6 Safety

For deploying wireless power transfer in public environments, it is necessary to evaluate how the exposed electromagnetic (EM) field affects people present within the charging coverage of the system. As measures for safety, the FCC and the Institute of Electrical and Electronics Engineers (IEEE) have adopted guidelines regarding EM field exposure [42]. These guidelines primarily focus on preventing localised heat stress and full-body heating at frequencies exceeding 100 kHz [42, 8]. Therefore, basic restrictions are imposed based on the specific absorption rate (SAR), which is a measure of the amount of power absorbed by biological tissue [8, 43]. The following analysis considers the compliance with restrictions on uncontrolled exposure of the general public, which limit the average SAR of the entire body to 0.08 W/kg and the localized SAR, defined as the average power absorbed by a 1 g tissue sample, to 1.6 W/kg.

The SAR is dependent on the input power and the power transfer efficiency[20, 43]. For instance, if the system is driven under non-loaded (*i.e.*, zero-efficiency) conditions, exposure levels tend to reach the regulatory limits even with a low input power, compared to high-efficiency conditions. This is because an increase in the power transfer efficiency increases the proportion of power delivered to the receiver; consequently, the proportion of reactive energy stored in the room-scale resonator decreases. As discussed in the previous section, the proposed system achieves a power transfer efficiency exceeding 50% in most (over 98%) of the room volume. Therefore, for subsequent analyses regarding safety, the input power at which the SAR reaches regulatory thresholds when the system operates at a power transfer efficiency of 50% was evaluated in order to determine a conservative threshold.

I conducted simulations of in-body SAR using Hyperworks FEKO, which is an EM solver that supports method of moments and FEM hybrid simulations; surroundings of the human body model were analyzed via FEM, which can calculate the SAR without a loss in accuracy within domains considerably smaller than the wavelength [8]. For the simulations, a 1.88 m full-body anatomical model comprising each tissue component annotated with its electromagnetic properties and mass was employed. This model was placed on three positions along the line between the center of the room and its walls (figure 3.11). Additionally, two resonant modes were considered; thus, a total of six configurations were investigated.

The obtained maximum input power values for the abovementioned configurations are shown in figure 3.12. For every configuration, the threshold of localised SAR was reached earlier than the threshold of the whole-body average SAR. As these results are based on a power transfer efficiency of 50%, the power delivered to the load is half of the input power. The input power threshold is greater than 100 W for all the tested configurations, and the results suggest

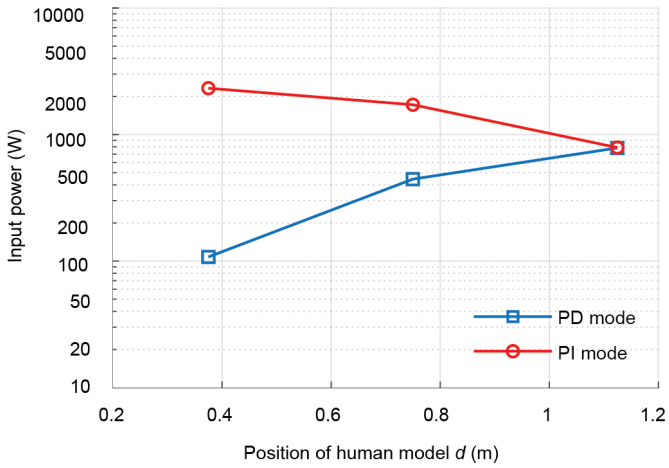

Figure 3.12 Input power limits derived from the specific absorption rate (SAR) evaluations.

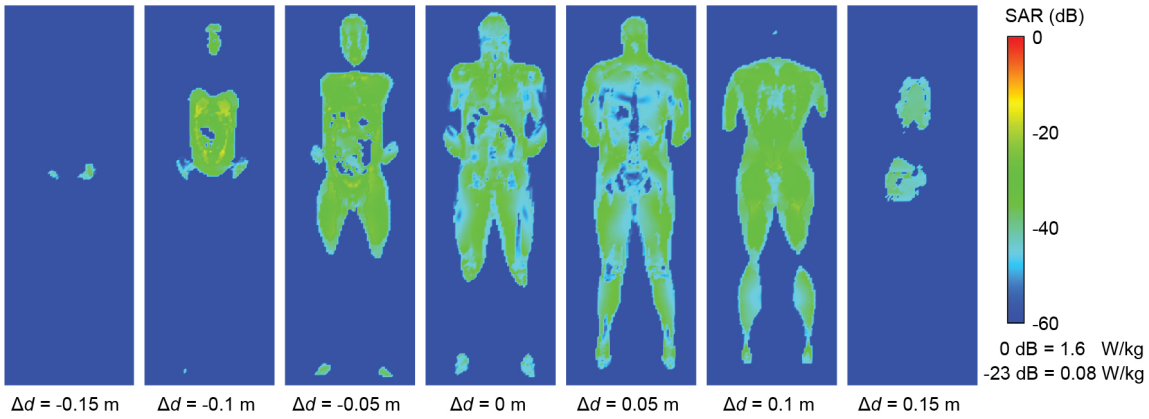

Figure 3.13 The SAR distribution when the input power reached the exposure limits.

that the input power can be increased further if people are appropriately positioned or restricted from certain areas. To provide a graphical representation of heat stress, the distribution of SAR at the threshold of input power is shown in figure 3.13. Here, 0 dB corresponds to the threshold for localised SAR (1.6 W/kg), whereas -23 dB corresponds to the threshold for average SAR (0.08 W/kg).

Figure 3.14 Demonstration of room-scale wireless power transfer in a living environment. I only used the pole independent (PI) mode for this demonstration. (a) shows an overview of the room; (b) shows a wirelessly powered light bulb (included inside the floor lamp in a), smartphone, and portable fan; (c) shows the wireless charging of a smartphone in the air; and (d) shows a wirelessly powered portable fan. I augmented these devices using simple wireless power transfer receivers, consisting of a receiver resonator, loop coil, full-bridge rectifier, and a linear voltage regulator. Figure 3.15) shows the details of these augmented devices.

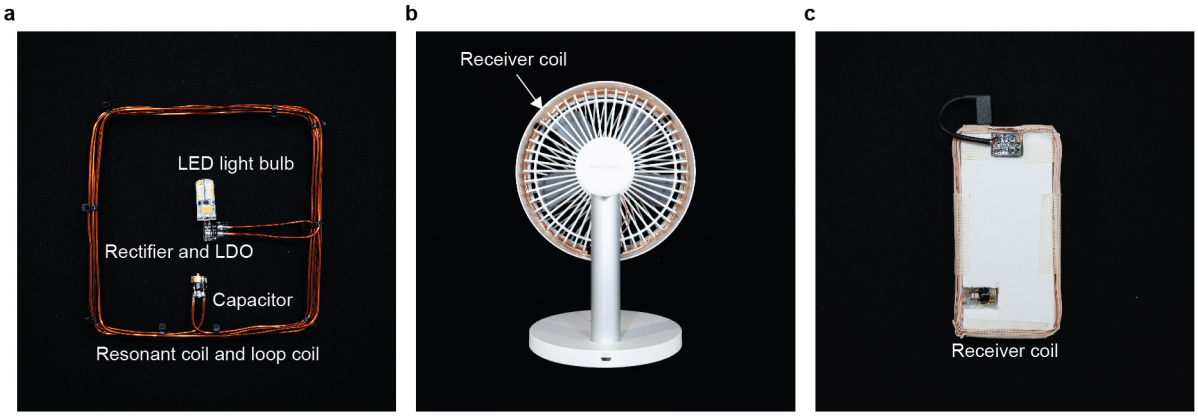

Figure 3.15 The electronics are augmented with wireless power receivers. (a) The light bulb in the floor lamp, fan, and the back of a smartphone. The receivers are composed of a receiver resonator, a loop coil for impedance tuning, a full-bridge rectifier, an LDO, and the load (*i.e.*, the empowered device).

3.7 Demonstration of wireless power transfer in living environments

To demonstrate the applicability of the proposed approach in daily life, the constructed wireless power room was furnished with typical devices such as floor lamps and smartphones. Figure 3.14 shows a photograph of the fully functional wireless power transfer room, where the central conductive pole is omitted and only the PI mode is used. The labelled devices were augmented with wireless power transfer receivers (figure 3.15). As shown in figure 3.14(a), the proposed technology enables seamless untethering of numerous electronic devices without interfering with conventional lifestyles.

3.8 Summary

In this chapter, multimode QSCR, which enables highly efficient and safe wireless transfer of large amounts of power within 3-D volumes, is presented. Analyses and measurements revealed that, by leveraging the multi-directional and widely distributed surface currents, efficient power transfer could be achieved throughout the room, unlike previous magnetoquasistatic wireless power methods, which were unable to cover the entire room. In addition, by using the repertoire of available resonant modes, the central pole, which was essential in previous approaches, could be omitted, while maintaining efficient power delivery

Table 3.2 Comparison with the previous quasistatic cavity resonator (QSCR).

	Previous approach	Proposed approach	
	QSCR (Single mode)	Multimode QSCR (Dual mode)	Multimode QSCR (PI mode)
Interaction with dielectrics (*e.g.* human, daily objects)	✓ Small	✓ Small	✓ Small
Full volume coverage	✗ Only near room-centre	✓ Full volume	✗ Only near the walls
Need for the central conductive pole	✗ Necessary	✗ Necessary	✓ Non-necessary

over a large portion of the room. The advantage of this method compared to the previous approach is summarized in table 3.2.

As the proposed approach uses magnetoquasistatic fields, room dimensions and receiver sizes can be flexibly determined, independently of the operating wavelength, by adjusting the values of the lumped capacitors. Another important benefit of using magnetoquasistatic fields is that the existence of everyday objects does not affect system operation significantly; simulations supporting this statement is provided in Methods H. Given the flexibility in system dimensions and the robustness to interference caused by external objects, the proposed technology is expected to be widely applicable in a wide range of scenarios, including charging cabinets, wireless charging rooms, and untethered factories.

Methods

A Construction details and the charging area

The dimensions of the constructed multimode QSCR-based wireless power transfer test room were 3 m × 3 m × 2 m. Figure 3.16 shows the charging area in this room. The room dimensions were determined based on the largest space I could find. Although the resonant structure has an octagonal shape, the charging volume is rectangular. Therefore, a rectangular room can be created using walls, a floor, and a ceiling within the charging area, as shown in figure 3.16; the images in figure 3.14 were obtained in this manner. The relation between receiver size

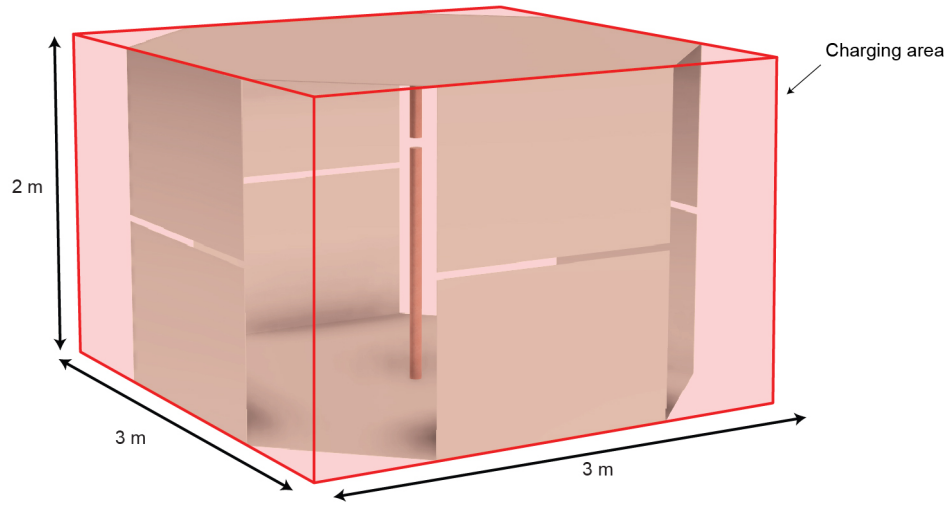

Figure 3.16 Considered charging area.

(figure 3.4(a), 150 mm × 150 mm square coil) and the charging area was obtained as follows:

$$(\text{Length of one side of the receiver})^3 : \text{room volume} \tag{3.13}$$

$$= 0.15^3\ \text{m}^3 : 18\ \text{m}^3 \tag{3.14}$$

$$= 1 : 5000 \tag{3.15}$$

Figure 3.17 shows the abstracted blueprint of the room. The room was constructed by first building a framework using typical aluminium frames; thereafter, 1100 aluminium alloy panels were bolted over these frames, which served as the conductive body of the wall, floor, and ceiling. The central pole was composed of C1220T copper alloy pipes and C1100 copper alloy plates, connected via braze welding. The lumped capacitors were bolted to the structure, as shown in figure 3.18, using custom printed circuit boards containing electrodes with an immersion gold surface finish. The panels composing the structure were carefully connected to ensure that high conductivity is maintained. The bottom half and top half of the structure need to be isolated, therefore I used Bakelite boards for good insulation while maintaining sufficient structural strength (figure 3.19). As shown in figure 3.3(b), the floor of the structure was lifted by approximately 200 mm for faciltating construction and to alleviate the effect of coupling with the building floor. The test room was built using ordinary hardware and tools; special construction techniques were not required.

For the demonstration of the furnished room (figure 3.14), I covered the ceiling and walls of the room with light-weight styrene boards to provide the appearance of an actual

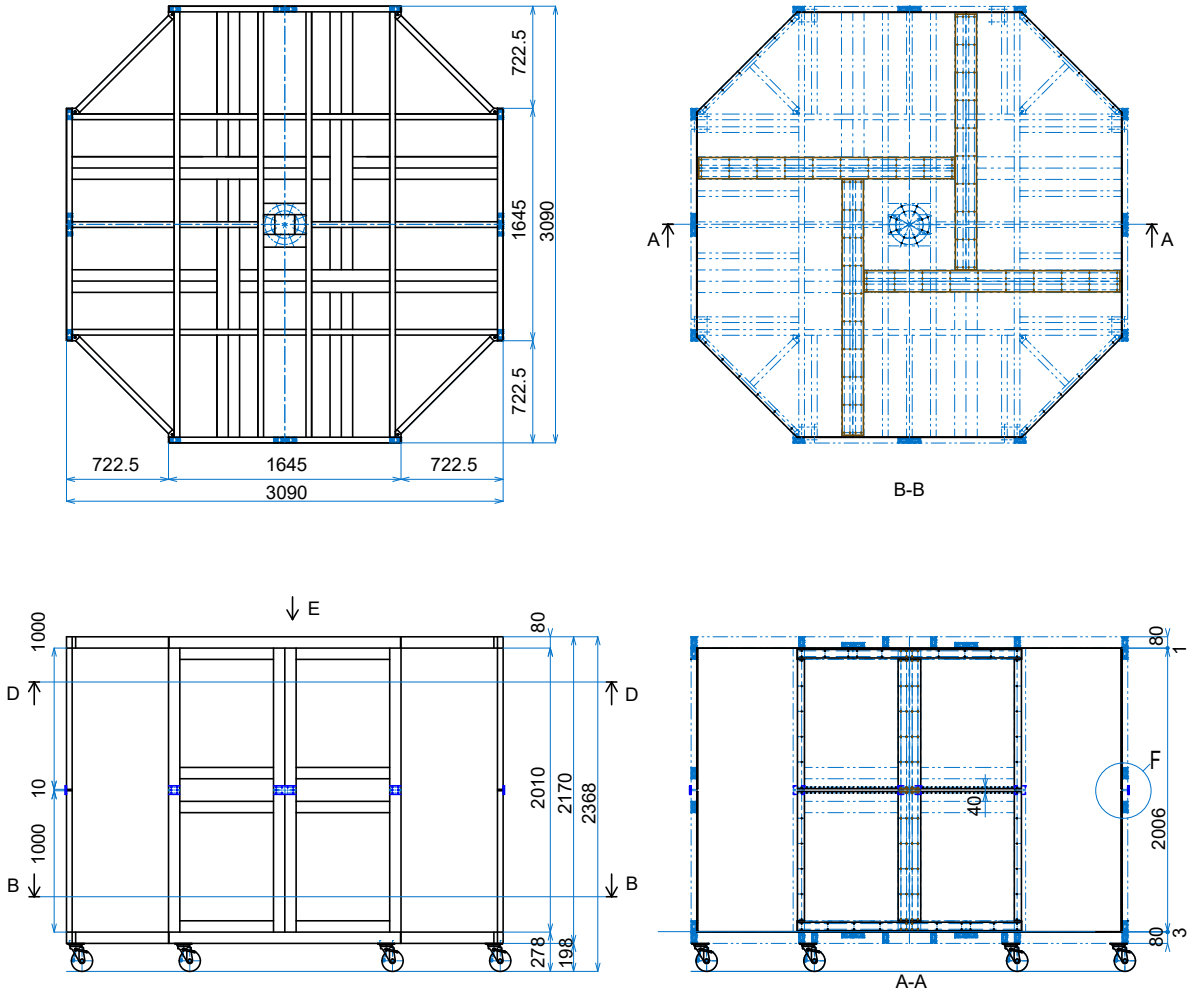

Figure 3.17 Blueprint of the implemented room-scale resonator (abstract).

room. In addition, the floor was covered with PVC flooring material. I placed the walls and floor materials along the charging area shown in figure 3.16 to form a rectangular room volume. Ordinary pieces of furniture were also placed within the room to further highlight the applicability of wireless power transfer in daily environments. Based on measurements of the quality factor and the resonant frequency of the room-scale resonator, these furnishing materials, as well as the people present within the room, did not significantly affect the system; thus, the conductive body of the resonant structure can be covered without affecting system performance, which is an advantage of this approach.

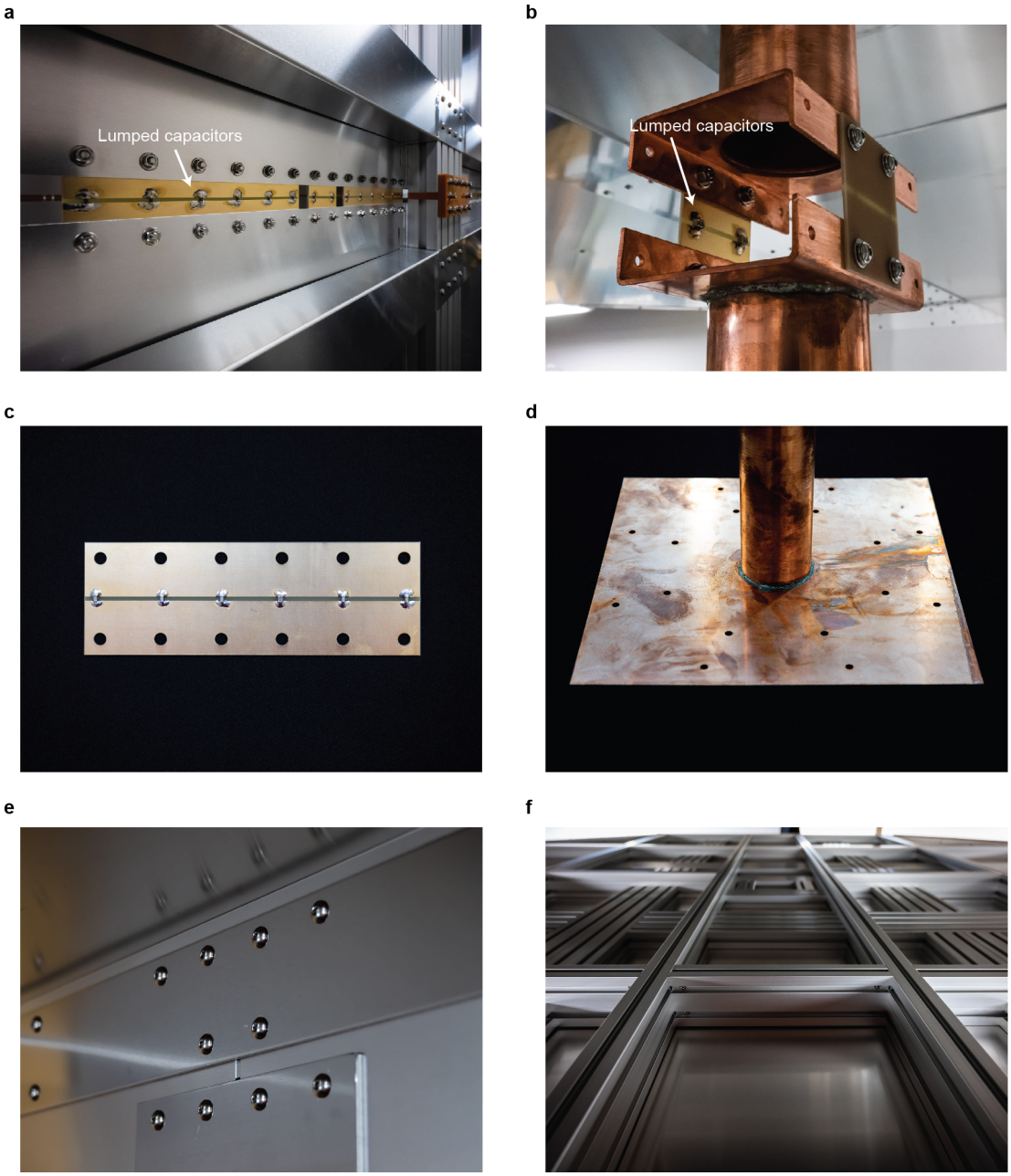

Figure 3.18 The mounting of the capacitors and how conductivity is maintained. (a) and (b) show the capacitors mounted in the pole and the wall. (c) shows the printed circuit boards used in (a) and (b). (d) shows the welded connection between the central pole and the floor/ceiling. (e) shows the connections of the edges of the structure. I used firm metallic plates to maintain uniform mechanical pressure and high-conductivity. (f) shows the outer view of the room-scale resonator. I bolted the aluminum sheets on the external aluminum frames.

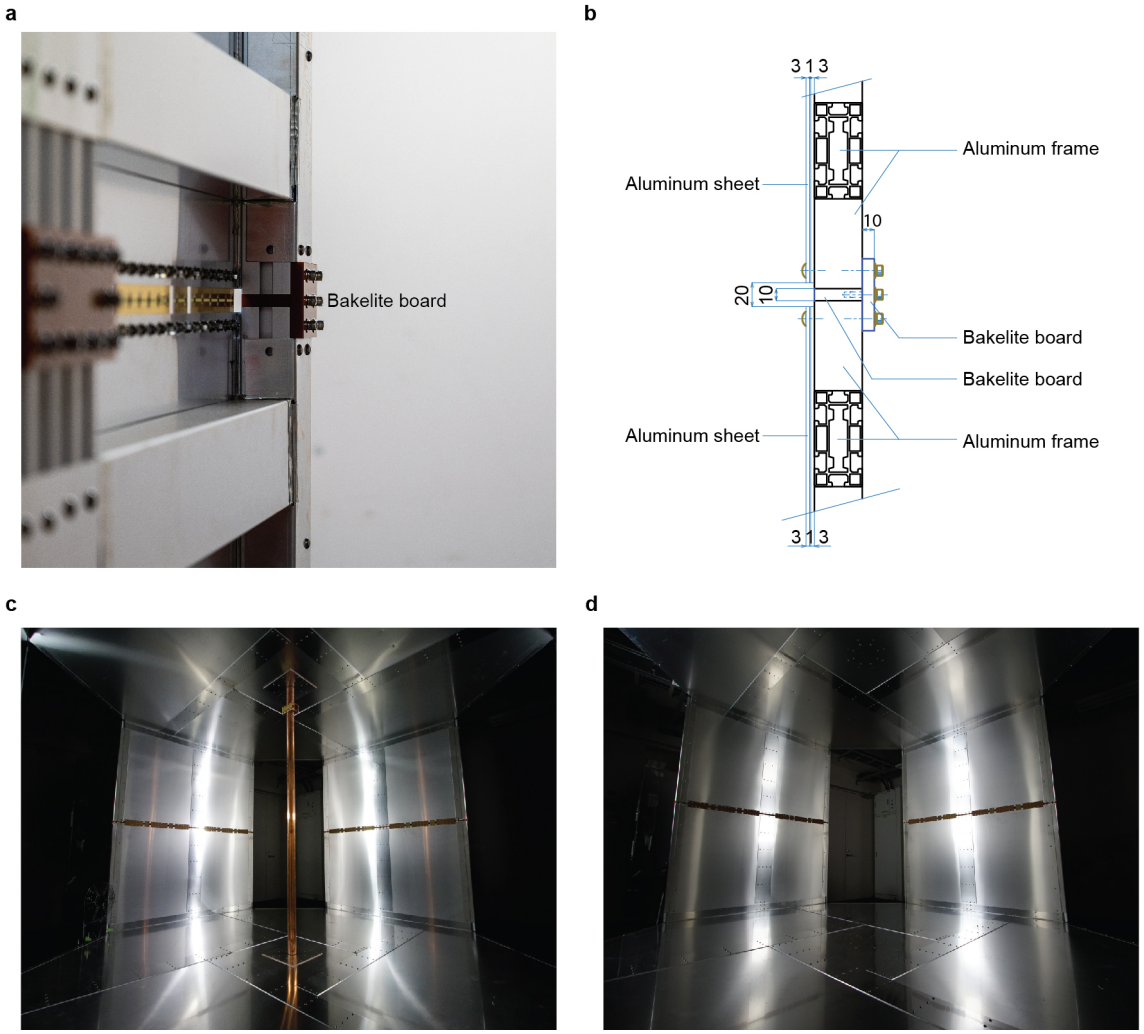

Figure 3.19 Details of the insulation within the structure and the inner view of the room. (a) and (b) show how I insulated the structure's bottom half and top half. I used Bakelite boards for good insulation while maintaining sufficient structural strength. (c) and (d) show the inner view of the room. (c) with and (d) without the central pole implemented.

B FEM simulations for determining eigenmodes of the structure

For extracting the eigenmodes of the structure, eigenfrequency analyses were conducted using the FEM-based electromagnetic field solver, COMSOL Multiphysics (RF module). I obtained the resonant frequencies, current distributions, and magnetic fields of the resonant modes through these simulations. As experimental values of the quality factor are typically lower than the simulated values, I used the measured quality factor for the efficiency and safety evaluations.

C Evaluating efficiency based on the coupled mode theory

The three parameters required to determine the transmission efficiency between coupled resonators are the quality factor of the transmitter, quality factor of the receiver, and the coupling coefficient between the transmitter and the receiver. For the coupled mode theory-based analysis, the following expression of the transfer efficiency between two coupled resonators with identical frequencies was used [20, 49]:

$$\eta_{\max} = \frac{\chi}{\left(1+\sqrt{1+\chi}\right)^2} \tag{3.16}$$

$$\chi = \frac{4Q_1Q_2|\kappa|}{\omega_0^2} \tag{3.17}$$

Here, Q_1, Q_2, κ, and ω_0 represent the quality factor of the transmitter (room-scale resonator), quality factor of the receiver, coupling rate between the transmitter and receiver, and angular resonant frequency of the two resonators, respectively. This expression yields the transfer efficiency when the load is tuned to a value that maximises efficiency. This is reasonable considering the development of maximum efficiency point tracking methods [50]. Measured values of the quality factor were used because it is difficult to obtain accurate values through simulations; meanwhile, FEM simulations were used to extract the coupling rate κ. The coupling rate κ was extracted through the following equations [39, 20]:

$$\kappa = \frac{\sqrt{2}}{4} \cdot \frac{\omega_1 \beta}{\sqrt{L_2 \alpha}} \tag{3.18}$$

$$\alpha = \iiint_V \frac{\mu_0}{2} \cdot \left|\vec{H}\right|^2 \mathrm{d}\boldsymbol{V} \tag{3.19}$$

$$\beta = \iint_A \mu_0 \vec{H} \cdot \vec{n}\, \mathrm{d}\boldsymbol{A} \tag{3.20}$$

Here, α is the total magnetic energy stored in the room, and β is the flux intersecting the receiver. In the abovementioned expressions, $\boldsymbol{V}$ is the entire volume of the room, $\vec{n}$ is the unit normal vector of the receiver surface, ω_0 is the resonant frequency of the QSCR, $\boldsymbol{A}$ is the area enclosed by the receiver, and L_2 is the receiver inductance.

For determining efficiency based on the coupled mode theory, the center of the receiver resonator was placed at 50 mm interval grid points within the volume of the room. The expression of the considered range of receiver positions (*i.e.*, coordinates of the center of the receiver) is as follows:

$$\max\left(|x|, |y|\right) \leq 1.4 \text{ m} \tag{3.21}$$

$$0.1 \text{ m} \leq |z| \leq 1.4 \text{ m} \tag{3.22}$$

I excluded a small region around the pole to accommodate the finite size of the receiver. As the cross-sections of the room and the receiver resonator differed by a factor of approximately 500, I assumed that the magnetic flux penetrating the receiver resonator was uniform. The efficiency calculated under this assumption was in good agreement with the measured efficiency. The orientation of the receiver resonator was set such that it maximises the power transfer efficiency at each position (*i.e.*, all the magnetic fluxes were normal to the coil).

D Evaluating efficiency based on two-port measurements

The measured efficiency, $\eta_{\max}$, was extracted using S-parameters measured by a VNA using the following expression from literature [50]:

$$\eta_{\max} = K - \sqrt{K^2 - 1} \tag{3.23}$$

$$K = \frac{1 - |S_{11}|^2 - |S_{22}|^2 + |S_{11}S_{22} - S_{12}^2|^2}{2|S_{12}|^2} \tag{3.24}$$

Similar to the expression for determining efficiency using the coupling mode theory, this expression also yields the transfer efficiency when the load is tuned to a value that maximises efficiency; this is reasonable and typical considering the development of maximum efficiency point tracking methods [18, 50, 53]. For each mode, the drive coil was placed at the positions shown in figure 3.7. Moreover, the receiver resonator was placed at the series of positions represented by lines (i) and (ii) in figure 3.7, with orientations that maximised the penetrating magnetic fluxes. For these evaluations, I used the receiver coil and the drive coil shown in figure 3.4.

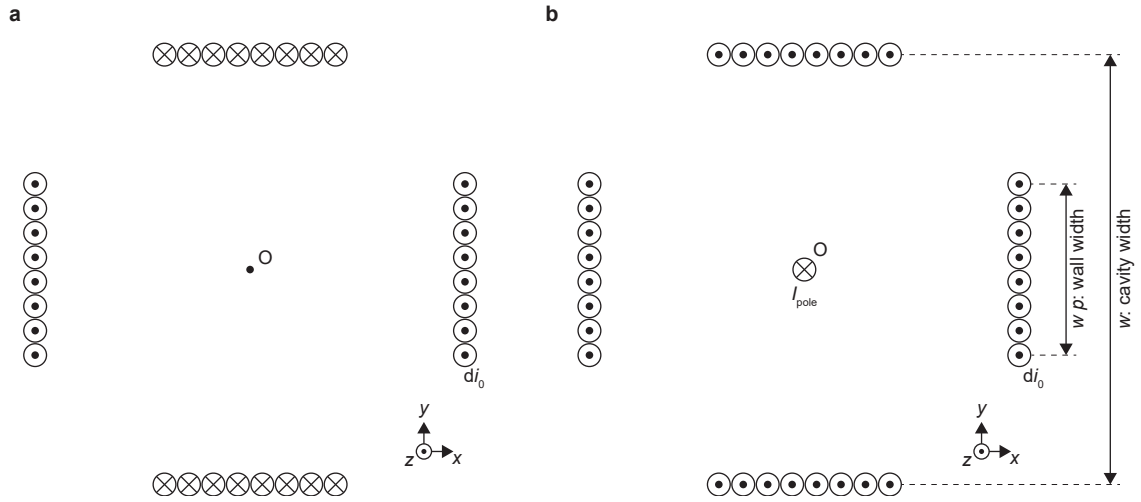

Figure 3.20 Approximate modeling of the multimode QSCR current. This model assumes uniform current elements that flow in $-\infty \leq z \leq +\infty$. (a) PI mode and (b) PD mode.

E Extraction of the approximate magnetic field formulation

Figure 3.20 shows the model used for extracting the approximate formulation. Because the magnetic field obtained by simulations and measurements did not have z-direction components, I modeled the multimode QSCR structure by assuming uniform current elements that flow in $-\infty \leq z \leq +\infty$.

Magnetic field $\vec{H}_{\text{line}}(\vec{r} = (x, y, z))$ generated by current element $\mathrm{d}i_0$ on $\vec{r'} = (x', y', z'), -\infty \leq z' \leq +\infty$ is,

$$\vec{H}_{\text{line}} = \frac{\mathrm{d}i_0 \mu_0}{2\pi \left((x - x')^2 + (y - y')^2\right)} \cdot \begin{pmatrix} -(y - y') \\ x - x' \\ 0 \end{pmatrix}. \tag{3.25}$$

Next, by assuming $x' = w/2$ (wall position),

$$\vec{H}_{\text{line}} = \frac{\mathrm{d}i_0 \mu_0}{2\pi \left((x - w/2)^2 + (y - y')^2\right)} \cdot \begin{pmatrix} -(y - y') \\ x - w/2 \\ 0 \end{pmatrix}. \tag{3.26}$$

Integrating $\vec{H}_{\text{line}}$ over $-w/2 \leq y' \leq w/2$ (wall width) gives,

$$\vec{H}_{\text{wall,A}} = \int_{-wp/2}^{wp/2} \vec{H}_{\text{line}} \mathrm{d}y' \tag{3.27}$$

$$= \frac{\mathrm{d}i_0\mu_0}{4\pi}\begin{pmatrix} -\log\left[1+\dfrac{8pwy}{\left(1+p^2\right)w^2-4w(x+py)+4\left(x^2+y^2\right)}\right] \\ -2\arctan\left[\dfrac{pw-2y}{w-2x}\right]-2\arctan\left[\dfrac{-pw-2y}{w-2x}\right] \\ 0 \end{pmatrix}. \tag{3.28}$$

In the same way,

$$\vec{H}_{\mathrm{wall,B}} = \frac{\mathrm{d}i_0\mu_0}{4\pi}\begin{pmatrix} -2\arctan\left[\dfrac{-pw+2x}{w-2y}\right]+\arctan\left[\dfrac{pw+2x}{w-2y}\right] \\ -\log\left[1-\dfrac{8pwx}{\left(1+p^2\right)w^2-4w(-px+y)+4\left(x^2+y^2\right)}\right] \\ 0 \end{pmatrix} \tag{3.29}$$

$$\vec{H}_{\mathrm{wall,C}} = \frac{\mathrm{d}i_0\mu_0}{4\pi}\begin{pmatrix} \log\left[1-\dfrac{8pwy}{\left(1+p^2\right)w^2+4w(x+py)+4\left(x^2+y^2\right)}\right] \\ -2\arctan\left[\dfrac{-pw+2y}{w+2x}\right]+2\arctan\left[\dfrac{pw+2y}{w+2x}\right] \\ 0 \end{pmatrix} \tag{3.30}$$

$$\vec{H}_{\mathrm{wall,D}} = \frac{\mathrm{d}i_0\mu_0}{4\pi}\begin{pmatrix} 2\arctan\left[\dfrac{-pw-2x}{w+2y}\right]-2\arctan\left[\dfrac{pw-2x}{w+2y}\right] \\ \log\left[1+\dfrac{8pwx}{\left(1+p^2\right)w^2-4w(px-y)+4\left(x^2+y^2\right)}\right] \\ 0 \end{pmatrix}, \tag{3.31}$$

can be derived. Because the pole current is equal to the total wall current,

$$I_{\mathrm{pole}} = 4\int_{-wp/2}^{wp/2}\mathrm{d}i_0\mathrm{d}y \tag{3.32}$$

$$= 4wp\mathrm{d}i_0. \tag{3.33}$$

Thus the magnetic field generated by the central pole can be calculated as the following:

$$\vec{H}_{\mathrm{pole}} = 4wp\vec{H}_{\mathrm{line}} \tag{3.34}$$

$$= 4wp\frac{\mathrm{d}i_0\mu_0}{2\pi\left(x^2+y^2\right)}\cdot\begin{pmatrix} -y \\ x \\ 0 \end{pmatrix}. \tag{3.35}$$

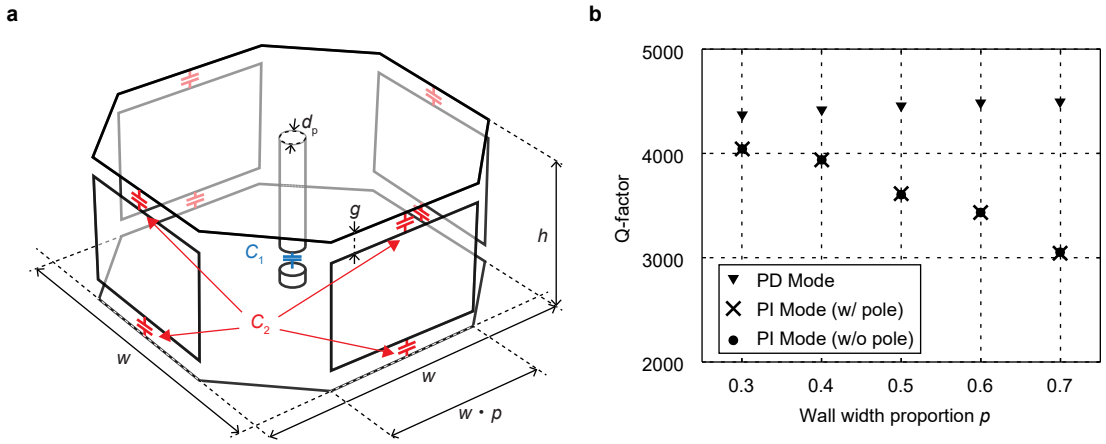

Figure 3.21 Wall opening size and the quality factor. (a) The considered setup. (b) The quality factors when the opening size is varied.

Finally, considering the current direction on each wall and the central conductive pole,

$$\vec{H}_{\mathrm{PD}} = \vec{H}_{\mathrm{pole}} + \vec{H}_{\mathrm{wall,A}} + \vec{H}_{\mathrm{wall,B}} + \vec{H}_{\mathrm{wall,C}} + \vec{H}_{\mathrm{wall,D}} \tag{3.36}$$

$$\vec{H}_{\mathrm{PI}} = \vec{H}_{\mathrm{wall,A}} - \vec{H}_{\mathrm{wall,B}} + \vec{H}_{\mathrm{wall,C}} - \vec{H}_{\mathrm{wall,D}}. \tag{3.37}$$

Simplifying this expression gives equations 3.4 and 3.5

F Varying the opening size

Before defining the size of the wall's opening, I observed how this opening size affects systems characteristics. The wall width proportion p in figure 3.21 (a) was varied from 0.3 to 0.7 with an interval of 0.1. Note that (i) I used the geometry of the previous quasistatic cavity resonator (4.9 m × 4.9 m × 2.3 m) for comparing the results with [20], and (ii) evaluations are based on simulations, which only consider copper-loss of the fundamental components, and does not consider losses that occur due to non-ideal setups (*e.g.*, contact resistance, resistance of the soldering, loss of capacitors, etc.).

The monitored figure of merit was the simulated Q-factors of each mode, which are presented in figure 3.21(b). The Q-factor of the PD mode was approximately constant, indicating that the QSCR operation can be extended to non-enclosed structures. On the other hand, the Q-factor drops for the PI mode with longer walls; however, the distribution of the magnetic field intensity of each mode (figure 3.22) also changes with varied p, which subsequently alters the coverage of where power transfer efficiency is high. Therefore, it is

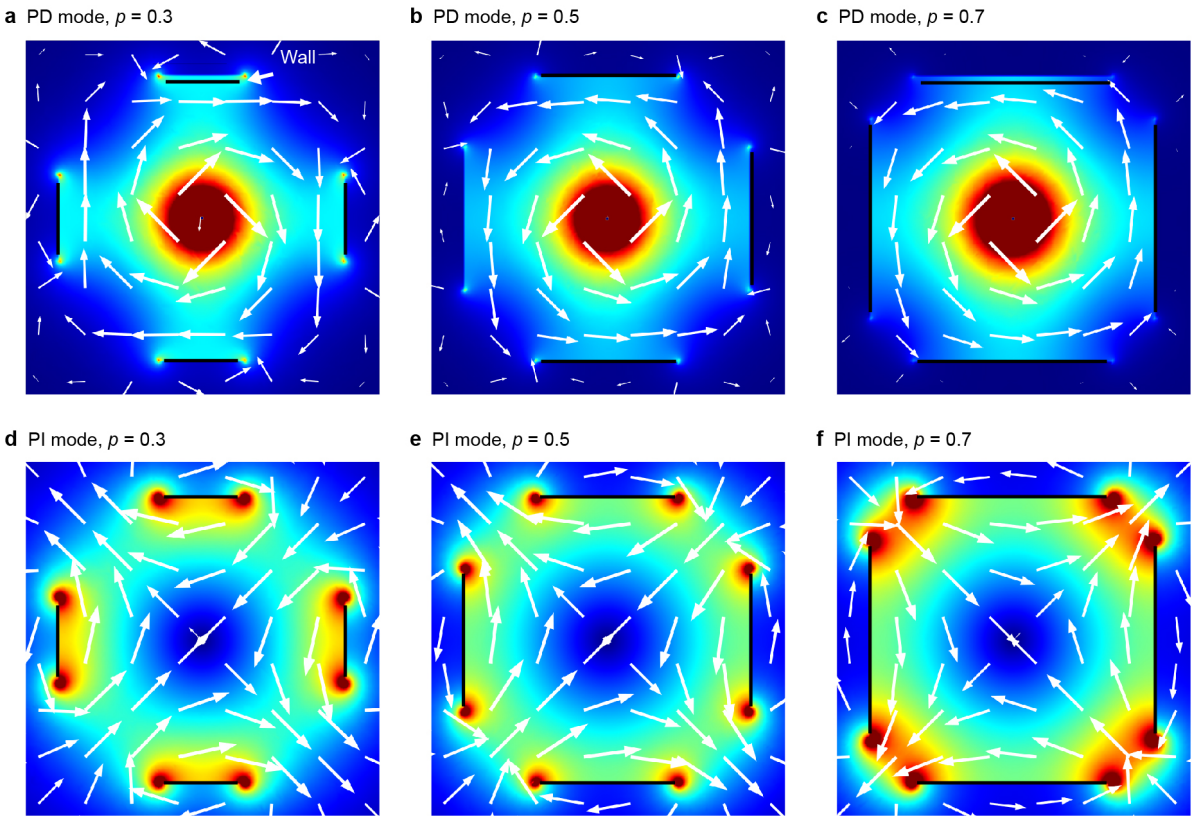

Figure 3.22 The magnetic field (top view) of each mode with different opening sizes. Refer to figure 3.21 (a) for the definition of wall width proportion p.

also necessary to consider the coverage in the selection of p. In both cases, the magnetic fields were approximately uniform in the z-direction.

G Power sources

In the initial experiments, I drove the room-scale wireless power systems using a 50 Ω linear power source. As many peripherals for measurements exist in 50 Ω systems, this setup is convenient for experiments. Meanwhile, as this system works in the MHz frequencies, many studies use switching power sources (*e.g.*, class-D amplifier, class-E amplifier) for enhancing the system efficiency. These sources typically have higher efficiency, leading to smaller power losses and removing the exaggerated cooling systems.

To this end, I operated the room-scale demonstrations (figure 3.14) using class-D amplifiers with two different setups shown in figure 3.23. Figure 3.23(a) shows the setup using lab equipment and off-the-shelf development boards. Figure 3.23(b) these functionalities

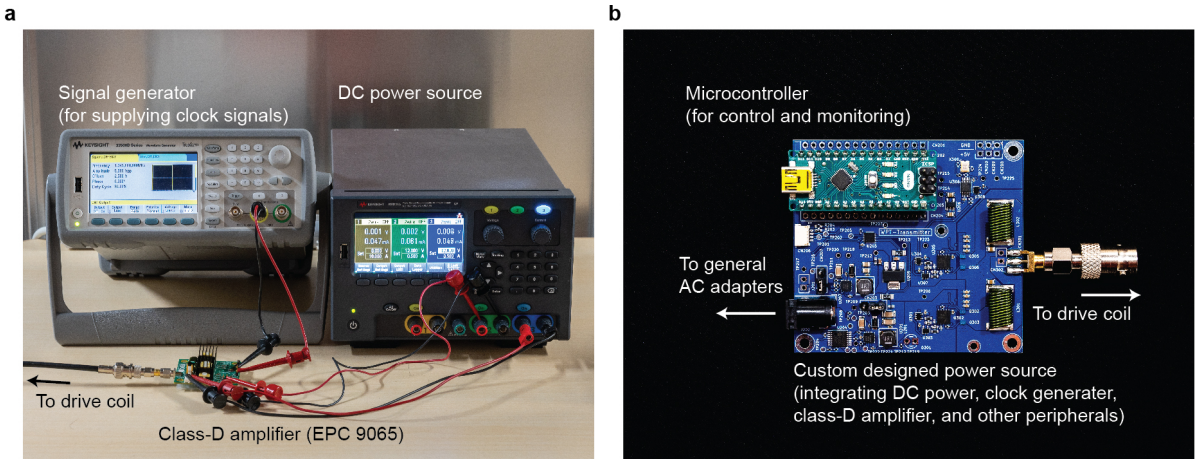

Figure 3.23 Power sources I used in the demonstrations. (a) A setup using off-the-shelf equipment. (b) The required elements integrated into a single printed circuit board (PCB).

integrated into a single printed circuit board (PCB) for exhibiting that the power sources can be minimized to below 100 mm.

H Interaction with foreign objects

Typical examples of foreign substances that could affect wireless powering systems could be classified into dielectrics, ferromagnetic, and conductors. Qualitatively thinking, dielectrics do not significantly interact with the magnetic field. Contrary, large ferromagnetics usually doesn't exist in the environment. Thus in this section, I discuss the undesired interaction between the room-scale wireless charging channel and foreign metallic objects present in the powering range.

As a fundamental premise, the QSCR-based systems studied in this chapter generates a quasistatic field distribution, not a far-field propagating wave. Therefore, interference in the form of multi-path, which typically affects microwave-based communication (*e.g.,* Wi-Fi, cellular, Bluetooth) do not occur in this system. The QSCR chamber operates in the deep sub-wavelength region. The ∼1 MHz carrier wavelength is approximately 300 m in free space, whereas the room's size is 3 m; this means the magnetic field distribution is effectively "static". The magnetic field does not beam from one point to another, nor is it pointed at the target. Instead, the current flows through the walls, floor, and ceiling. This current generates the field at all points within the cavity volume. Thus, if I place a metallic object in the QSCR room, the magnetic field will form around the object instead of penetrating it.

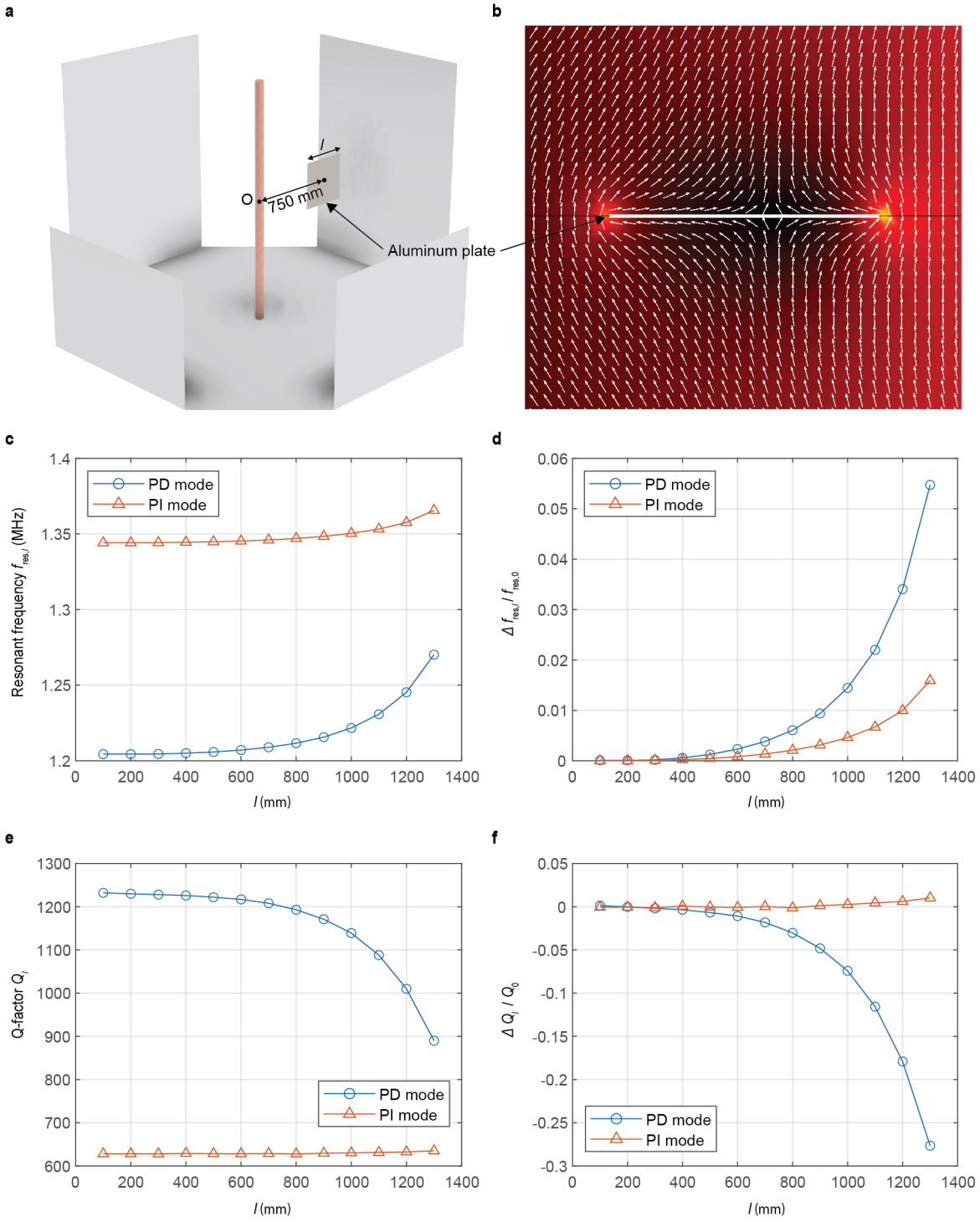

Figure 3.24 (a) Simulation setup for evaluating the effect of foreign metallic objects within the powering range. I placed an aluminum sheet with a side length l between the wall and the pole. (b) The magnetic field in the proximity of the aluminum plate (l = 400mm). (c-f) The performance change when the aluminum plate size is varied; (c) resonant frequency, (d) variation rate of resonant frequency, (e) quality factor, and (f) variation rate of quality factor.

To observe this effect, I evaluated the magnetic channel's characteristic when a metallic sheet is present within the channel. Figure 3.24 (a) shows the COMSOL simulation model of the QSCR room with an obstructive aluminum sheet placed halfway from the pole to the wall with the worst-orientation. I used a square aluminum sheet with a side length l and a thickness of 10 mm.

Figure 3.24 (b) shows the magnetic field occurring around the metallic sheet with sheet size $l = 40$ mm using the pole independent (PI) mode. This figure shows that the magnetic field generated by the QSCR room forms around the metallic sheet's boundary condition with the magnetic flux "flowing" around it. Figure 3.24 (c) shows the variation of resonant frequency $f_{\text{res},l}$ with increasing l and Figure 3.24 (d) shows the ratio of this variation of resonant frequency in a normalized form. Note that $f_{\text{res},0}$ is the resonant frequency when the aluminum sheet is not present. Generally, these graphs show an increase in resonance frequency with increasing l. We can qualitatively understand that the blocked magnetic field subsequently decreases the magnetic energy confined in the cavity and the effective inductance, leading to the increase in resonant frequency due to the relationship of equation 3.1. The frequency only shifts ~1% when a 1000 mm square aluminum sheet exists, which can be easily dealt via dynamic impedance tuning mechanisms [9].

Figure 3.24 (e) shows the variation of quality factor Q_l with increasing l and Figure 3.24 (f) shows the ratio of this variation of Q-factor in a normalized form. Note that Q_0 is the resonant frequency when the aluminum sheet is not present. These figures show that the quality factor significantly decreases in the pole dependent (PD) mode and slightly increases for the pole independent (PI) mode. The factors attributing to the decrease is the additional copper loss and the reduction in inductance. Meanwhile, the factor attributing to the increase in quality factor is the increased resonant frequency. The figures 3.24 (e,f) indicate that the dominant factors within these candidates differ, resulting in a non-uniform trend. As shown in equation 3.9, this variation in quality factor alters the power transfer efficiency.

Figure 3.25 (a–l) shows the magnetic field when I placed the obstructive aluminum sheet for attaining a visual understanding. These figures show the magnetic field distribution (top view) with arrows indicating direction and color showing the field strength's magnitude. Moreover, the overall magnetic field distribution, which directly correlates to power transfer, is generally unaffected by the aluminum sheet's presence. In contrast, the region in proximity of the sheet experiences a decay in field intensity. These distributions and figure 3.24(c-f) indicate that mobile-scale (<300 mm) devices hardly affect the systems' performance. As this obstructive grows to the size of a furniture (~1 m) and inhabit a significant portion of the space between the pole and the wall, it will begin to block the flux like a Faraday cage. This interference alters

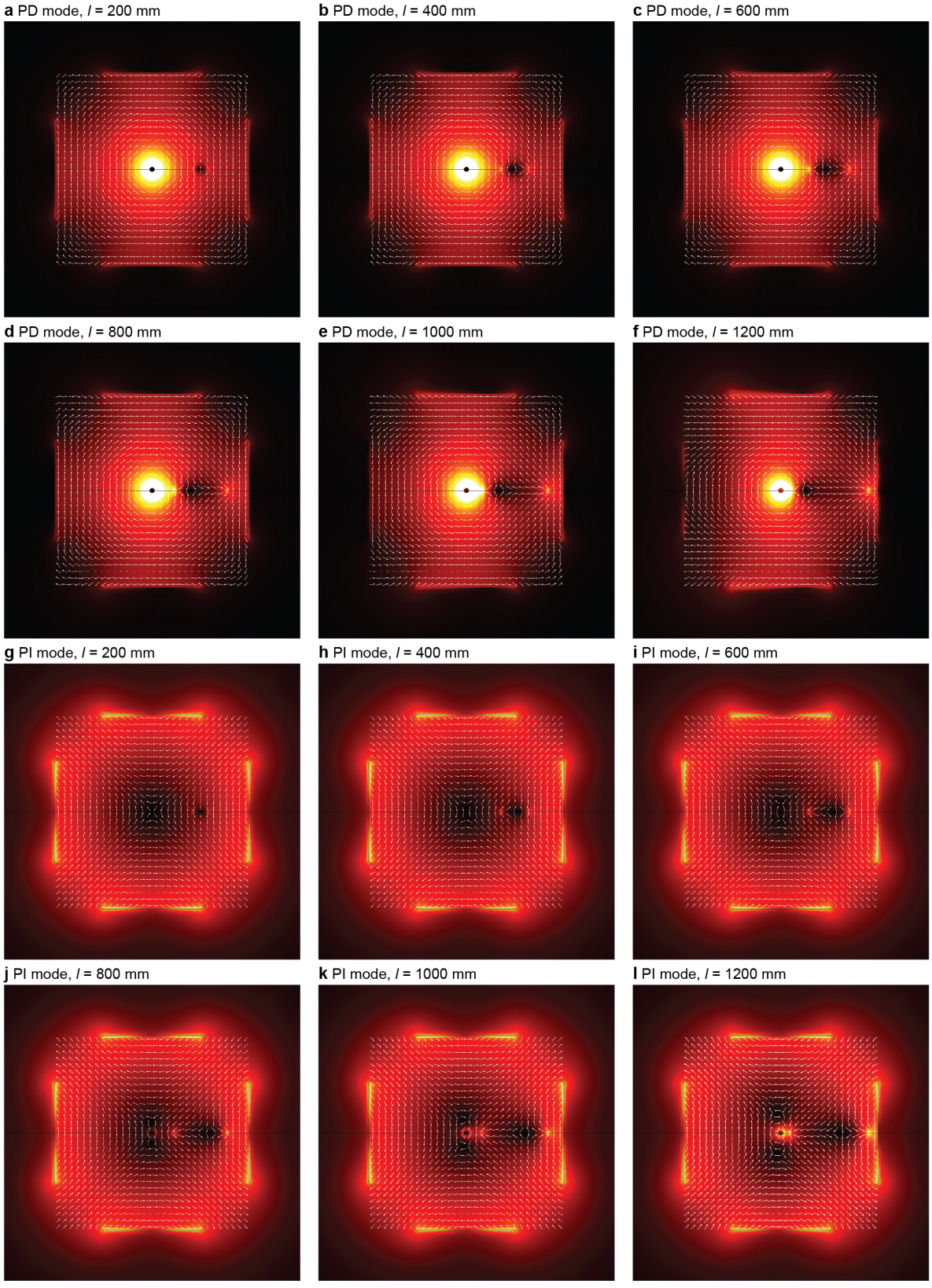

Figure 3.25 The top view of the simulated magnetic field with foreign aluminum sheets. The simulation model in figure 3.24. (PD: Pole dependent; PI: Pole independent)

the QSCR room's behavior, changing the resonant frequency, the Q-factor, and the magnetic field distribution in the sheet's proximity.

Chapter 4

Room-wide wireless power and communication via quasistatic cavity resonance

Current IoT systems suffer from a lack of access to energy sources, and this drawback will further expose as the devices increase along with the development of this technology. The concept of wireless power can overcome this problem and in fact, the advancement in semiconductor technology and microwave power delivery succeeded in deploying battery-less computation devices (*e.g.*, RFID) in public. However, the microwave power transfer, which these systems leverage, only supports micro-Watt order power delivery within a few meters in line-of-sight conditions [24, 54]. These are magnitudes below the desired power levels in most IoT nodes. Thus, these devices' functions are limited to returning fixed IDs or driving low-power microcontroller units (MCU) with primitive sensors in around a meter range.

Besides, QSCR technology has three vital benefits for driving indoor IoT systems using ubiquitously deployed nodes, which were not collectively available with former techniques: (i) the capability for transmitting several ten Watts of power to small footprint receivers, (ii) a room-scale powering range including out-of-sight areas, and (iii) the minimum interference with external objects and people. Thereby, this chapter demonstrates how we can empower IoT nodes using quasistatic cavity resonators (QSCR). Furthermore, I offer guidelines for designing hardware front-ends of power delivery and low-power communication that rides on the QSCR channel (figure 4.1 and figure 4.2).

This chapter cannot be publicized because a certain copyright holder's consent has not been obtained.

Please refer to the following paper for the contents of this chapter:

Takuya Sasatani, Chouchang Jack Yang, Matthew J. Chabalko, Yoshihiro Kawahara, and Alanson P. Sample, "Room-Wide Wireless Charging and Load-Modulation Communication via Quasistatic Cavity Resonance," PACM on Interactive, Mobile, Wearable and Ubiquitous Technologies (ACM IMWUT), Vol. 2, No. 4, Article No. 188, Dec. 2018.

Chapter 5

Wide-area wireless power delivery to pebble-sized devices via hierarchical resonators

Wireless power transfer via magnetic resonant coupling, which can safely deliver high power levels without interacting with daily objects, have been intensely explored for powering IoT devices operating in various environments [13, 59]. However, we still need strong coupling between the transmitter/receiver pair for efficient power delivery (*i.e.,* a large portion of magnetic flux generated by the transmitter has to flow through the receiver for efficient powering). This feature introduces the following requirements: (a) The transmitter/receiver pair is placed close and is well aligned, and (b) the transmitter/receiver pair has a similar form factor [60]. Recently presented technologies such as quasistatic cavity resonance (QSCR) demonstrated that we could mitigate this requirement in coupling by composing high quality-factor (*i.e.,* low loss) transmitters that generate nearly uniform fields within large-scale volumes [20, P3]. These approaches enabled efficient (over 50%) power delivery to mobile (∼100 mm) devices within room-scale volumes. However, when we scale down the devices to pebble-scale (∼10 mm) for ubiquitous deployment, the decreased coupling results in the rapid degradation of the power supply link (*i.e.,* below 1% efficiency).

Hypothetically, we can efficiently link pebble-scale devices with large-scale wireless power transfer systems by selectively focusing the magnetic field to where small devices are. However, in contrast to far-field studies in which beamforming approaches are established [61, 23], focusing the magnetic field in 3-D volumes is still an unsolved issue. Thus in this paper, I present wireless power transfer via hierarchical resonators that focuses the magnetic field to where the small devices operate by introducing intermediate relay modules. Theoretical

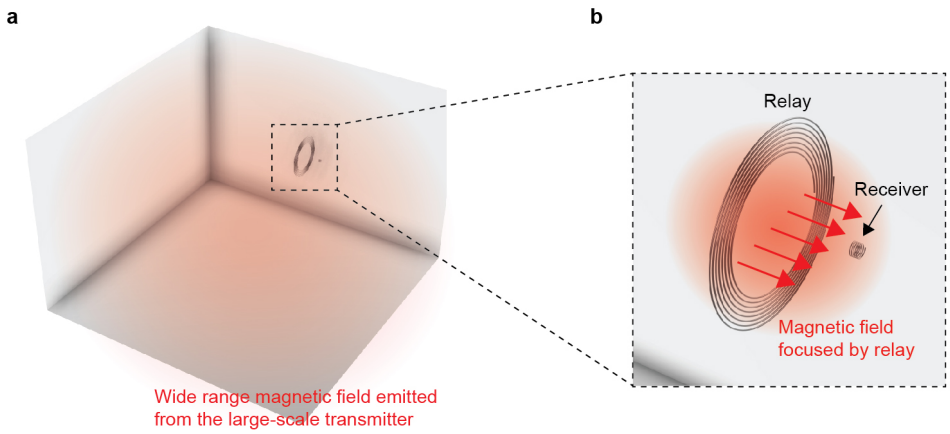

Figure 5.1 The concept of the proposed approach—wireless power transfer via hierarchical resonators—. (a) The overview of the entire system, in which the transmitter emits a wide-range magnetic field via the current flowing through the surrounding metallic wall/floor/ceiling [20, P3, P2]. (b) A magnified view of (a), which shows the magnetic field "focused" to where the small receivers are.

studies of coupled resonators present that coupled oscillators can passively pass down energy [49]. This effect is often used in wireless power transfer systems composed of homogeneous elements such as 2-D transmitter arrays (*i.e.,* a 2-D surface densely packed with transmitters) [62, 63, P10, 64]. Inspired by these studies, I leverage this phenomenon to bridge highly asymmetric elements that otherwise can not be efficiently connected. Our relay modules receive energy via the magnetic field emitted by the large-scale transmitter, which is composed of walls and floor made with conductive sheets, and re-emits it in the surroundings of itself (see figure 5.1 [20, P2, P3]). Because the relay module locally-generates the re-emitted field, it is narrowly focused nearby the module; thus, nearby small receivers gain access to the transmitter via this focused field.

While this approach requires a nearby relay module, it is much easier to deploy these low-cost, low-power, maintenance-free modules than to distribute active wireless chargers everywhere, requiring power supplies and expensive RF amplifiers. Because the large-scale transmitter generates the source magnetic field, this relay module (i) only consumes a small portion of power for state transition, (ii)does not need facilities for actively emitting magnetic fields, and (iii) can be used with general large-scale inductive transmitters. Because many small devices operate nearby mid-scale objects, where I can embed relay modules, there are many potential usage scenarios for this approach. For instance, by deploying pebble-sized sensors within industrial spaces (*e.g.,* vegetable cultivation factories [65], production lines, clean-rooms) and embedding relay modules within ubiquitous objects (*e.g.,* trays, tables,

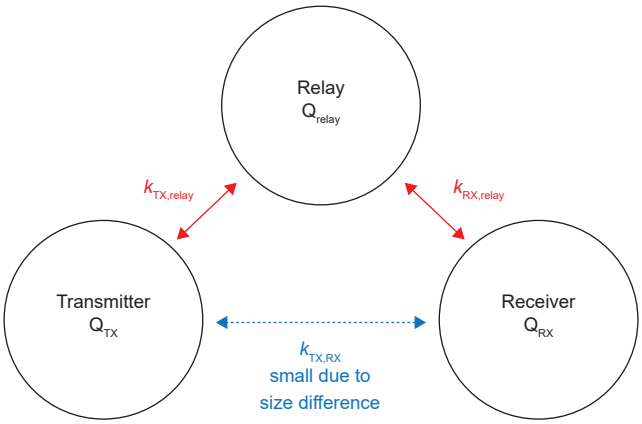

Figure 5.2 The relationship between the transmitter, relay, and receiver in the proposed approach. Q represents each component's quality factor, whereas k represents the coupling coefficient between components.

racks), we can precisely monitor local environmental parameters for efficient production at long-term.

To summarize, the contributions of this study are as follows:

- Proposal of wireless power transfer via hierarchical resonators, which efficiently bridges the gap between wide-area inductive systems and small (∼10 mm) sensor nodes.
- Theoretical analysis of the proposed hierarchical link.
- Design and prototype implementation of the receiver module and relay module.
- Performance evaluation with small receivers placed within air and water.
- Demonstration of power delivery in significantly asymmetric inductive systems.

5.1 The concept of hierarchical resonators

In this approach, I premise transmitters that satisfy the following requirement:

- The transmitter generates a nearly uniform magnetic field distribution in wide ranges compared to the receiver device dimension.
- The transmitter has a high quality factor.

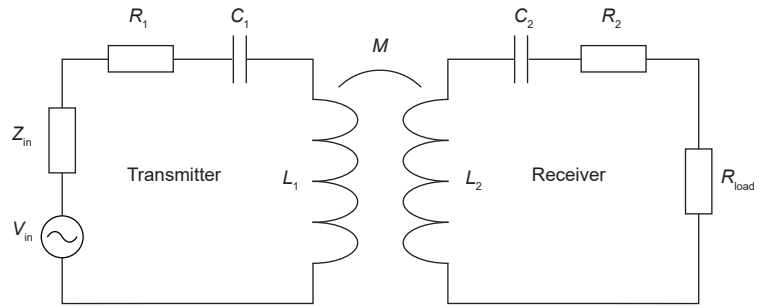

Figure 5.3 The circuit diagram of typical wireless power transfer via magnetic resonance coupling systems, composed by a pair of inductively coupled LC resonators. V_{in}, Z_{in}, R_{load} represent the source voltage, source impedance, and load. L, C, and R are the coil's inductance, the lumped capacitors' capacitance, and copper loss, respectively.

Applicable transmitters are useful for empowering receivers in the scale of mobile devices (∼100 mm), which can capture a sufficient amount of flux with itself's dimension. However, smaller "pebble-sized" receivers can not directly capture a sufficient amount of flux, which results in small coupling and low power transfer efficiency. Consequently, it is needed to enhance the flux near the receivers, or in other words, "focus" the field to where the receivers are. My approach uses a relay module in the proximity of receivers that capture the surrounding magnetic field and re-emits an oscillating magnetic field nearby itself. Because the magnetic field's source is the transmitter, a *passive* coil-based resonator can achieve the relay effect. Therefore this module only requires a small amount of power (which the system can also seamlessly supply from the transmitter via the wireless power transfer system) for turning ON/OFF the relay effect using switches. In the remainder of this section, I provide a theoretical backbone and a graphical representation of the proposed method to offer the basic understandings of the proposed method.

Theoretical background

While this relay module plays a similar role as "lenses", which focuses the propagating waves through the controlled boundary of diffraction index, this system works in the near-field domain; therefore, the underlying physics is different. Our analysis begins with the following expression of power transfer efficiency between coupled oscillators, which is often used to analyze wireless power transfer systems based on magnetic resonance coupling. In this section, I explain why hierarchical links (figure 5.2) can enhance power transfer efficiency by a mixture

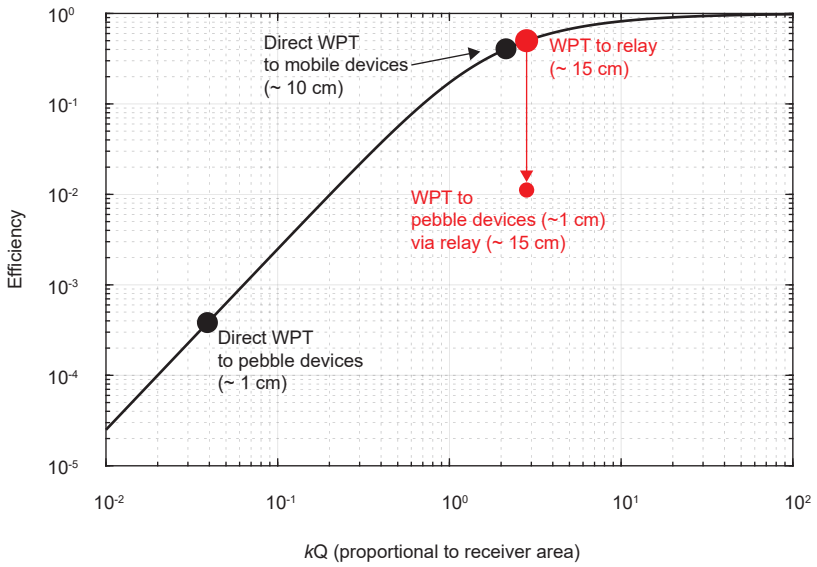

Figure 5.4 The relationship between the kQ-product $k_{1,2}\sqrt{Q_1 Q_2}$ and power transfer efficiency (see equation 5.3). This figure illustrates the operation point of each approach to offer an intuitive understanding of the proposed method and the challenge for efficiently powering pebble-sized sensors. The red arrow represents the loss that occurs in the power transfer between the relay to the receiver. (WPT: wireless power transfer.)

of circuit theory and coupling mode theory, which are both standard tools for analyzing relevant power transfer systems.

The two fundamental parameters that define the power transfer efficiency between two coupled resonators (*i.e.,* the transmitter and receiver) are the following: (i) The transmitter and receiver's quality factor (*i.e.,* ratio of the peak energy stored in the resonator in a cycle of oscillation to the energy lost per radian of the cycle), and (ii) coupling coefficient, which in this study is equivalent to the amount of flux generated by the transmitter that intersects with the receiver (see figure 5.1(a)). For reference, the quality factor of series LCR resonators (see figure 5.3) are known to be the follows:

$$Q_{LCR} = \frac{\omega_0 L}{R} \tag{5.1}$$

$$\omega_0 = \frac{1}{\sqrt{LC}} \tag{5.2}$$

L is the coil's inductance, C is capacitance, and R is series resistance (*i.e.*, copper loss). By using the quality factor of the transmitter and receiver, Q_1, Q_2, and the coupling coefficient between the resonator pair, $k_{1,2}$, the transmission efficiency of inductively coupled systems is

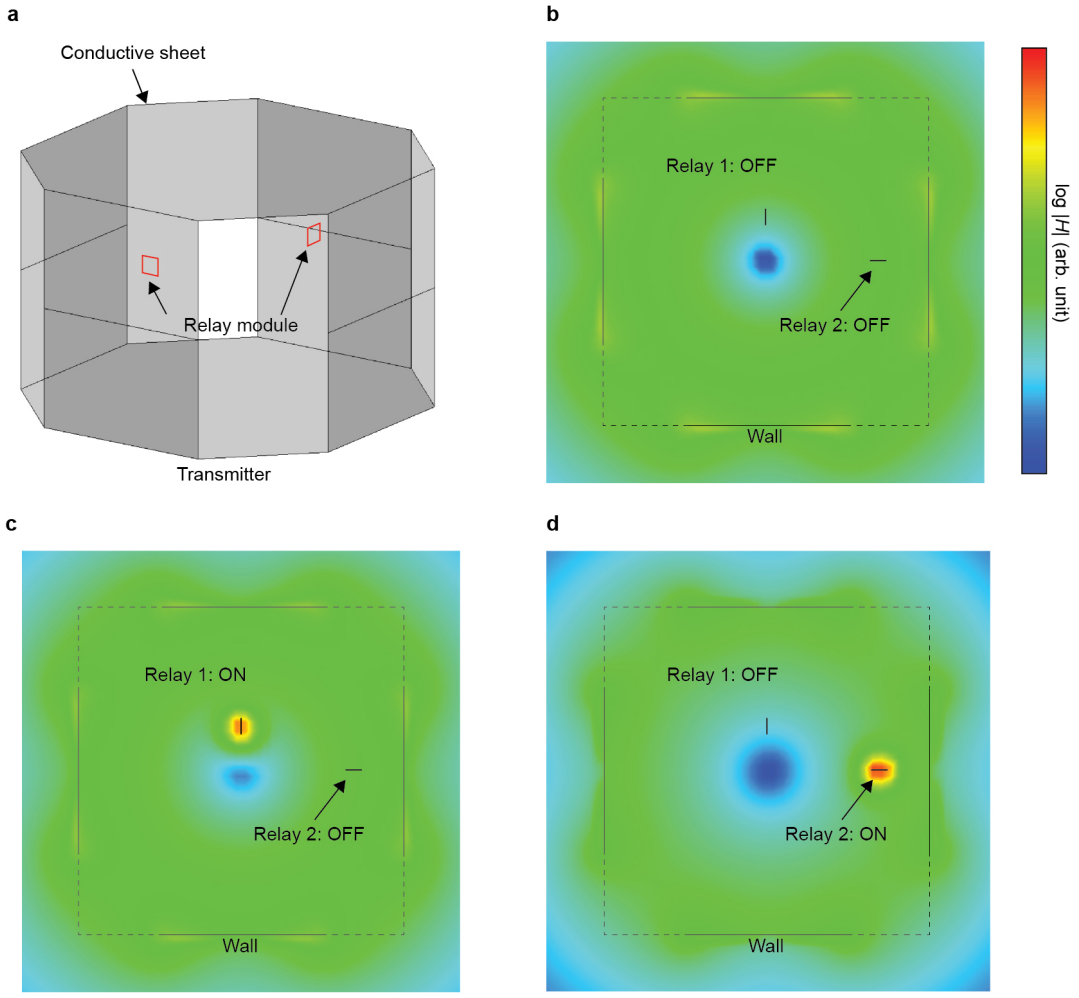

Figure 5.5 The magnetic field distribution with and without the relay module. The input power is consistent for all three plots. (a) shows the 3-D model of the transmitter used in this analysis, which is presented in chapter 3. As described in chapter 3, conductive sheets, which accommodate the oscillating current, are placed in the surrounding of the powered volume. I inserted lumped capacitors within these sheets to enable an operation resembling a coil resonator (*i.e.*, magnetic field is exposed and the electric field is confined in the lumped capacitors). This transmitter generates a magnetic field parallel to the floor. (b-d) shows the top view of the magnetic field distribution. (b) is the original magnetic field distribution, which is strong near the walls of the room and decays as it approaches the center (refer to the PI mode of [P3] for the detailed distribution.) (c) and (d) shows the field when I turned ON each relay coil. We can see that the relay modules successfully amplify the magnetic field in the proximity of itself.

known to be as follows:

$$\eta_{\max} = \frac{k_{1,2}^2 Q_1 Q_2}{\left(1 + \sqrt{1 + k_{1,2}^2 Q_1 Q_2}\right)^2} \tag{5.3}$$

Note that this $\eta_{\max}$ is the maximum efficiency obtainable from this resonator pair under optimum loading conditions. This system does not obtain this *exact* maximum value; therefore, I will proceed with this discussion by treating this equation as a trend, while it is not a rigorous solution.

Equation 5.3 shows that $k_{1,2}\sqrt{Q_1 Q_2}$ is the figure of merit (FOM) for transfer efficiency. Based on methods developed in prior work, the coupling coefficient, $k_{1,2}$, can be expressed as follows, using the total peak magnetic field within the volume, α, and the flux penetrating the dimension of the receiver, β [39]:

$$k_{1,2} = \frac{\beta}{\sqrt{2L_2\alpha}} \tag{5.4}$$

$$\beta = \iint_A \left(\mu_0 \vec{H}_1 \cdot \vec{n}\right) \mathrm{d}A_2 \tag{5.5}$$

$$\alpha = \iiint_V \left(\mu_0 \frac{|\vec{H}_1|^2}{2}\right) \mathrm{d}V \tag{5.6}$$

$\vec{H}_1$, L_2, μ_0, V, and A_2 represent the magnetic field generated by the transmitter, the inductance of coil receiver, the permeability of vacuum, the total volume, and the area enclosed by the coil receiver, respectively. In highly asymmetric systems (*i.e.,* the transmitter is much larger than the receiver), we can treat the magnetic flux penetrating the receiver to be uniform; under this condition, $k_{1,2}$, β, and the face vector of the area enclosed by the receiver $\vec{A}_2$ satisfy the following relationship.

$$k_{1,2} \propto \beta \propto \vec{H}_1 \cdot \vec{A}_2 = H_1 A_2 \cos\theta_2 \tag{5.7}$$

θ_2 is the angular misalignment between the face vector of the receiver $\vec{A}_2$ and the local magnetic flux $\vec{H}_1$. From equation 5.7, $k_{1,2}$ is proportional to the field intensity and the area enclosed by the receiver coil.

The relationship of efficiency and the kQ-product $k_{1,2}\sqrt{Q_1 Q_2}$ is plotted in figure 5.4(b). This figure shows that while in the high kQ (over 1) domain, efficiency slowly decays with decreasing kQ, a rapid decay occurs in the smaller kQ (below 1) part. This curve also

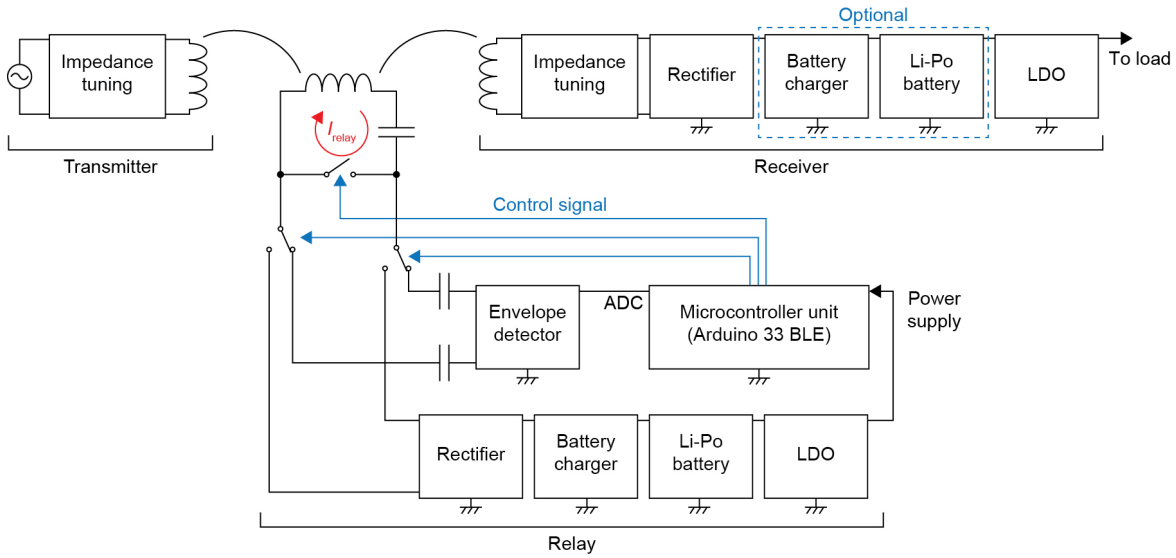

Figure 5.6 The system diagram of the transmitter-relay-receiver link.

indicates that although prior work [20, P2, P3] achieved power transfer with around 50% efficiency using mobile (∼100 mm) receivers, the efficiency will significantly drop with smaller receivers (∼10 mm). Our proposed method's fundamental idea is to ride on the channel composed between the large-scale transmitter and mid-scale relay module; thereby, cushion the size difference between the transmitter and receiver. We can qualitatively understand this idea as riding on the mid-efficiency zone (around $1 \leq kQ \leq 5$) of the "kQ vs. efficiency plot" twice, instead of attempting direct power transfer on the extremely low-efficiency region ($k \ll 1$) of the curve. I plotted a conceptual trace of this procedure in figure 5.4 as "wireless power transfer (WPT) to pebble devices via relay", whereas the red arrow expresses the loss occurring from the power transfer between the relay and receiver. This analysis omits the coupling between the transmitter and receiver, which is reasonable for the considered scale difference. However, I note that this omitting would be invalid for significantly larger receivers.

5.2 Visualization of focused field

This section offers an intuitive understanding of the proposed method by visualizing the modified magnetic field using the hierarchical approach. For the visualization software, I used Hyperworks FEKO, an electromagnetic field solver based on the method of moments (MoM). Figure 5.5(a) shows the 3-D model of the room-scale transmitter, built based on the theory developed in [P3]. Although this resonator can generate two sets of magnetic fields, I solely

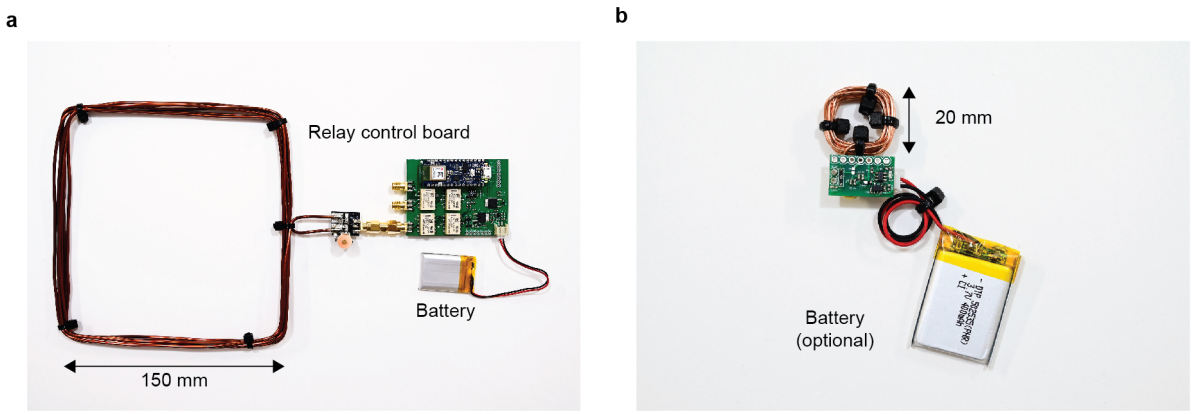

Figure 5.7 The developed (a) relay module and (b) receiver module.

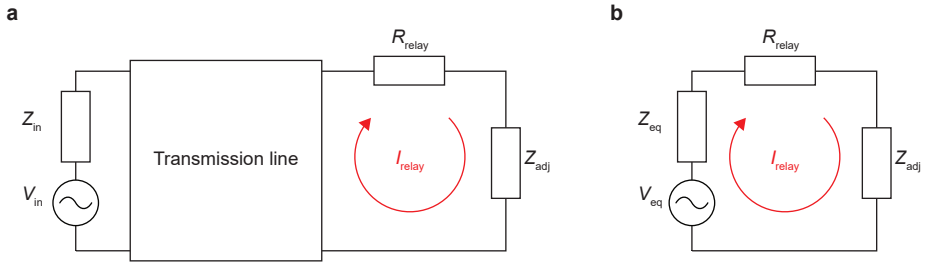

Figure 5.8 The circuit model for determining the Z_{adj} value. Any circuit in the form of (a) can be transformed into (b), using Thevenin's theorem. V_{in}, Z_{in}, and R_{relay} are source voltage, source impedance, and the copper loss of the relay. Z_{adj} shows the impedance value controllable from the relay module.

used the PI mode (resonant frequency: 1.35 MHz) throughout this study. I can see that the original field distribution is more intense near the room walls, and it monotonically decays as it reaches the center of the structure. Also, as described in [P3], the generated magnetic field is parallel to the floor. Note that although I use this transmitter for demonstration, this approach is not specific to this structure.

Figure 5.5(b) shows the magnetic field when both relays are OFF. This distribution corresponds to the magnetic field initially generated and shows a nearly uniform distribution. Figure 5.5(c) and d show the field patterns when relay 1 and relay 2 are ON, respectively. When the relay module is active, it gathers energy from ambient fields and re-emits it in the proximity of itself. The input power of all three plots in figure 5.5(b-d) are the same. Furthermore, when an active relay module exists within the room, the original field's field intensity decreases. This decrease shows that the relay is absorbing the energy from the room via ambient fields.

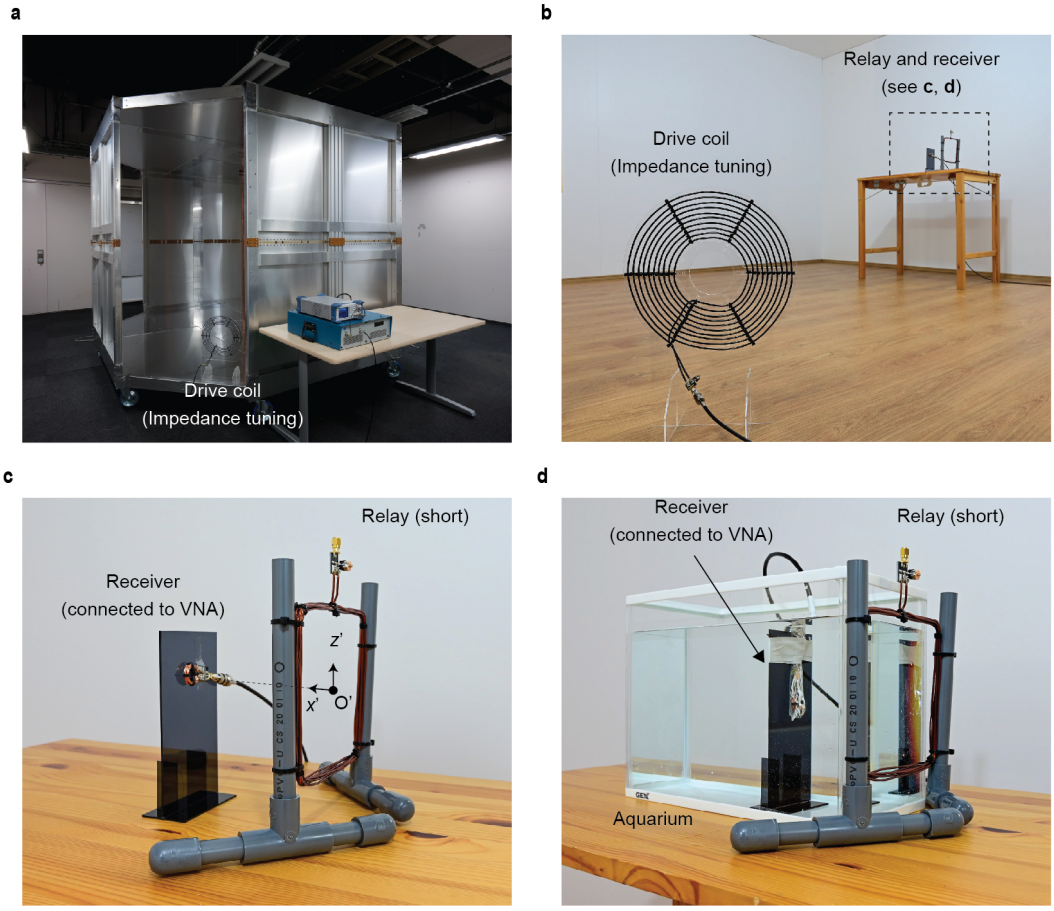

Figure 5.9 The measurement setup. (a) The room-scale transmitter used for measurements and demonstration (chapter 3). The metal sheets surrounding the volume accommodate an oscillating current in resonant conditions and generate a three-dimensional magnetic field within the cavity. Power is input via the drive coil, which works as an impedance tuning network that mediates the power source and the room-scale transmitter. The presented method is independent of the transmitter itself. (b) The inner view of the transmitter. Note that I furnished the cavity to hide the metal sheets behind the wall/floor/ceiling. (c,d) Zoom view of (b), which shows the setup of the relay and receiver when the receiver is (c) in air and (d) in water. I defined relative coordinates based on the relay position for measurements, as shown in (c). I omitted the y'-axis because it is 0 throughout the study.

5.3 System design and implementation

Next, I proceed to the system design that achieves the basic principles presented in the previous sections. Figure 5.6 shows the functional diagram of the most simple implementation. The main operation procedure for power delivery is the follows:

1. A power input (sine wave) matching the wide-range transmitter's resonant frequency is input.
2. The wide-range transmitter oscillates and generates a widely distributed magnetic field.
3. The relay module receives energy via the ambient oscillating magnetic field
4. The relay module re-emits the magnetic field in the proximity of itself.
5. The pebble-sized devices equipped with receivers receive energy through this focused magnetic field.

This approach is compliant with any wide-range inductive transmitters fulfilling the requirements presented in section 5.1. Therefore the design of the transmitter itself is out of the scope of this chapter. For the evaluation and demonstration later in this chapter, I will use the 3 m $\times$ 3 m $\times$ 2 m room-scale resonator developed in chapter 3.

Relay module

Figure 5.6(a) shows the developed relay module. It consists of a microcontroller unit (MCU) with integrated BLE SoC (Arduino nano 33 BLE), an active envelope detector, a power harvester, mechanical latched relays, a Li-Po battery, and a 150 mm, 6-turn square coil fabricated with ϕ2 mm copper wire. The peak detector can detect the external magnetic field's amplitudes and the ADC (in the MCU) reads out this value. Based on this read-out value, the MCU controls the mechanical relays' states to choose whether the relay effect is activated. Because this module equips a BLE SoC, they can cooperate with other relay modules when multiple relay modules exist (see section 5.7). I also note that this module needs power only when transiting between the states because I used latched (bi-stable) mechanical relays. This relay module equips a battery for running the minimum active operations, which can also be charged by the wireless power transfer system. Thus, this module can operate without manual maintenance. The power harvester that takes care of charging the relay module consists of a full-bridge rectifier, an LDO, and a battery charger.

Table 5.1 Circuit parameters used in measurements

Q_{TX}	Q_{relay}	L_{relay}	Q_{RX}	L_{RX}	$C_{RX,P}$	$C_{RX,S}$
540	202	13.6 µH	53	1.8 µH	7.2 nF	570 pF

Although this relay coil can adopt complex control schemes, I maximize the re-emitted magnetic field's amplitude in unloaded conditions in this chapter. Figure 5.8 shows a simplified circuit model of the system, and the controllable parameter within this circuit model is impedance Z_{adj}. Note that if the receiver consumes power (*e.g.,* charges itself.), this impedance Z_{adj} expresses the received energy. Because the magnetic field in proximity of the receiver will increase with current I_{relay}, I simply maximize this current, whereas I_{relay} in unloaded conditions can be expressed as follows:

$$I_{ryelay,unloaded} = \frac{V_{eq}}{R_{relay} + Z_{eq} + Z_{adj}} \tag{5.8}$$

Assuming Z_{eq} is real as typical resonators under resonant conditions are, it is obvious that minimizing Z_{adj} will maximize the current, therefore I defined Z_{adj} as a short circuit. Alternative designs of the relay module is also presented in section 5.7.

Receiver module

Figure 5.6(c) shows the implemented receiver module. The module consists of a 20 mm, 10-turn receiver coil fabricated with ϕ1 mm copper wire, an impedance tuning circuit, and a power receiver. The received energy can be either used for charging an appended battery or directly powering sensor devices. The battery charger and the battery are optional. Therefore, battery-less applications can exclude these components. I built the impedance tuning circuit using lumped capacitors, and I explain the details of this tuning in section 5.4. The power harvester consists of a full-bridge rectifier, a linear battery charger, and an LDO for 3.3 V output for driving connected devices. The module does not include any fundamentally large components. Therefore, I can miniaturize the module size to the coil's footprint through additional engineering effort (see section 5.7).

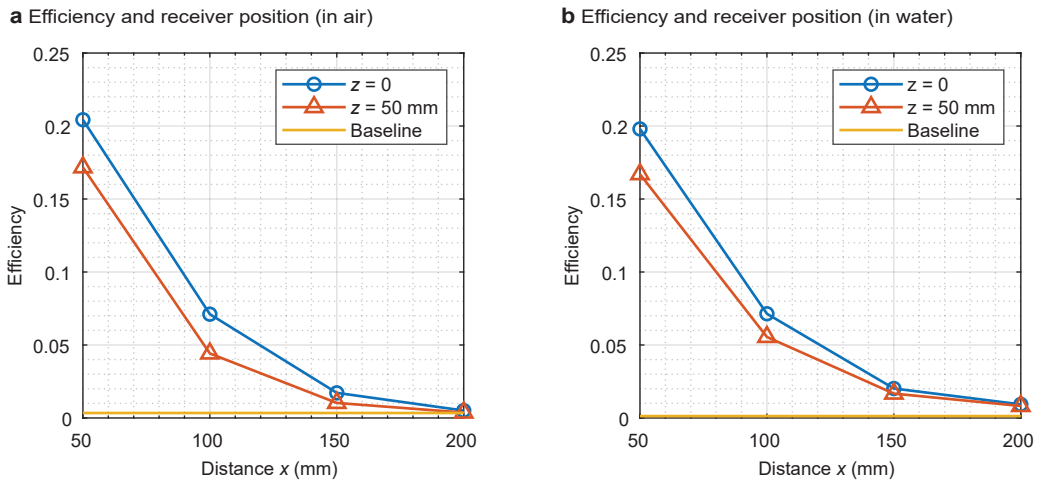

Figure 5.10 The measured power transfer efficiency when the position of the receiver is varied. The baseline in each plot refers to the efficiency when the relay module is not present. (a) Efficiency plot when I moved the receiver in the air. (b) Efficiency plot when I moved the receiver in water.

5.4 Evaluation of power transfer efficinecy

In this section, I first conduct a set of measurements. Then I demonstrate the battery-less operation of a microcontroller board and wireless charging of a Li-Po battery, using the modules developed in section 5.3. In this evaluation, I conducted two types of measurements: (i) two-port measurements and (ii) DC-to-DC measurements. Two-port measurement evaluates the pure characteristics of the transmission line, or in other words, the performance in AC-to-AC. I conducted this series of measurements using a vector network analyzer (VNA). In addition to two-port measurements, which gives a fundamental understanding of the channel, I conducted DC-to-DC measurements. DC-to-DC measurement reveals the presented approach's end-to-end performance, including the loss of the power amplifiers and rectifiers. I note that the optimization of power conversion circuits is out of this chapter's scope; thus, I built conversion circuits with off-the-shelf components.

This approach can be developed on general wide-range inductive transmitters fulfilling the requirements presented in section 5.1. As for this study, I conducted the evaluations using a 3 m × 3 m × 2 m room-scale transmitter, developed in chapter 3 (see figure 5.9(a,b)). Although the referred room-scale transmitter possesses two resonant modes, I solely used the PI mode with the resonant frequency of 1.35 MHz. I input power to the room-scale transmitter through a drive coil, which I can treat as an impedance tuning network [20, P2, P3]. When I input

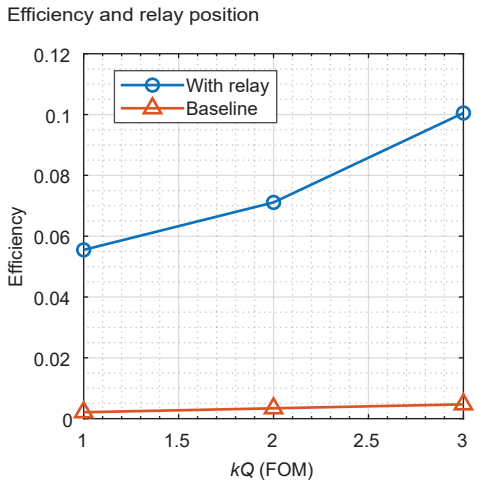

Figure 5.11 Efficiency plot when I moved the relay. kQ refers to the kQ-product between the relay and the transmitter, which denotes the relay position in this study. The baseline in each plot refers to the efficiency when the relay module is not present.

a tone corresponding to the resonant frequency of the room-scale transmitter, the transmitter generates a magnetic field that permeates the room volume (figure 5.5(b)).

The placements of the relay and receiver module in the system affect these evaluations' results; however, defining position based on the raw coordinate will give a solution specific to the transmitter. To explore the fundamental characteristics of this approach, I denoted the position of the relay module using the kQ-product between the transmitter and relay, $k_{\mathrm{TX,relay}}\sqrt{Q_{\mathrm{TX}}Q_{\mathrm{relay}}}$. Note that in near-field systems, the coupling coefficient represents the interaction between the two components. Meanwhile, quality factors are position-independent; therefore, it is reasonable to use the kQ-factor as the relay position in this analysis. As for the receiver position, I used the relative coordinates based on the relay's placement because I omitted the direct coupling between the transmitter and receiver, as discussed in section 5.1. Figure 5.9(c) shows this relative coordinate (x', y', z').

As for the relay coil, I used a 150 mm, 6 turn coil, which follows the receivers used in prior work [20, P3]. Through these studies, I can see that the kQ-product between this size coil and the transmitter is over 3 (*i.e.,* efficiency is over ~50%) in most positions with perfect angular alignment. Because the kQ-product degrades as the angle gets misaligned, I consider $1 \leq k_{\mathrm{TX,relay}}\sqrt{Q_{\mathrm{TX}}Q_{\mathrm{relay}}} \leq 3$ as a typical range of relay placement. Table 5.1 shows the Q-factors and inductance of the used transmitter, relay, and receiver. I tuned the resonant frequencies of these modules to 1.35 MHz, corresponding to the room-scale transmitter.

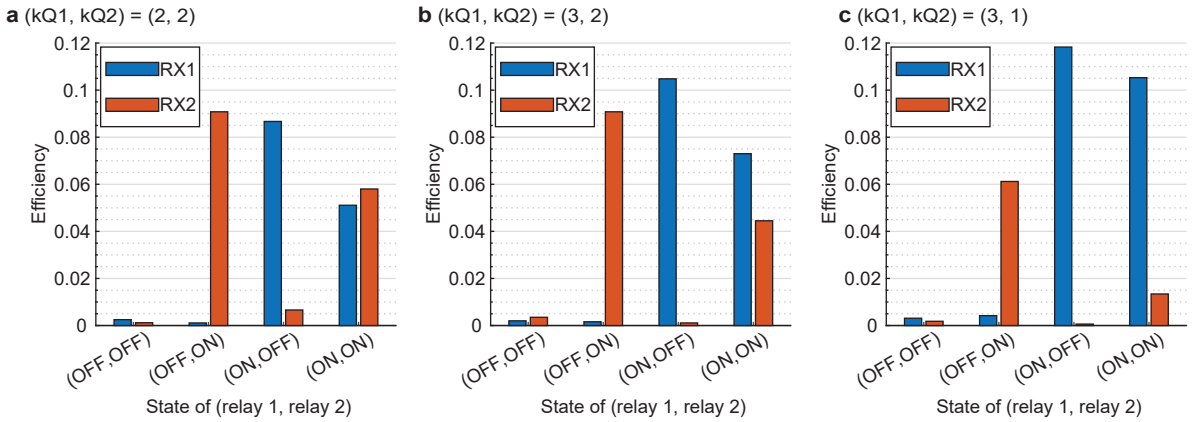

Figure 5.12 The power transfer efficiency $\eta_{\max}$ when multiple relay-receiver pairs exist in the large scale transmitter's operating range. $kQi(i = 1, 2)$ refers to the kQ-product between the i-th relay and the transmitter. I conducted the measurement for each ON/OFF state of the relays.

Note that I omitted the transmitter's inductance because it can not be defined using typical expressions of inductance [P3].

Two-port measurements (AC-to-AC)

I measured the power transfer efficiency to investigate the effect of critical design parameters. Methods A present the detailed methods for extracting efficiency.

RX position, embedded medium, and transfer efficiency $\eta_{\max}$

Figure 5.10(a,b) shows the measured power transfer efficiency when the receiver position is varied from 50 mm to 200 mm. These two plots showed the measurement results when I placed the receiver (a) in free-space or (b) in still-water. Each plot shows results with 0 or 50 mm misalignment in the z-axis direction. The baseline shows the efficiency when there are no relay modules. Therefore, it corresponds to the efficiency of direct power transfer from the transmitter to the receiver. In this baseline measurement, barely any change in efficiency was observed with position variations in the range of $0 \leq x \leq 200$ mm; thus, the baseline efficiency shows the efficiency when I placed the receiver on $(x', y', z') = (0, 0, 0)$. From these two plots, we can find the following:

- The transfer efficiency significantly improves when I use the relay module.
- The hierarchical link can send the same degree of power to devices placed in water.

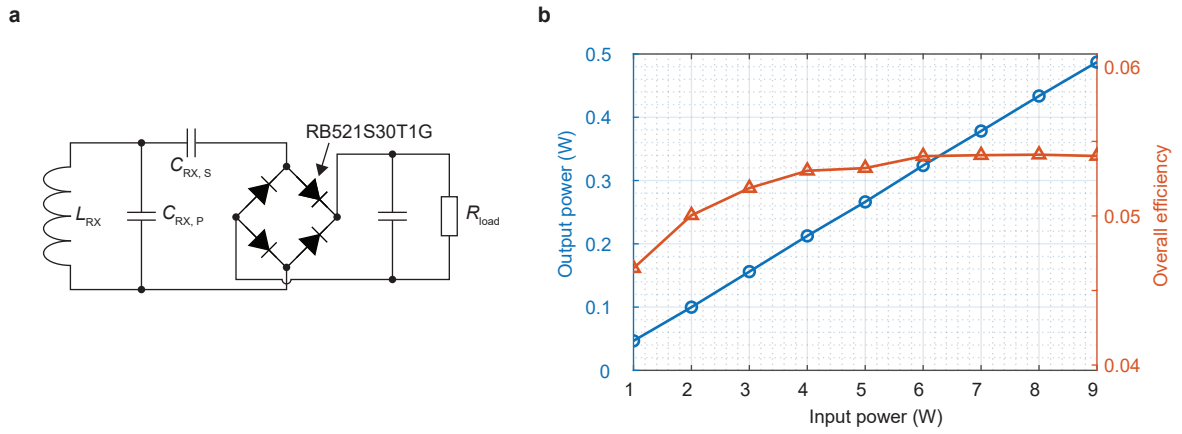

Figure 5.13 Measurements of DC-to-DC power transfer. (a) The receiver circuit used for measurements. Table 5.1 shows the circuit parameters. (b) The output power and DC-to-DC efficiency when the input power is varied.

- 50 mm misalignment (z-axis direction) introduces a small efficiency loss.
- The efficiency exponentially decays with increasing distance from the relay.

Relay position and transfer efficiency $\eta_{\max}$

Figure 5.11 shows the measured power transfer efficiency when the relay position (*i.e.*, kQ-product between the transmitter and relay) is varied within the range of $1 \leq k_{\mathrm{TX,relay}}\sqrt{Q_{\mathrm{TX}}Q_{\mathrm{relay}}} \leq 3$. The positions of the receivers were fixed to $(x', y', z') = (100, 0, 0)$ mm in these measurements. The baseline plot corresponds to the power transfer efficiency with no relay; I fixed the receivers at $(x', y', z') = (100, 0, 0)$ mm in these measurements too. These figures show that the baseline's efficiency also increases with increasing kQ-product; this is because the transmitter field intensity and higher kQ-product here positively correlate. From this plot, I can find the following:

- The transfer efficiency significantly increases in every position by using this approach.
- The transfer efficiency increases with the increased kQ-product between the transmitter and relay.
- The rise of transfer efficiency is steeper with the relay introduced.

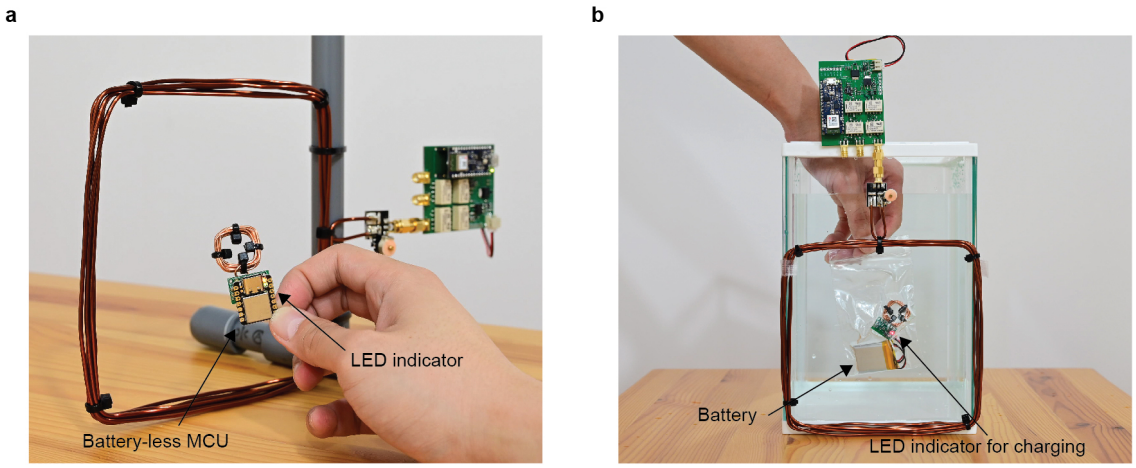

Figure 5.14 Demonstration of DC-to-DC power transfer. (a) Power delivery to a battery-less computation device. (b) Power delivery to a wireless battery charger (1 cell, 50 mA). Note that (a,b) uses the modules I developed in section 5.3.

Multiple relays and transfer efficiency $\eta_{\max}$

Next, I evaluated the efficiency when multiple sets of a relay and a receiver exist within the transmitter's powering range. The results of these measurements are shown in figure 5.12, whereas $kQ1$ and $kQ2$ represent the $k_{\mathrm{TX,relay}}\sqrt{Q_{\mathrm{TX}}Q_{\mathrm{relay}}}$ value between the transmitter and each relay. I selected the kQ value pairs for observing the interference between (a) relays with the same degree of coupling with the transmitter, (b) relays with the small difference of coupling with the transmitter, and (c) relays with a large difference of coupling with the transmitter. I measured the S-parameter between the transmitter and the receiver, with the other receiver terminated with a 50 Ω RF load. These figures indicate the following:

- The transfer efficiency degrades when both relays are ON, compared to the configuration where the relay associated with the measured receiver is solely ON.
- As the coupling difference between the transmitter and each relay becomes large, this trend accelerates. The receiver associated with the small kQ relay receives significantly small power when both relays are ON.

In addition to these confirmed trends, these results suggest that we can enhance the total power transfer efficiency (*i.e.,* proportion of total delivered power within input power) by activating multiple relays and powering multiple receivers at once. I will discuss this topic in section 5.7.

End-to-end measurement (DC-to-DC)

Next, I proceed to the measurement of end-to-end power transfer efficiency. This efficiency refers to the proportion of power delivered to the 100 Ω DC load connected to the receiver within the power input from the DC power source. The relay was placed so the $k_{\mathrm{TX,relay}}\sqrt{Q_{\mathrm{TX}}Q_{\mathrm{relay}}}$ is 2, whereas the positions of the receivers were fixed to $(x', y', z') = (100, 0, 0)$ mm. I built a matching circuit to maximize transfer efficiency under these conditions, which resulted in a network shown in figure 5.13(a). Table 5.1 provides the circuit parameters in this network. For the transmitter side, I used a DC power source (Keysight E36312A) for inputting power to a high-frequency ZVS (zero voltage switching) class-D power amplifier development board (EPC9065). The output of this amplifier was input to the room-scale transmitter via the drive coil. I note that I treated the DC input of the amplifier as the system's DC power input. I omitted the clock source's power consumption and the logic power supply because these are not essential for evaluating the system performance. As for received power, I measured the power supplied to R_{load} in figure 5.13(a) using a digital multimeter (Keysight 34410A). Figure 5.13(b) presents the measured output power and end-to-end efficiency with varied input power. The power transfer efficiency was around 5% and power levels up to approximately 500 mW, which can afford driving a broad range of sophisticated devices. This figure also shows degradation in efficiency from AC-to-AC efficiency (around 8%). However, this loss is in a reasonable range, considering the loss of the power amplifier and rectifier. Different from 50 Ω systems, it is challenging to isolate each stage's loss in DC-to-DC evaluation; thus, I will not investigate this topic in-depth.

5.5 Demonstration of wirelessly powering pebble-sized devices

Finally, I demonstrate power delivery to a (a) pebble-sized battery-less device and a (b) pebble-sized battery charger. Figure 5.14(a) shows a pebble-sized battery-less device and figure 5.14(b) shows a 50 mA battery charger, both driven through the developed modules (see figure 5.7). One large benefit of pulling up these power transfer systems' power levels is that we can use non-power optimized devices (*i.e.,* Arduino, Raspberry Pi, sensor sub-modules.) for prototyping. This advancement enables us to use low-cost and easy prototyping tools to develop and test applications where we can not manually charge devices frequently.

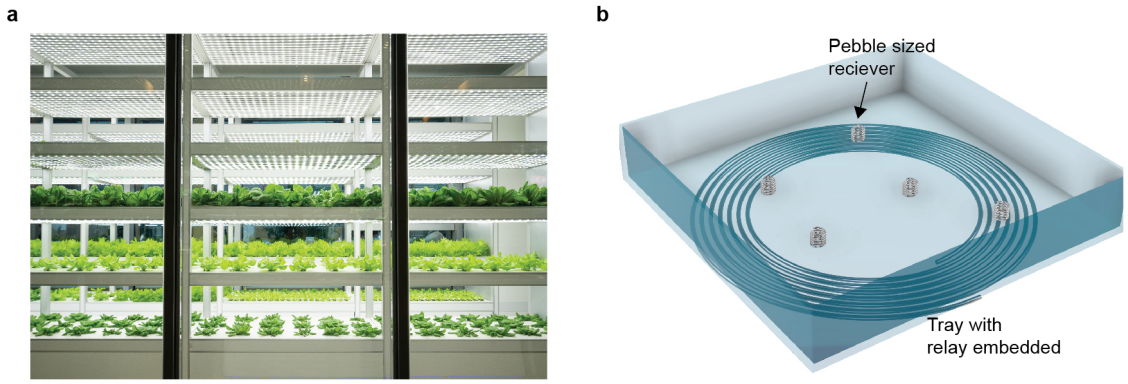

Figure 5.15 (a) A photo of a vegetable cultivation factory, which I envision as a motivating application. (b) A sketch of a relay module embedded within a tray, which manages the seedlings. By introducing a wide-range wireless powering system in the factory room and using these modified trays, power gets efficiently delivered to embedded small devices within the system's range.

5.6 Potential applications

We have acknowledged the need for untethering small-sized devices for a long time. However, previous attempts usually fall into approaches that drive these devices in a strictly limed area [66, 67, 17]. This approach needs to place or embed a relay module nearby. However, it is much easier to integrate these stand-alone, maintenance-free relay modules than deploy wireless charging facilities requiring wires and power amplifiers. Besides, we place many small devices nearby larger objects, where we can embed these modules. For instance, one of my motivating applications is powering sensor devices deployed in vegetable cultivation factories (see figure 5.15(a)), which manage seedlings in units of trays [65]. Cultivation under controlled factory environments has a promise for efficiently and stably producing vegetables. However, the challenge in finding optimal environmental parameters for cultivating each vegetable is limiting the advancement of this emerging agriculture. A sophisticated, continuous, and non-destructive sensing system that monitors numerous local environments is highly desired in this technical field. However, the power supply issue exists as a bottleneck. By leveraging the tray to embed these relay modules, we can develop high-spec and non-destructive sensing systems without batteries' strict limitations (see figure 5.15(b)). Furthermore, we can deploy useful sensing devices, such as cameras, formerly non-affordable due to the limited power capacity.

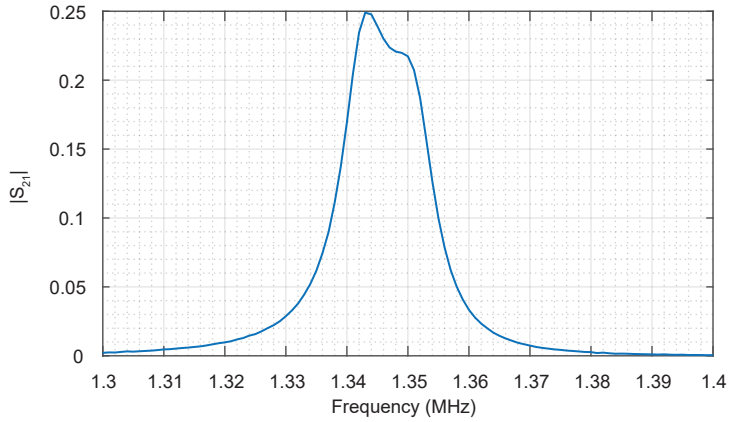

Figure 5.16 Frequency plot of forward voltage gain $|S_{21}|$ from the transmitter input to the pebble-sized receiver. I executed this measurement using the matching circuit shown in figure 5.13(a); therefore, it was not strictly impedance matched with 50 Ω.

5.7 Discussion

Communication via the hierarchical link

Wireless communication on the developed inductive link will enable communication robust to ambient lossy dielectric mediums (*i.e.,* where electromagnetic waves can not efficiently propagate). These domains include water, soil, and biological tissue. Therefore, extending the studied approach to data communication should benefit sensor devices operating in such inaccessible environments.

Figure 5.16 shows The frequency plot of forward voltage gain $|S_{21}|$, revealing over 10 kHz half voltage bandwidth. Thus is likely that I can build wireless communication systems on this link. To be more specific, applying load-modulation communication approaches or appending active RF front-ends will enable inductive communication at a wide range. A previous study establishes a 10 kHz on-off keying (OOK) load-modulation communication system on a similar channel [P2]. These systems will work in the same principle as near-field communication (NFC) protocols. I note that regulations, in Japan only, permits experiments using a sine wave input and prohibits the emission of modulated signals, including backscatter or load-modulation communication. Therefore, I could not conduct experiments to examine this issue. I note that although this regulatory limitation becomes a problem in public spaces, it could be feasible in controlled environments, such as industrial spaces, by attaining regulatory permission.

Safety

Guidelines for electromagnetic field exposure are used for evaluating the safety of these wireless systems. For instance, the Federal Communications Commission (FCC) and the Institute of Electrical and Electronics Engineers (IEEE) have issued guidelines of EM field exposure [43]. In the frequency bands above 100 kHz, preventing localized heat stress and full-body heating is the main interest of these guidelines. Therefore, these guidelines offer basic restrictions based on specific absorption rate (SAR), which is the amount of power getting absorbed in biological tissue. The guideline for uncontrolled exposure for the general public, which is the most conservative guideline, limits the whole-body average SAR is limited to 0.08 W/kg. Besides, localized SAR, defined as the average SAR over a 1 g tissue sample, is restricted to 1.6 W/kg.

The work presented in chapter 3 conducted safety evaluations using full-body anatomical models, which show that we can safely transmit over a hundred Watts. Furthermore, as shown in figure 5.5(c,d), this approach has control over the locations where the electromagnetic field is focused. This distribution indicates that by detecting proximity users and gathering the field when no one is nearby, this system can safely deliver a larger amount of power than systems developed in chapter 3.

Optimizing systems with multiple relay modules

Measurements in section 5.4 showed that when multiple relays exist within the range of the transmitter, they interfere with each other. A straightforward solution to detour this interference is to activate one relay at a time. We can use the BLE SoC on the relay modules to activate them based on the control packets sent from a central control unit by simple firmware modifications of the developed module.

As a clue for further improvement, we can observe that the sum of the harvested power in figure 5.12(a) in the (ON, ON) state is higher than any relay turned ON alone. This trend suggests that I can increase the total efficiency (*i.e.,* sum of the power delivered to the receivers over total power input) by powering multiple receivers at once. Besides, figure 5.12(c) shows that the relay/receiver pair with smaller coupling gets significantly affected when we turn on multiple relays. One necessary research direction is to develop charging protocols, which can achieve the following collectively: (a) power transfer with high total efficiency and (b) meeting the real-time needs of power at each node.

I also note that I did not consider the time-slots for charging the relays in this study. The relay modules only consume power when it changes the state of the mechanical relays.

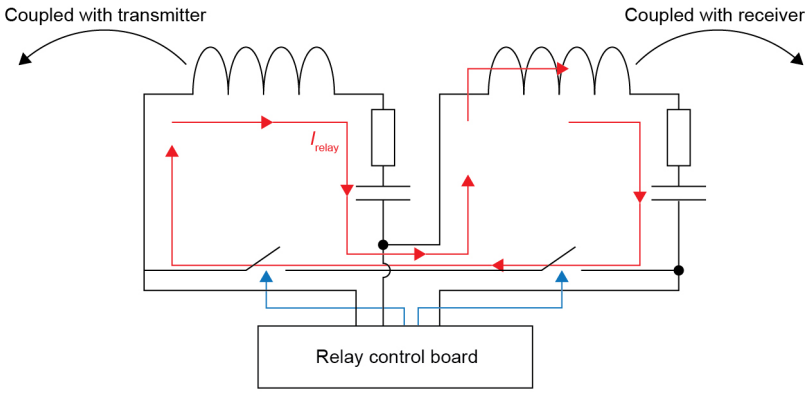

Figure 5.17 Circuit diagram of a relay module with two coils resonators. This alternative implementation works under the same principle as the relay module presented in figure 5.6.

Furthermore, the large footprint enables easy charging from the large-scale transmitter. Thus, a possible straightforward operation would be to start receiving power when the battery capacity falls under a pre-defined threshold. However, this causes a pause in power delivery to the receiver because the absorbed energy appears in the Z_{adj} in figure 5.8. Thereby the re-emitted field will be decreased when the relay gets charged. Therefore, possible future research directions are the following: (a) defining a protocol that detects the receiver's power needs and the relay and allocates optimized time-slots for the charging of each or (b) re-designing the relay hardware so the system can simultaneously charge the relay and receiver.

More layers in the hierarchical architecture

Our hierarchical architecture defined three layers, which consist of the transmitter, relay, and receiver. However, it is worth investigating the addition of more layers. I assume that more layers would enable cushioning a much more significant size difference between receiver size and charging range. For instance, we could charge a dust-scale sensor node within a factory-scale charging system. Still, there should be an inevitable trade-off because each appended layer will expose copper loss. Further investigation and optimizing systems with more than four layers should be another exciting direction for future work.

Miniaturization of the modules

As figure 5.6 shows, the components integrated into this control board all made of common electronic parts. Therefore, we can deploy the components except for the battery and the BLE

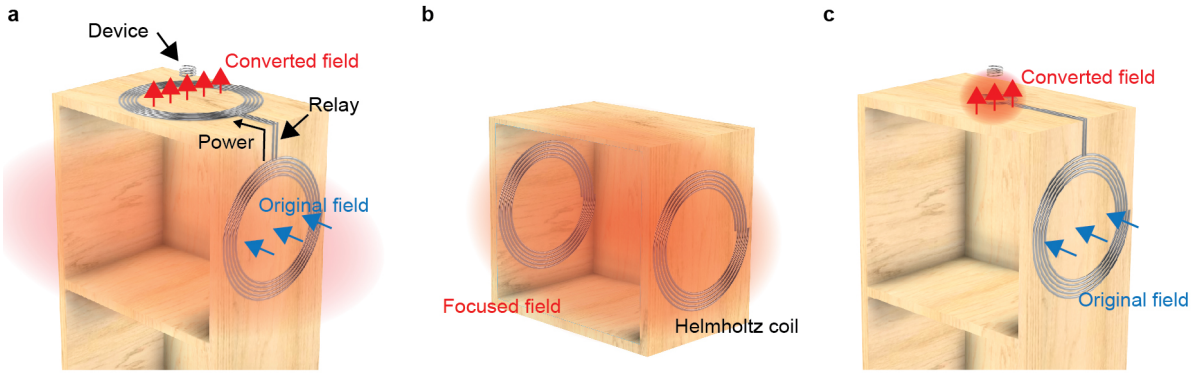

Figure 5.18 Example of the primitives that relay modules with multiple resonators can achieve. (a) Converting the field direction, (b) making a 3-D field on a smaller scale by using Helmholtz coils, and (c) intensively focusing the field by varying the scales of the two coils.

SoC onto a single IC through extensive engineering effort. We can also omit batteries if the device only wakes up when the system emits a magnetic field nearby. This way, the battery can also be omitted, which will enable further miniaturization of the sensor devices.

Beyond focusing

This chapter discussed using hierarchical links for "focusing" the ambient magnetic fields on the relays' proximity. Abstractly, we can understand this operation that the relays are converting the room-generated field to a field receivable by the end devices. This section discusses how the technology of hierarchical resonance can further manipulate the field in this conversion.

Figure 5.8 shows a simple alternative configuration with two coils; this design uses different coils for receiving and re-emitting magnetic fields. This design and the design presented in figure 5.6 operates under the same principle presented in section 5.1. Furthermore, the module I developed can adapt to both designs by modifying the firmware. For instance, this architecture can achieve the following primitives shown in figure 5.18(a-c) by leveraging the freedom of relative coil position and form-factor: (a) converting the field direction, (b) making a 3-D field on a smaller scale by using Helmholtz coils, and (c) intensively focusing the field by varying the scales of the two coils. Furthermore, we can dynamically switch ON/OFF this manipulation and switch between multiple primitives as long as the hardware is embedded beforehand.

Figure 5.19 demonstrates the bending of the fields (figure 5.18(a)) in a scenario where the receiver's orientation is misaligned with the room-generated field (this is noted as a limitation in chapter 3). We need to stand up the smartphone for efficiently coupling with the external field.

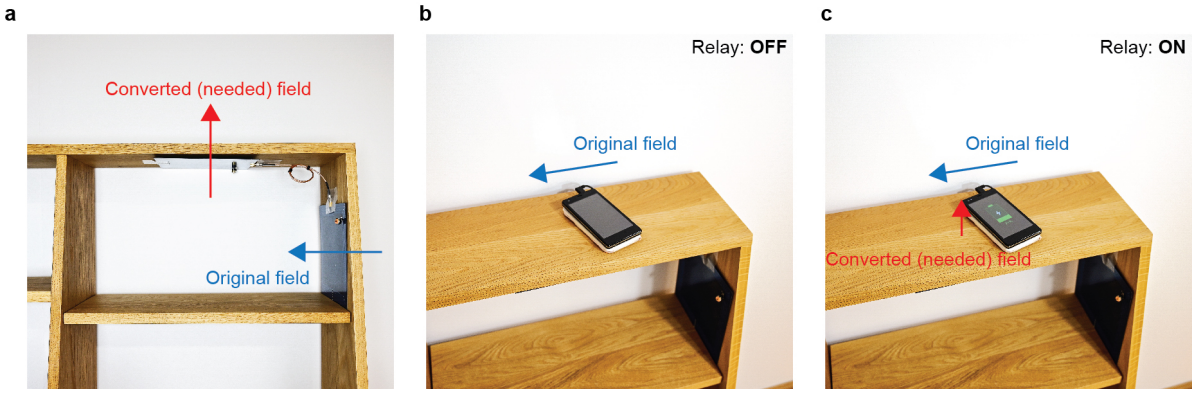

Figure 5.19 Demonstration of converting the "physically defined field" to an "affordance defined field" in an ad-hoc manner. This demonstration is based on the primitive shown in figure 5.18(a). (a) Placement of the relay module within the shelf. (b) The phone can't receive power when the relay is OFF. (b) The phone can receive power when the relay is ON.

However, considering the shelves' affordance, we usually don't place smartphones in such ways; thus, the smartphone doesn't get charged (figure 5.19(b)). Figure 5.19(c) demonstrates turning ON the embedded relay module, which converts the direction of the magnetic field in the direction where the "naturally" placed smartphone can receive power.

As I described in chapters 1-3, efficiently generating a room-scale magnetic field is generally a challenge because it conflicts with the governing physics of near-field electromagnetics. Thus at the current state of this technology, the magnetic field still needs to be designed with priority given to physical limitations for achieving high-efficiency. Meanwhile, the environment's affordance usually defines the device's placement (*i.e.*, the needed magnetic field). The mismatch in these "physically defined field" and "affordance defined field" often cause inconveniences. Hierarchical resonance shows a way to mitigate this mismatch by converting the "physically defined field" to an "affordance defined field" in an ad-hoc manner. Further exploration and systematization of this conversion is a promising direction of future development of hierarchical resonance.

5.8 Summary

I introduced wireless power transfer via hierarchical resonators, which efficiently bridges highly asymmetric transmitter/receiver links by selectively focusing the ambient magnetic field. We can build this hierarchical link on general large-scale inductive transmitters by placing low-cost, low-power, maintenance-free relay modules within the powering range. I

showed that the technique could efficiently and robustly connect pebble-sized sensors, which we could not empower using large-scale transmitters. Furthermore, I demonstrated 500 mW power delivery to pebble-sized (20 mm) devices. These magnitudes higher transferable power levels than other methods will grant access to new sensor modalities, drastically extend the lifetime of devices, and lower the threshold for developing sensor systems due to the mitigated power restriction.

Methods

A Extracting power transfer efficiency

For two-port measurements, I used a vector network analyzer (Keysight FieldFox) for obtaining the S-parameter matrix (*i.e.,* scattering matrix). I processed these obtained parameters to evaluate the power transfer efficiency. I calculated the efficiency, $\eta_{\max}$, from the following formula, which corresponds to the maximum power transfer efficiency of a given two port network [50].

$$\eta_{\max} = \frac{\chi}{(1+\sqrt{1+\chi})^2} \tag{5.9}$$

$$\chi = \frac{|Z_{12}|^2}{\mathrm{r}Z_{11}\mathrm{r}Z_{22} - \mathrm{r}Z_{12}^2} \tag{5.10}$$

Here, $\mathrm{r}Z = \mathrm{re}\{Z\}$ and $\mathrm{i}Z = \mathrm{im}\{Z\}$. Z is the Z-parameter matrix, converted from the measured S-parameter matrix. The power transfer efficiency of two-port networks is dependent on the load impedance. Therefore, the system can reach this efficiency $\eta_{\max}$ when the connected load impedance is a particular optimum impedance value. The power usage of applications define the load impedance (*i.e.,* the operating voltage and current) Thus, methods using impedance tuning networks [68], switching voltage converters [69, 18], and 4-coil systems [9], have been presented to convert the application-defined load impedance value to this optimum value. In the latter DC-to-DC evaluations and demonstrations, I used an impedance tuning network for this operation. Furthermore, the development of power conversion technologies made the use of maximum efficiency $\eta_{\max}$ defined by equation 5.9 practical.

Chapter 6

Conclusion and future work

In this thesis, I explored the fundamental physics, system design, and implementation of cavity-inspired, magnetoquasistatic wireless power technologies for drastically extending the powering range of high-power wireless power transfer techniques. This advancement granted distributed electronic devices with seamless access to large amounts of energy. Beyond this vision, people would not have to care about power cords and battery capacity, sensor systems would work forever without maintenance, and power outlets would no longer constrain the layout of electrical equipment. Furthermore, the removal or minimization of batteries will allow previously non-available form-factors and enable operation in various areas where prior devices can not access.

An important novelty of the technologies I introduced is that they leverage the magnetic field, which is robust and safe. Compared to other wireless power approaches, such as microwave, electronic, light, etc., the magnetic field interacts less with biological tissue and daily objects. This feature makes these approaches safe for the human body and less affected by ambient objects. Besides, such systems' resonant frequency is free tunable independently with the system dimensions. We can freely define the resonant frequency and structure size by tuning the capacitor values'. This feature enhances utility compared to former cavity-based methods, in which the dimension of the system strictly defines the resonant frequency. Thus, we can install these systems in various sized spaces and situations while keeping the operation frequency compliant with regulations.

These technologies have the promise to empower computation without affecting or negatively changing our lifestyles with these benefits achieved collectively. In the rest of this chapter, I will describe future research directions beyond this thesis.

6.1 Facilitating the system deployment

The technologies studied in this thesis are still emerging; therefore, I mostly focused on basic physics and the fundamental system design. As the theory governing this technique develops, interest should shift into more comprehensive system designs.

An exciting direction for future work in this domain is facilitating system deployment. I built the prototype demonstration systems out of standard aluminum frames, aluminum sheets, and copper components, which worked well for prototyping. Besides, it will be beneficial to facilitate system deployment by riding on former construction techniques. For instance, by implementing the whole system leveraging the area within the drywall, wallpaper, or conductive paint, ordinary construction procedures could form the transmitter structure. Integrating the emerging construction-scale 3-D printing could also be another exciting direction.

The underlying challenges are the lack of conductivity of the existing materials and connection methods. The conductivity of existing paint and 3-D printable substrates is still not high enough to attain the high-quality factor (*i.e.*, low loss) required for high-efficiency power transfer. Embedding copper sheets or metal nets within wallpaper or drywall is an alternative method, which will not suffer from material conductivity. However, a technical challenge exists in maintaining the low-resistance contacts with other compositions since it is difficult to build large structures out of bulk. As this domain is interdisciplinary, cooperation between electrical and other (*e.g.*, material science, structure, etc.) is needed to overcome this challenge.

6.2 Deploying in other shapes

I assumed rectangular rooms as the target volume in this study since many rooms are rectangular (excluding openings). This assumption also simplified the analysis and system design. Meanwhile, walls, ceilings, and floors exist in many places, including vehicles, rooms, boxes, trains, machines, etc. Suppose we can deploy the presented technologies in many other shapes. In that case, we could leverage such structures for embedding cavity-inspired wireless power transfer systems. This advancement will offer people a wireless powering experience without any (explicit) dedicated structures. For instance, this will enable scenarios such as the car's shell working as an invisible wireless power transmitter, which unnoticeably powers devices located within the vehicle.

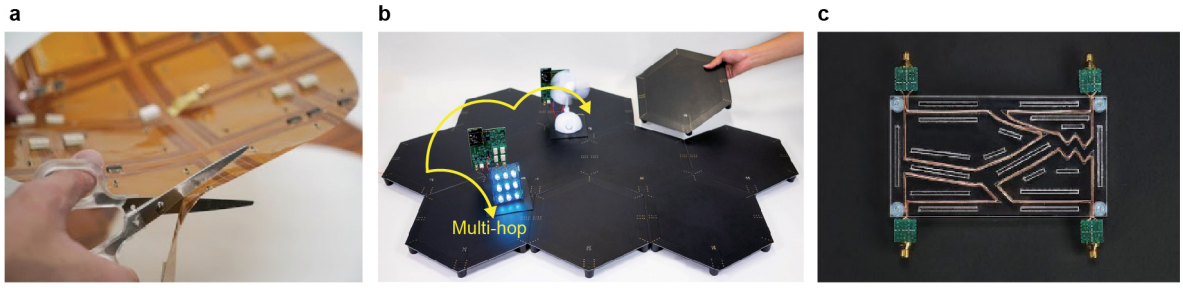

Figure 6.1 Two-dimensional wireless power transfer systems that we developed. Note that I excluded these studies from this thesis's scope. (a) A cuttable wireless power transfer sheet [P11]. (b) A reconfigurable wireless power surface that we can introduce by arranging panel-shaped modules [P10]. (c) A receiver array designed using genetic algorithm, which prevents the significant drop of efficiency throughout the wireless powering surface [P5, P23].

From the engineering perspective, this design process differs from the presented studies because there would be nearly no symmetry. As the structures become more geometrically complex, the designing process would be too difficult to handle by heuristic design. Therefore, a promising direction of future work is to establish computational design techniques to analyze and optimize the transmitter structure based on the intended charging volume and the shell for embedding.

6.3 Integrating with other technologies

This thesis pushed up the trade-off curve between "deliverable power levels" and "powering range," however, this trade-off still apparently exists. Thereby, it is unlikely that this technology covers every application, at least for the near future. For instance, the two-dimensional systems we developed lack in powering range compared to the three-dimensional approaches developed in this thesis (figure 6.1). However, suppose the surface is the primary domain of interest. In that case, these 2-D approaches could be more efficient and capable of delivering higher power levels (*e.g.*, over hundreds of Watts). Thus, it would be interesting to explore system architectures that seamlessly integrate 2-D and 3-D wireless powering systems.

Furthermore, microwaves and optical techniques are much less efficient, and the power-levels are magnitudes lower than this thesis's approaches in indoor setups. However, they can be more effective when it is challenging to deploy current cavity-inspired approaches. Such conditions include situations when the operating distance is more extended and in outdoor environments.

Apparently, there is still no *one-covers-all* technology in the wireless power transfer field. Thereby, the integration of various charging systems should be another exciting topic to explore. Suppose the receivers equip several types of receivers (*e.g.*, optical and inductive) and autonomously changes the charging mode depending on the situation (*e.g.*, indoor/outdoor, line-of-sight/non-line-of-sight, high-power/low-power). In that case, the operation range could further expand than any other technology alone. For enabling such systems, we need to investigate the integration at both physical level (*e.g.*, interference between the technologies) and systems level (*e.g.*, protocols for determining the appropriate technology).

6.4 Designing peripheral circuits for specific applications

Because most of this study focused on enhancing the link efficiency between the transmitter/receiver pair, I did not optimize peripheral circuits' efficiency. Such non-optimized portions include the power amplifier, rectifier, DC-DC converters, battery managers, etc. Besides, I did not implement any dynamic impedance tuning approaches for maximum efficiency point tracking.

I regard the obtained performance satisfactory for many IoT applications, such as empowering mobiles and sensor nodes. However, if significantly higher power-levels need to be transmitted (*e.g.,* charging electric vehicles), it would be necessary to optimize these peripheral circuits and aim for the upper edge of efficiency [70, 71].

6.5 Electromagnetic compatibility (EMC)

Any system that exposes oscillating electromagnetic fields can affect electronic devices within the operation range. Examples of this effect include appending noises to electrical or even damage components. Thereby, EMC/EMI is usually controlled via standards such as the CISPR standard determined by the International Electrotechnical Commission (IEC) [72].

Because wireless power transfer systems generally emit higher power levels than typical communication systems, EMC/EMI has been a general concern for such technologies. However, the testing of EMC/EMI is highly application-specific. Thereby, I leave the detailed exploration of this term for future work and only provide the electrical field intensity in the room's proximity for attaining a quantitative understanding. Figure 6.2 shows the electrical field intensity around the room-scale wireless power transfer system presented in Chapter 3. These figures show that the electrical field is concentrated near the lumped capacitors and eventually decays with increasing distance. Thus, one counterpart is to optimize the capacitive

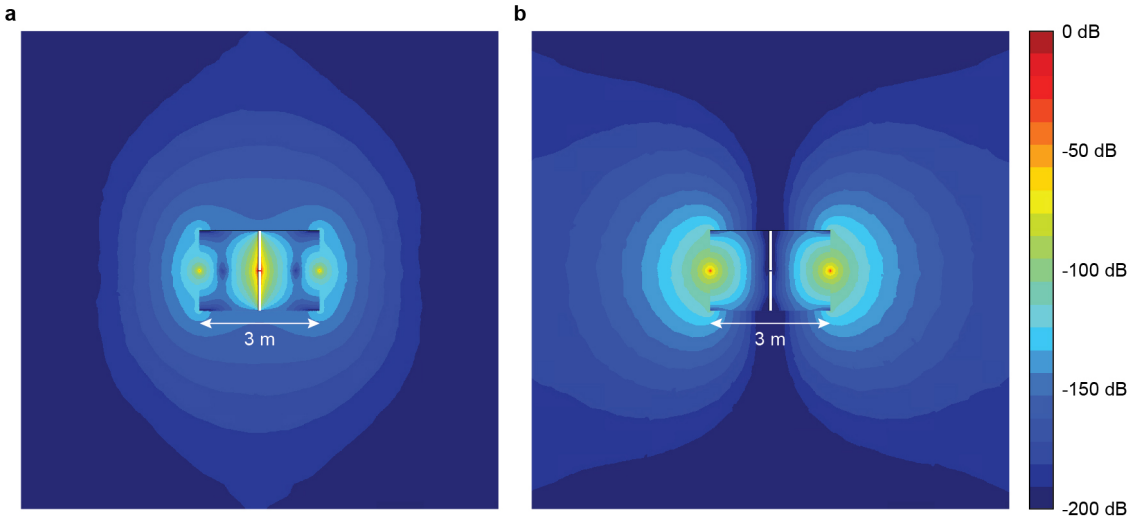

Figure 6.2 The electrical field density inside and outside of the multimode QSCR. Note that these distributions only show relative values. (a) Pole dependent (PD) mode. (b) Pole independent (PI) mode.

lumped elements' positions for controlling the exposed areas. Furthermore, it would be interesting to distribute the lumped capacitors across the current trace to decrease each capacitor's voltage stress [73]. This distributed placement should subsequently suppress the electric field amplitude exposed near each capacitor.

6.6 Unlocking new device modalities

Untethering power cords will subtract cables associated with users and change the design and modalities of devices. For instance, batteries are the most space/weight consuming component in many electronics. Thereby, the elimination or even the reduction of battery size will lead to drastic changes in the design of ongoing electronic devices.

Furthermore, speculatively thinking, such technologies have a promise to be a unique power source for devices that can not equip batteries. Some instances of these devices are flexible electronics, stretchable electronics [74], and small electronics [75], which the unique form factor does not allow equipping rigid and bulky batteries. In laboratory setups, these devices are often powered by external and wired power sources (because most studies consider the power supply out of scope), which significantly limits practicality. As a primitive proof of concept Figure. 6.3 demonstrates these technologies' capability for empowering flexible, film-type devices. Besides, reliable power sources that can

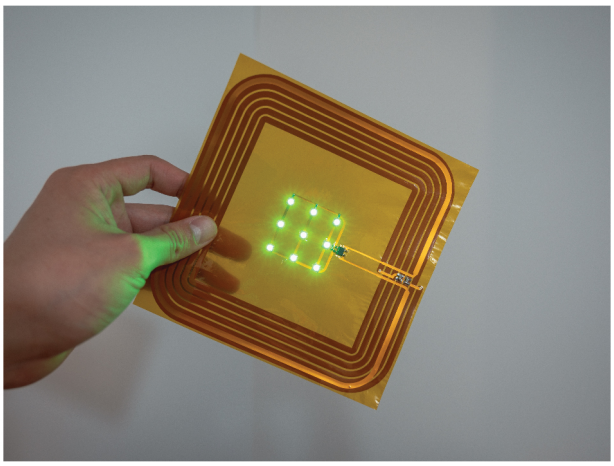

Figure 6.3 Powering an LED array implemented on a flexible substrate.

drive numerous particle scale devices will work as a backbone of futuristic computing concepts, such as smart dust [32] and programmable matter [75], by solving the critical bottleneck of power distribution. Thereby we proposed a concept of "wirelessly cooperated" shape-changing computing particles [P12] (Figure 6.4) for seamlessly empowering clusters of unrecognizably small computers woven into everyday artifacts. We proposed integrating wireless communication [76] and powering technologies into millimeter-scale IC chips for achieving computers that we can directly and naturally manipulate as we interact with clay.

We can extend such discussions to robotics, which often requires numerous actuating and sensing functionalities integrated into various form factors. As an example of "excluding" electrical systems, previous work demonstrated an utterly soft robot powered by chemical reaction controlled with a microfluidic logic [77]. However, the utility of such non-electronic approaches is limited because it lacks means for communication, precise control, complex processing abilities, and speed.

We previously demonstrated wirelessly driven soft-robotics in two-dimensional setups. In this work, we connected the actuators that cause locomotion to wireless power receivers sensitive to different frequency bands. External wireless power transmitters can remotely and selectively drive these actuators [P6, P8]. This demonstration showed the proof of concept for off-loading the power source to the external of the robotic form factor (which holds the robotics' softness).

Another expected innovation is extending the operating range of devices to fields where it is difficult to reach with wires. Examples of these domains are underwater, within solids, biological tissue, in air, etc. As the technologies developed in this thesis are relatively less

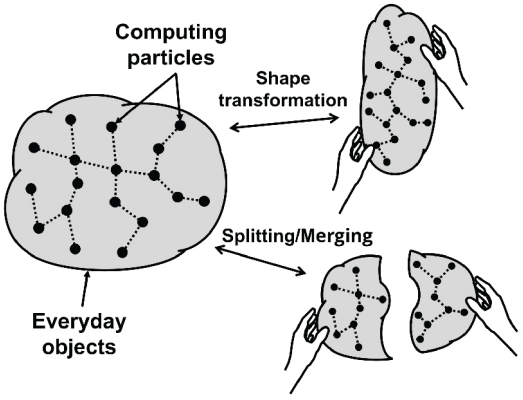

Figure 6.4 The concept of wirelessly cooperated shape-changing computing particles [P12]. This concept will seamlessly empower clusters of unrecognizably small computers woven into everyday artifacts via wireless power and communication among millimeter-scale IC chips. Such technology would lead to computers that we can directly and naturally manipulate as we interact with clay.

affected by the external environment, it has the promise of empowering devices operating in such domains. For instance, balloon robots, or drones in general, maneuver using actuators, typically powered by batteries since wiring in the air is usually infeasible. However, as the payload of these devices is limited, the loadable battery capacity and the flight time is strictly limited. To investigate proof of concept for this instance, we explored a wireless powered balloon robot's design. Therefore, we delivered a pilot study on wirelessly powering balloon robots [P43], which indicated that power could be delivered to floating drones using realistic setups.

A critical finding from these works is that the powering performance and the receiver's form-factor are highly-dependent. Wider (*i.e.*, heavier) conductive patterns usually deliver a higher quality factor (Q). Besides, a larger receiver area typically results in a larger coupling coefficient (k). However, the exclusion of batteries and continuous power supply in remote conditions is a unique and convenient benefit. Thereby offering analysis tools and protocols for investigating these pros and cons should be a promising future work direction.

6.7 Contributions from the applied physics perspective

Up to now, this thesis has discussed the electrical engineering and application perspective of wireless power technologies. Meanwhile, wireless power transfer is an interdisciplinary field, which is intensely engaged with applied physics [59]. Thus in this last section, I will provide

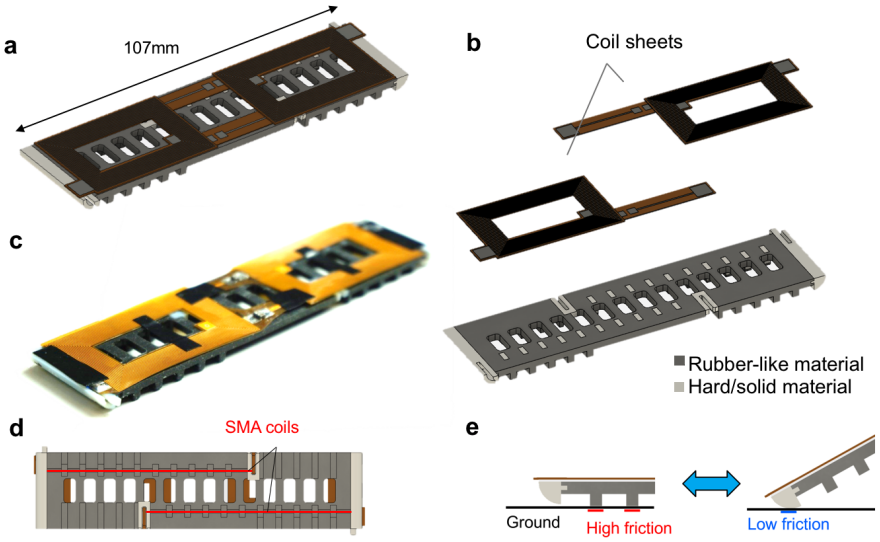

Figure 6.5 Wirelessly powered soft robotic caterpillar [P8]. We drove the shape memory alloys (SMAs) remotely and selectively for generating locomotion. (a) 3D model of the soft robotic caterpillar with integrated wireless power receiver coils. (b) The two receiver coils attributed to each shape memory alloy (SMA) actuator. (c) Photograph of the assembled wirelessly powered soft robotic caterpillar. (d) The underside of the soft robotic caterpillar showing the two assembled SMAs. (e) Mechanism for generating locomotion.

a perspective on the positioning and contribution of this thesis's technologies in the domain of applied physics. My discussion starts by briefly positioning existing wireless power transfer approaches based on figure 6.6.

Existing similar technologies and easy-to-use analysis techniques worked as a driving force for developing many wireless power transfer technologies. For instance, inductive coupling approaches are inspired by transformers, and we often use lumped circuit models for analysis [16]. This approach rides on the magnetoquasistatic domain of Maxwell's equations, which leads to little interference with dielectrics (*e.g.,* biological tissue, everyday objects, furniture) [7]. Besides, approaches leveraging radiated electromagnetic waves (*e.g.,* microwave, laser) ride on the technical body of communication technologies. Mature engineering tools such as wave physics and the Friis transmission equation have helped develop this approach [4].

The introduction of magnetic resonance coupling has significantly enlarged the overlap between wireless power transfer and applied physics [13]. We can understand this technology as a "resonant" version of inductive coupling techniques because we can formulate most of this technique's features using lumped circuit analysis [10]. Importantly, this also revealed

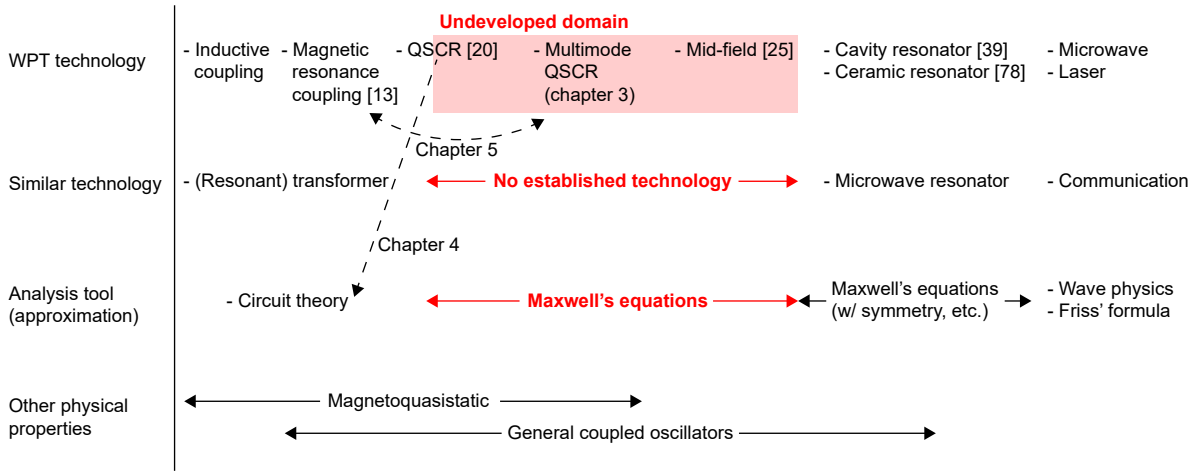

Figure 6.6 Wireless power transfer technologies organized from the physics perspective. (QSCR: quasistatic cavity resonance; WPT: wireless power transfer)

that we could treat the inductively coupled resonators as general oscillators, which are usually analyzed by coupled-mode theory [49]. This advancement also triggered the development of another domain which uses classic resonators (*e.g.,* cavity resonators) for wireless power transfer for attaining properties that coil resonators don't possess [39, 78]. Although these techniques often require the calculation of Maxwell's equations, most of these techniques use structures that can be solved analytically, such as highly symmetric ones.

Now, let's focus on the undeveloped domain with no original technology nor easy-to-use analysis tools. Although this domain is apparently challenging to use, recent advances indicate that this area could offer superior and unique characteristics, which we could not achieve using the realms with established analysis techniques or similar technologies. One technology in this domain is mid-field wireless power transfer, which uses electromagnetic fields between the far-field and near-field domain [25]. This approach actively leverages the interaction with the surrounding dielectrics to focus energy on the implanted devices much smaller than the wavelength; this shows magnitudes higher performance than other approaches riding on well-known approximations in such situations.

This undeveloped domain strongly engages with the technologies developed in this thesis. This domain formerly included quasistatic cavity resonance [20]; however, the formulation in chapter 4 linked this technology with circuit theory, which partially pulled this technology into the domain where engineering becomes relatively easy. The multimode quasistatic cavity resonance (chapter 3) is an exploration outside of the umbrella of well-known analysis tools leading to a unique performance that we could not reach otherwise (*e.g.,* full-volume coverage).

Furthermore, we can understand hierarchical resonance (chapter 5) as a fusion of these unique room-scale systems and ordinary coil-based resonators. By bridging these two domains, we demonstrated custom-designing the field distributions of quasistatic cavity resonance, which was previously difficult because of the lack of accessible engineering tools.

In summary, the 3-D wireless power primitives developed in this thesis are additional proof of the potential for leveraging the "undeveloped" zone for wireless power applications, and it encourages the further exploration of this domain. Furthermore, it indicates the importance of developing system-level technologies that bridge different technological domains, which I discussed in section 6.3.

References

[1] L. D. Xu, W. He, and S. Li, "Internet of things in industries: A survey," *IEEE Transactions on Industrial Informatics*, vol. 10, no. 4, pp. 2233–2243, 2014.

[2] M. Weiser, " The computer for the 21 st century ," *ACM SIGMOBILE Mobile Computing and Communications Review*, vol. 3, no. 3, pp. 3–11, 1999.

[3] P. Kamalinejad, C. Mahapatra, Z. Sheng, S. Mirabbasi, V. C. Victor, and Y. L. Guan, "Wireless energy harvesting for the Internet of Things," *IEEE Communications Magazine*, vol. 53, no. 6, pp. 102–108, 2015.

[4] W. C. Brown, "The History of Power Transmission by Radio Waves," *IEEE Transactions on Microwave Theory and Techniques*, vol. 32, no. 9, pp. 1230–1242, 1984.

[5] N. Shinohara, "Power Without Wires," *IEEE Microwave Magazine*, vol. 12, no. 7, pp. S64–S73, 2011.

[6] B. Strassner and K. Chang, "Microwave power transmission: Historical milestones and system components," *Proceedings of the IEEE*, vol. 101, no. 6, pp. 1379–1396, 2013.

[7] J. Garnica, R. A. Chinga, and J. Lin, "Wireless power transmission: From far field to near field," *Proceedings of the IEEE*, vol. 101, no. 6, pp. 1321–1331, 2013.

[8] Institute of Electrical and Electronics Engineers Standards Coordinating Committee 28 (IEEE-SCC 28) Standards, "C95.3-2002 IEEE recommended practice for measurements and computations of radio frequency electromagnetic fields with respect to human exposure to such fields," 2002.

[9] A. P. Sample, D. A. Meyer, and J. R. Smith, "Analysis, experimental results, and range adaptation of magnetically coupled resonators for wireless power transfer," *IEEE Transactions on Industrial Electronics*, vol. 58, no. 2, pp. 544–554, 2011.

[10] D. S. Ricketts, M. J. Chabalko, and A. Hillenius, "Experimental demonstration of the equivalence of inductive and strongly coupled magnetic resonance wireless power transfer," *Applied Physics Letters*, vol. 102, no. 5, 2013.

[11] S. Assawaworrarit, X. Yu, and S. Fan, "Robust wireless power transfer using a nonlinear parity-time-symmetric circuit," *Nature*, vol. 546, no. 7658, pp. 387–390, 2017.

[12] S. Assawaworrarit and S. Fan, "Robust and efficient wireless power transfer using a switch-mode implementation of a nonlinear parity-time symmetric circuit," *Nature Electronics*, vol. 3, no. 5, pp. 273–279, 2020.

[13] A. Kurs, A. Karalis, R. Moffatt, J. D. Joannopoulos, P. Fisher, and M. Soljačić, "Wireless power transfer via strongly coupled magnetic resonances," *Science*, vol. 317, no. 5834, pp. 83–86, 2007.

[14] A. Kurs, R. Moffatt, and M. Soljačić, "Simultaneous mid-range power transfer to multiple devices," *Applied Physics Letters*, vol. 96, no. 4, 2010.

[15] J. Zhou, B. Zhang, W. Xiao, D. Qiu, and Y. Chen, "Nonlinear Parity-Time-Symmetric Model for Constant Efficiency Wireless Power Transfer: Application to a Drone-in-Flight Wireless Charging Platform," *IEEE Transactions on Industrial Electronics*, vol. 66, no. 5, pp. 4097–4107, 2019.

[16] S. Y. Hui, W. Zhong, and C. K. Lee, "A critical review of recent progress in mid-range wireless power transfer," *IEEE Transactions on Power Electronics*, vol. 29, no. 9, pp. 4500–4511, 2014.

[17] Y. Uno, H. Qiu, T. Sai, S. Iguchi, Y. Mizutani, T. Hoshi, Y. Kawahara, Y. Kakehi, and M. Takamiya, "Luciola," *Proceedings of the ACM on Interactive, Mobile, Wearable and Ubiquitous Technologies*, vol. 1, no. 4, pp. 1–17, 2018.

[18] A. P. Sample, B. H. Waters, S. T. Wisdom, and J. R. Smith, "Enabling seamless wireless power delivery in dynamic environments," *Proceedings of the IEEE*, vol. 101, no. 6, pp. 1343–1358, 2013.

[19] T. Ohira, "Extended k-Q product formulas for capacitive- and inductive-coupling wireless power transfer schemes," *IEICE Electronics Express*, vol. 11, no. 9, pp. 1–7, 2014.

[20] M. J. Chabalko, M. Shahmohammadi, and A. P. Sample, "Quasistatic cavity resonance for ubiquitous Wireless power transfer," *PLoS ONE*, vol. 12, no. 2, pp. 1–14, 2017.

[21] V. Talla, B. Kellogg, S. Gollakota, and J. R. Smith, "Battery-Free Cellphone," *Proceedings of the ACM on Interactive, Mobile, Wearable and Ubiquitous Technologies*, vol. 1, no. 2, pp. 1–20, 2017.

[22] V. Talla, B. Kellogg, B. Ransford, S. Naderiparizi, J. R. Smith, and S. Gollakota, "Powering the next billion devices with Wi-Fi," *Communications of the ACM*, vol. 60, no. 3, pp. 83–91, 2017.

[23] X. Fan, H. Ding, S. Li, M. Sanzari, Y. Zhang, W. Trappe, Z. Han, and R. E. Howard, "Energy-Ball: Wireless Power Transfer for Batteryless Internet of Things through Distributed Beamforming," *Proceedings of the ACM on Interactive, Mobile, Wearable and Ubiquitous Technologies*, vol. 2, no. 2, pp. 1–22, 2018.

[24] V. Liu, A. Parks, V. Talla, S. Gollakota, D. Wetherall, and J. R. Smith, "Ambient backscatter: Wireless communication out of thin air," *Computer Communication Review*, vol. 43, no. 4, pp. 39–50, 2013.

[25] J. S. Ho, S. Kim, and A. S. Poon, "Midfield wireless powering for implantable systems," *Proceedings of the IEEE*, vol. 101, no. 6, pp. 1369–1378, 2013.

[26] D. R. Agrawal, Y. Tanabe, D. Weng, A. Ma, S. Hsu, S. Y. Liao, Z. Zhen, Z. Y. Zhu, C. Sun, Z. Dong, F. Yang, H. F. Tse, A. S. Poon, and J. S. Ho, "Conformal phased surfaces for wireless powering of bioelectronic microdevices," *Nature Biomedical Engineering*, vol. 1, no. 3, pp. 1–16, 2017.

[27] J. S. Ho, Y. Tanabe, S. M. Iyer, A. J. Christensen, L. Grosenick, K. Deisseroth, S. L. Delp, and A. S. Poon, "Self-tracking energy transfer for neural stimulation in untethered mice," *Physical Review Applied*, vol. 4, no. 2, pp. 1–6, 2015.

[28] H. Basaeri, D. B. Christensen, and S. Roundy, "A review of acoustic power transfer for bio-medical implants," *Smart Materials and Structures*, vol. 25, no. 12, 2016.

[29] N. Arora, S. Zhang, F. Shahmiri, D. Osorio, Y.-C. Wang, M. Gupta, Z. Wang, T. Starner, Z. L. Wang, and G. Abowd, "SATURN: A Thin and Flexible Self-powered Microphone Leveraging Triboelectric Nanogenerator," *Proceedings of the ACM on Interactive, Mobile, Wearable and Ubiquitous Technologies*, vol. 2, no. 2, pp. 1–28, 2018.

[30] J. Jang and F. Adib, "Underwater backscatter networking," *Proceedings of the 2019 Conference of the ACM Special Interest Group on Data Communication (SIGCOMM 2019)*, pp. 187–199, 2019.

[31] V. Iyer, E. Bayati, R. Nandakumar, A. Majumdar, and S. Gollakota, "Charging a Smartphone Across a Room Using Lasers," *Proceedings of the ACM on Interactive, Mobile, Wearable and Ubiquitous Technologies*, vol. 1, no. 4, pp. 1–21, 2018.

[32] B. Warneke, M. Last, B. Liebowitz, and K. S. Pister, "Smart dust: communicating with a cubic-millimeter computer," *Computer*, vol. 34, no. 1, pp. 44–51, 2001.

[33] Q. Zhang, W. Fang, Q. Liu, J. Wu, P. Xia, and L. Yang, "Distributed Laser Charging: A Wireless Power Transfer Approach," *IEEE Internet of Things Journal*, vol. 5, no. 5, pp. 3853–3864, 2018.

[34] I. Laakso, S. Tsuchida, A. Hirata, and Y. Kamimura, "Evaluation of SAR in a human body model due to wireless power transmission in the 10MHz band," *Physics in Medicine and Biology*, vol. 57, no. 15, pp. 4991–5002, 2012.

[35] T. Sekitani, M. Takamiya, Y. Noguchi, S. Nakano, Y. Kato, T. Sakurai, and T. Someya, "A large-area wireless power-transmission sheet using printed organic transistors and plastic MEMS switches," *Nature Materials*, vol. 6, no. 6, pp. 413–417, 2007.

[36] J. Jadidian and D. Katabi, "Magnetic MIMO: How to charge your phone in your pocket," *Proceedings of the Annual International Conference on Mobile Computing and Networking 2014 (MOBICOM 2014)*, pp. 495–506, 2014.

[37] H. D. Lang, A. Ludwig, and C. D. Sarris, "Convex optimization of wireless power transfer systems with multiple transmitters," *IEEE Transactions on Antennas and Propagation*, vol. 62, no. 9, pp. 4623–4636, 2014.

[38] S. Kashyap, E. Björnson, and E. G. Larsson, "Can wireless power transfer benefit from large transmitter arrays?" *2015 IEEE Wireless Power Transfer Conference, WPTC 2015*, pp. 1–3, 2015.

[39] M. J. Chabalko and A. P. Sample, "Resonant cavity mode enabled wireless power transfer," *Applied Physics Letters*, vol. 105, no. 24, 2014.

[40] ——, "Three-Dimensional Charging via Multimode Resonant Cavity Enabled Wireless Power Transfer," *IEEE Transactions on Power Electronics*, vol. 30, no. 11, pp. 6163–6173, 2015.

[41] H. Mei, K. A. Thackston, R. A. Bercich, J. G. Jefferys, and P. P. Irazoqui, "Cavity resonator wireless power transfer system for freely moving animal experiments," *IEEE Transactions on Biomedical Engineering*, vol. 64, no. 4, pp. 775–785, 2017.

[42] A. Christ, M. Douglas, J. Nadakuduti, and N. Kuster, "Assessing human exposure to electromagnetic fields from wireless power transmission systems," *Proceedings of the IEEE*, vol. 101, no. 6, pp. 1482–1493, 2013.

[43] A. Christ, M. G. Douglas, J. M. Roman, E. B. Cooper, A. P. Sample, B. H. Waters, J. R. Smith, and N. Kuster, "Evaluation of wireless resonant power transfer systems with human electromagnetic exposure limits," *IEEE Transactions on Electromagnetic Compatibility*, vol. 55, no. 2, pp. 265–274, 2013.

[44] S. A. Ahson and M. Ilyas, *RFID handbook: applications, technology, security, and privacy*. CRC press, 2017.

[45] J. F. Ensworth and M. S. Reynolds, "BLE-Backscatter: Ultralow-Power IoT Nodes Compatible with Bluetooth 4.0 Low Energy (BLE) Smartphones and Tablets," *IEEE Transactions on Microwave Theory and Techniques*, vol. 65, no. 9, pp. 3360–3368, 2017.

[46] C. Yang, J. Gummeson, and A. Sample, "Riding the airways: Ultra-wideband ambient backscatter via commercial broadcast systems," *Proceedings of the IEEE International Conference on Computer Communications 2017 (IEEE INFOCOM 2017)*, pp. 1–9, 2017.

[47] S. Li, L. D. Xu, and S. Zhao, "The internet of things: a survey," *Information Systems Frontiers*, vol. 17, no. 2, pp. 243–259, 2015.

[48] D. Kajfez and E. J. Hwan, "Q-factor measurement with network analyzer," *IEEE Transactions on Microwave Theory and Techniques*, vol. 32, no. 7, pp. 666–670, 1984.

[49] H. A. Haus and W. Huang, "Coupled-Mode Theory," *Proceedings of the IEEE*, vol. 79, no. 10, pp. 1505–1518, 1991.

[50] M. Zargham and P. G. Gulak, "Maximum achievable efficiency in near-field coupled power-transfer systems," *IEEE Transactions on Biomedical Circuits and Systems*, vol. 6, no. 3, pp. 228–245, 2012.

[51] D. Lin, C. Zhang, and S. Y. Hui, "Mathematic Analysis of Omnidirectional Wireless Power Transfer-Part-II Three-Dimensional Systems," *IEEE Transactions on Power Electronics*, vol. 32, no. 1, pp. 613–624, 2017.

[52] J. S. Choi, E. S. Lee, B. G. Choi, S. H. Han, and C. T. Rim, "Six degrees of freedom wide-range IPT for multiple IoT by DQ rotating magnetic field," *Proceedings of the IEEE Applied Power Electronics Conference and Exposition (IEEE APEC)*, pp. 3730–3737, 2017.

[53] H. Li, J. Li, K. Wang, W. Chen, and X. Yang, "A maximum efficiency point tracking control scheme for wireless power transfer systems using magnetic resonant coupling," *IEEE Transactions on Power Electronics*, vol. 30, no. 7, pp. 3998–4008, 2015.

[54] A. P. Sample, D. J. Yeager, P. S. Powledge, A. V. Mamishev, and J. R. Smith, "Design of an RFID-based battery-free programmable sensing platform," *IEEE Transactions on Instrumentation and Measurement*, vol. 57, no. 11, pp. 2608–2615, 2008.

[55] GS1, "EPC UHF Gen2 Air Interface Protocol," https://www.gs1.org/standards/epc-rfid/uhf-air-interface-protocol, Accessed: 2020-12-3.

[56] D. K. Klair, K. W. Chin, and R. Raad, "A survey and tutorial of RFID anti-collision protocols," *IEEE Communications Surveys and Tutorials*, vol. 12, no. 3, pp. 400–421, 2010.

[57] P. Grover and A. Sahai, "Shannon meets tesla: Wireless information and power transfer," *Proceedings of the IEEE International Symposium on Information Theory*, pp. 2363–2367, 2010.

[58] S. Bi, C. K. Ho, and R. Zhang, "Wireless powered communication: Opportunities and challenges," *IEEE Communications Magazine*, vol. 53, no. 4, pp. 117–125, 2015.

[59] M. Song, P. Belov, and P. Kapitanova, "Wireless power transfer inspired by the modern trends in electromagnetics," *Applied Physics Reviews*, vol. 4, no. 2, 2017.

[60] B. H. Waters, B. J. Mahoney, G. Lee, and J. R. Smith, "Optimal coil size ratios for wireless power transfer applications," *Proceedings of the IEEE International Symposium on Circuits and Systems (IEEE ISCAS)*, vol. 1, no. 2, pp. 2045–2048, 2014.

[61] N. Shinohara, "Beam control technologies with a high-efficiency phased array for microwave power transmission in Japan," *Proceedings of the IEEE*, vol. 101, no. 6, pp. 1448–1463, 2013.

[62] W. Zhong, C. K. Lee, and S. Y. Ron Hui, "General analysis on the use of tesla's resonators in domino forms for wireless power transfer," *IEEE Transactions on Industrial Electronics*, vol. 60, no. 1, pp. 261–270, 2013.

[63] G. Lee, B. H. Waters, Y. G. Shin, J. R. Smith, and W. S. Park, "A reconfigurable resonant coil for range adaptation wireless power transfer," *IEEE Transactions on Microwave Theory and Techniques*, vol. 64, no. 2, pp. 624–632, 2016.

[64] D. Ahn and S. Hong, "A study on magnetic field repeater in wireless power transfer," *IEEE Transactions on Industrial Electronics*, vol. 60, no. 1, pp. 360–371, 2013.

[65] L. SPREAD Co., "Techno farm™," https://technofarm.com/, Accessed: 2020-06-30.

[66] M. Boyvat, J. S. Koh, and R. J. Wood, "Addressable wireless actuation for multijoint folding robots and devices," *Science Robotics*, vol. 2, no. 8, pp. 1–10, 2017.

[67] C. Holz, T. Grossman, G. Fitzmaurice, and A. Agur, "Implanted user interfaces," *Proceedings of the 2020 CHI Conference on Human Factors in Computing Systems*, pp. 503–512, 2012.

[68] Y. Lim, H. Tang, S. Lim, and J. Park, "An adaptive impedance-matching network based on a novel capacitor matrix for wireless power transfer," *IEEE Transactions on Power Electronics*, vol. 29, no. 8, pp. 4403–4413, 2014.

[69] D. Ahn and S. Hong, "Wireless power transfer resonance coupling amplification by load-modulation switching controller," *IEEE Transactions on Industrial Electronics*, vol. 62, no. 2, pp. 898–909, 2015.

[70] T. C. Beh, T. Imura, M. Kato, and Y. Hori, "Basic study of improving efficiency of wireless power transfer via magnetic resonance coupling based on impedance matching," *IEEE International Symposium on Industrial Electronics*, pp. 2011–2016, 2010.

[71] J. Park, Y. Tak, Y. Kim, Y. Kim, and S. Nam, "Investigation of adaptive matching methods for near-field wireless power transfer," *IEEE Transactions on Antennas and Propagation*, vol. 59, no. 5, pp. 1769–1773, 2011.

[72] International Electrotechnical Commission (IEC), "Technical committee CISPR: International special committee on radio interference (CISPR)," https://www.iec.ch, Accessed: 2020-12-3.

[73] Y. Narusue and Y. Kawahara, "Distributed reactance compensation for printed spiral coils in wireless power transfer," *Proceedings of the IEEE Wireless Power Transfer Conference (WPTC 2017)*, pp. 9–12, 2017.

[74] J. A. Rogers, T. Someya, and Y. Huang, "Materials and mechanics for stretchable electronics," *Science*, vol. 327, no. 5973, pp. 1603–1607, 2010.

[75] S. C. Goldstein, J. D. Campbell, and T. C. Mowry, "Programmable matter," *Computer*, vol. 38, no. 6, pp. 99–101, 2005.

[76] J. Kadomoto, H. Irie, and S. Sakai, "WiXI: An inter-chip wireless bus interface for shape-changeable chiplet-based computers," *Proceedings of the 2019 IEEE International Conference on Computer Design (ICCD 2019)*, pp. 100–108, 2019.

[77] M. Wehner, R. L. Truby, D. J. Fitzgerald, B. Mosadegh, G. M. Whitesides, J. A. Lewis, and R. J. Wood, "An integrated design and fabrication strategy for entirely soft, autonomous robots," *Nature*, vol. 536, no. 7617, pp. 451–455, 2016.

[78] M. Song, P. Belov, and P. Kapitanova, "Wireless power transfer based on dielectric resonators with colossal permittivity," *Applied Physics Letters*, vol. 109, no. 22, p. 223902, 2016.

Publication list

Publications included in this thesis

[P1] T. Sasatani, A. P. Sample, and Y. Kawahara, "Room-wide magnetoquasistatic wireless power transfer using a cavity-based multimode resonator," *Nature Electronics*, **Under review**.

[P2] T. Sasatani, CJ. Yang, M. J. Chabalko, Y. Kawahara, and A. P. Sample, "Room-Wide Wireless Charging and Load-Modulation Communication via Quasistatic Cavity Resonance," *Proceedings of the ACM on Interactive, Mobile, Wearable and Ubiquitous Technologies (ACM IMWUT)*, Vol. 2, No. 4, Article No. 188, Dec. 2018.

[P3] T. Sasatani, M. J. Chabalko, Y. Kawahara and A. P. Sample, "Multimode Quasistatic Cavity Resonators for Wireless Power Transfer, " *IEEE Antennas and Wireless Propagation Letters*, vol. 16, No. 1, pp. 2746–2749, Aug. 2017.

[P4] T. Sasatani, Y. Hirai, A. P. Sample, and Y. Kawahara, "Wide-Area Wireless Power Delivery to Pebble-Sized Devices via Hierarchical Resonators," **To be submitted**.

Publications excluded from this thesis

International journals

[P5] T. Sasatani, Y. Narusue, and Y. Kawahara, "Genetic Algorithm-Based Receiving Resonator Array Design for Wireless Power Transfer," *IEEE Access*, vol. 8, pp. 222385–222396, Dec. 2020.

[P6] Y. Nishizawa, T. Sasatani, M. Ishige, Y. Narusue, T. Umedachi, Y. Kawahara, "Ramus: A Frequency-Multiplexed Power Bus for Powering, Sensing and Controlling Robots," *IEEE Robotics and Automation Letters (Proceedings of the 3rd IEEE International Conference on Soft Robotics ‐RoboSoft 2020)*, Vol. 5, No. 3, pp. 4126–4132, April 2020.

[P7] S. Yoshida, Y. Kawahara, T. Sasatani, K. Kiyono, Y. Kobayashi, and H. Funato, "Infants show physiological responses specific to parental hugs," *iScience*, Vol. 23, No.4, 2020, 10996, April 2020.

[P8] C. Caffrey, T. Umedachi, W. Jiang, T. Sasatani, Y. Narusue, R. Niiyama and Y. Kawahara, "Soft robotic caterpillar with wirelessly powered shape memory alloy actuators, " *The International Journal of Robotics Research*, Vol. 7, No. 6, March 2020.

[P9] T. Cheng*, K. Narumi*, Y. Do, Y. Zhang, T. D. Ta, T. Sasatani, E. Markvicka, Y. Kawahara, L. Yao, G. D. Abowd, and H. Oh, "Silver Tape: Inkjet-Printed Circuits Peeled-and-Transferred on Versatile Substrates," *Proceedings of the ACM on Interactive, Mobile, Wearable and Ubiquitous Technologies (ACM IMWUT)*, Vol. 4, No. 1, No. 6, Mar. 2020 (* Authors contributed equally).

[P10] K. Sumiya, T. Sasatani, Y. Nishizawa, K. Tsushio, Y. Narusue, and Y. Kawahara, "Alvus: A Reconfigurable 2-D Wireless Charging System," *Proceedings of the ACM on Interactive, Mobile, Wearable and Ubiquitous Technologies (ACM IMWUT)*, Vol. 3, No. 2, Article No. 68, June 2019. **Distinguished paper award**

[P11] R. Takahashi, T. Sasatani, F. Okuya, Y. Narusue, and Y. Kawahara, "A Cuttable Wireless Power Transfer Sheet," *Proceedings of the ACM on Interactive, Mobile, Wearable and Ubiquitous Technologies (ACM IMWUT)*, Vol. 2, No. 4, Article No. 190, Dec. 2018.

[P12] J. Kadomoto, T. Sasatani, K. Narumi, N. Usami, H. Irie, S. Sakai, and Y. Kawahara, "Toward Wirelessly Cooperated Shape-Changing Computing Particles," *IEEE Pervasive Computing*, **Under review**.

[P13] T. Sasatani, M. J. Chabalko, and A. P. Sample, "Analysis and Design of Quasistatic Cavity Resonators for Wireless Power Transfer," **To be submitted**.

International conferences (full paper, refereed)

[P14] Y. Kawahara, T. Sasatani, "Wireless Power Transfer for Internet of Things (Invited)," *The Annual International Electron Devices Meeting (IEDM) 2020*, To appear.

[P15] H. Hayashi, K. Hata, T. Sasatani, H. Sato, R. Yamamura, Y. Seong, R. Niiyama, and Y. Kawahara, "Effect of Body Materials on Transmission Efficiency and Resonant Frequency in Wirelessly Powered Personal Mobility Devices," *Proceedings of IEEE Wireless Power Transfer Conference (WPTC) 2020*, Seoul, Korea, Nov. 2020.

[P16] R. Takahashi, M. Fukumoto, Changyo Han, T. Sasatani, Y. Narusue, and Y. Kawahara, "TelemetRing: A Batteryless and Wireless Ring-shaped Keyboard using Passive Inductive Telemetry," *Proceedings of the 33rd Annual ACM Symposium on User Interface Software and Technology (UIST' 20)*, Virtual (previously Minneapolis, US), Oct. 2020.

[P17] K. Takaki, T. Sasatani, H. Kasashima, Y. Kawahara, and T. Naemura "Coil Design for Wireless Power Transfer and Communication over Hinges of Smart Glasses," *Proceedings of the 2020 International Symposium on Wearable Computers (ISWC)*, pp. 79–83, Virtual, Mexico, Sept. 2020.

[P18] M. Morita, T. Sasatani, R. Takahashi, and Y. Kawahara, "Topology Construction Protocol for Wireless Power Transfer System with a 2-D Relay Resonator Array," *Proceedings of 2020 IEEE International Conference on Consumer Electronics (ICCE)*, Las Vegas, NV, Jan. 2020.

[P19] H. Hayashi, T. Sasatani, Y. Narusue, and Y. Kawahara, "Design of Wireless Power Transfer Systems for Personal Mobility Devices in City Space," *Proceedings of the 2019 IEEE 90th Vehicular Technology Conference (IEEE VTC)*, Honolulu, Hawaii, Sept. 2019.

[P20] T. Sasatani, Y. Narusue, and Y. Kawahara, "Dynamic Complex Impedance Tuning Method Using a Multiple-Input DC/DC Converter for Wireless Power Transfer," *Proceedings of the IEEE Wireless Power Transfer Conference 2018 (IEEE WPTC)*, pp. 1–4, Montreal, Canada, June 2018. **Best student paper finalist**

[P21] T. Sasatani, Y. Narusue, Y. Kawahara, and T. Asami, "DC-Based Impedance Tuning Method Using Magnetic Saturation for Wireless Power Transfer," *Proceedings of the IEEE Wireless Power Transfer Conference 2017 (IEEE WPTC)*, pp. 1–4, Taipei, Taiwan, May 2017.

[P22] T. Hashizume, T. Sasatani, K. Narumi, Y. Narusue, Y. Kawahara, and T. Asami, "Passive and Contactless Epidermal Pressure Sensor Printed with Silver Nano-particle Ink, " *Proceedings of the ACM International Joint Conference on Pervasive and Ubiquitous Computing (UbiComp) 2016*, pp. 190–195, Heidelberg, Germany, Sept. 2016.

[P23] T. Sasatani, Y. Narusue, Y. Kawahara, and T. Asami, "Genetic Algorithm-Based Design of Receiving Resonator Arrays for Wireless Power Transfer via Magnetic

Resonant Coupling," *Proceedings of the IEEE Wireless Power Transfer Conference 2016 (IEEE WPTC)*, pp. 1–4, Aveiro, Portugal, May 2016.

International conference (demo, contest, others)

[P24] S. Yoshida, Y. Kawahara, T. Sasatani, K. Kiyono, Y. Kobayashi, and H. Funato, "Measurement of heart rate variability during hugs in parents and infants," *The International Congress of Infant Studies (ICIS)*, Virtual Poster Presentation, July 2020.

[P25] T. Sasatani, A. P. Sample, and Y. Kawahara, "3-D Wireless Charging for Indoor Electronics Using Multimode Quasistatic Cavity Resonators," *Adjunct Proceedings of ACM Ubicomp 2018*, Singapore, Oct. 2018.

[P26] K. Sumiya, T. Sasatani, Y. Nishizawa, Y. Narusue, K. Tsushio, Y. Kawahara, "A Reconfigurable 2-D Wireless Charging System," *Adjunct Proceedings of ACM Ubicomp 2018*, Singapore, Oct. 2018.

[P27] R. Takahashi, T. Sasatani, F. Okuya, Y. Narusue, Y. Kawahara, "Design of Cuttable Wireless Power Transfer Sheet," *Adjunct Proceedings of ACM Ubicomp 2018*, Singapore, Oct. 2018.

[P28] T. Sasatani, and Y. Kawahara, "Multimode Quasistatic Cavity Resonators for Wireless Power Transfer: Towards Empowering Freely Moving Animal Experiments in 3-D Environments," *International Symposium on Systems Science of Bio-Navigation 2018*, Kyoto, Japan, Sept. 2018.

[P29] Y. Narusue, A. Hashizume, T. Sasatani, X. Shi, Y, Mizutani, Y. Kawahara, and T. Asami, "Indoor Wireless Power Transfer, " *TECO Green Tech Contest 2016*, Taipei, Taiwan, Aug. 2016. **Bronze medalist**

Japanese Conferences (In Japanese)

[P30] 山川凌太郎, 飯塚達哉, 石毛真修, 笹谷拓也, 高木健, 川原圭博, "マスク越しフレーズ認識に向けたミリ波レーダによる口の形状変化の検出手法, " 情報処理学会第 83 回全国大会, March 2021, 発表予定.

[P31] 林寛将, 笹谷拓也, 畑勝裕, 山村亮介, 川原圭博, "電動パーソナルモビリティのシェアリング事業に向けた無線充電システムの導入とインセンティブスキームに関する検討, " 情報処理学会第 83 回全国大会, March 2021, 発表予定.

[P32] 高橋亮, 雪田和歌子, 笹谷拓也, 横田知之, 染谷隆夫, 川原圭博, "バッテリレスなウェアラブルの無線センシングに向けた衣類型リーダコイルの設計, " 電子情報通信学会総合大会, March 2021, 発表予定.

[P33] 高橋亮, 笹谷拓也, 川原圭博, “体内への電磁界暴露を抑制可能な無線給電・通信用テキスタイルコイルの設計, ” 電子情報通信学会ソサイエティ大会, B-15, Sept. 2020.

[P34] 吉田さちね, 川原圭博, 笹谷拓也, 清野健, 小林洋, 船戸弘正, “親との触れ合いで起こるヒト乳児の生理反応, ” 第 43 回日本神経科学大会, 1O07m-3-01, July 2020.

[P35] 林寛将, 笹谷拓也, 畑勝裕, 山村亮介, 川原圭博, “電動パーソナルモビリティのシェアリング事業に向けた無線充電システムのシミュレーションによる解析, ” マルチメディア, 分散, 協調とモバイル (DICOMO2020) シンポジウム, 4A-2, pp. 520–525, June 2020.

[P36] 笹谷拓也, 川原圭博, “準静空洞共振器を用いた無線給電の自動車技術への応用可能性, ” 自動車技術会 2020 年春季大会, May 2020.

[P37] 高木健, 笹谷拓也, 笠島博信, 川原圭博, 苗村健, “眼鏡型デバイスにおけるヒンジ部の配線の無線化, ” 電子情報通信学会総合大会, B-15-14, March 2020.

[P38] 平井雄太, 笹谷拓也, 高橋亮, 川原圭博, “マルチモード準静空洞共振器を用いた無線給電における中継器の構成についての検討, ” 電子情報通信学会総合大会, B-20-11, March 2020.

[P39] 平井雄太, 笹谷拓也, 川原圭博, “マルチモード準静空洞共振器を用いた無線電力伝送における中継共振器の配置についての一検討, ” 電子情報通信学会ソサイエティ大会, B-20-19, Sept. 2019.

[P40] 笹谷拓也, 川原圭博, “部屋全域への無線電力伝送に向けたマルチモード準静空洞共振器,” 研究報告ユビキタスコンピューティングシステム（UBI）, 2019-UBI-62, pp. 1–8, June 2019. (山下記念論文賞 & 優秀論文賞)

[P41] 笹谷拓也, 川原圭博, “三次元無線電力伝送のための面電流を用いたマルチモード共振器についての一検討, ” 電子情報通信学会総合大会, B-21-37, March 2019.

[P42] 高橋亮, 韓燦教, 笹谷拓也, 成末義哲, 福本雅朗, 川原圭博, 苗村健, “ワイヤレスな指輪型キーボードのバッテリレス化手法, ” 電子情報通信学会総合大会, B-15-13, March 2019.

[P43] 黒澤蓮, 笹谷拓也, 鳴海紘也, 川原圭博, “三次元無線給電システムにより駆動する空中浮遊デバイスに向けたペイロードと給電効率の検証, ” 電子情報通信学会ソサイエティ大会, B-15-24, Sept. 2019.

[P44] 西澤勇輝, 笹谷拓也, 成末義哲, 川原圭博, “センサフィードバックの統合が可能な周波数選択性電力バスによる多数アクチュエータの独立駆動システム, ” 電子情報通信学会総合大会, A-1-20, March 2019.

[P45] 林寛将, 笹谷拓也, 成末義哲, 川原圭博, “パーソナルモビリティの走行中無線電力伝送に向けた送電コイル設計に関する一検討, ” 情報処理学会第 81 回全国大会, 4Y-06, March 2019.

[P46] 角谷和宣, 西澤勇輝, 笹谷拓也, 高橋亮, 成末義哲, 川原圭博, “[依頼講演] 1MHz 磁界共振結合方式を用いた無線給電プラレールの設計と製作, ” 信学技報, vol. 118, no. 227, WPT2018-50, pp. 111–114, Oct. 2018.

[P47] 笹谷拓也, 川原圭博, “三次元無線電力伝送のための Multimode Quasistatic Cavity Resonator の実装, ” 電子情報通信学会ソサイエティ大会, B-21-14, Sept. 2018.

[P48] 西澤勇輝, 成末義哲, 笹谷拓也, 川原圭博, “Ramus: 周波数選択性電力バスによる多数アクチュエータの独立駆動システムの検討, ” 電子情報通信学会ソサイエティ大会, A-1-6, Sept. 2018.

[P49] 林寛将, 笹谷拓也, 成末義哲, 川原圭博, “パーソナルモビリティへの磁界共振結合型無線電力伝送における位置ずれの影響評価, ” 電子情報通信学会ソサイエティ大会, B-21-5, Sept. 2018.

[P50] 中原健一, 成末義哲, 笹谷拓也, 鳴海紘也, 川原圭博, “渦電流を利用した非接触駆動による相転移アクチュエータの高速化, ” 電子情報通信学会ソサイエティ大会, B-18-6, Sept. 2018.

[P51] Z. Li, T. Sasatani, Y. Nishizawa, Y. Kawahara, “Coil Design for Wireless Power Transfer through Walls with Metallic Lattice,” Proceedings of IEICE Society Conference, B-21-9, Sept. 2018.

[P52] 笹谷拓也, 成末義哲, 川原圭博, “無線電力伝送のための DC/DC コンバータを用いた複素インピーダンス変換手法についての一検討, ” 電子情報通信学会総合大会, B-21-2, March 2018.

[P53] 高橋亮, 笹谷拓也, 奥谷文徳, 成末義哲, 川原圭博, “切断により形状の変更が可能な無線電力伝送シートの設計の一検討, ” 電子情報通信学会総合大会, March 2018.

[P54] 角谷和宣, 西澤勇輝, 笹谷拓也, 橋詰新, 成末義哲, 川原圭博, “二次元共振器アレイを用いた給電領域を自由に変更可能な無線給電システムの構成, ” 電子情報通信学会総合大会, March 2018.

[P55] 笹谷拓也, 成末義哲, 川原圭博, 浅見徹, “磁界共振結合型無線電力伝送ツールキットの設計および実装, ” 電子情報通信学会総合大会, B-18-40, March 2017.

[P56] W. Jiang, H. Zhu, T. Sasatani, Y. Narusue, M. Fukumoto, and Y. Kawahara, “A design of an asymmetric resonator for wirelessly powered wearable ring device,” Proceedings of IEICE Society Conference, BS-7-20, Sept. 2017.

[P57] 水谷陽太, 笹谷拓也, 成末義哲, 川原圭博, 浅見徹, “受電器アレイとシート型送電器を用いた電界結合型無線電力伝送における極板形状に関する一検討, ” 電子情報通信学会技術研究報告, vol.116, no.321, WPT2016-38, pp. 7–11, Nov. 2016.

[P58] 橋爪崇弘, 笹谷拓也, 成末義哲, 川原圭博, 浅見徹, “銀ナノインクを用いた非接触読み取り可能なパッシブ型静電容量式圧力センサと着圧測定への応用, ” マルチメディア, 分散, 協調とモバイル (DICOMO2016) シンポジウム, 4G-1, pp. 840–845, July 2016.

[P59] 笹谷拓也, 成末義哲, 川原圭博, 浅見徹, “磁界共振結合型無線電力伝送における遺伝的アルゴリズムを用いた受電共振器アレイの設計, ” 電子情報通信学会総合大会, B-21-22, March 2016.

[P60] 橋爪崇弘, 笹谷拓也, 成末義哲, 川原圭博, 浅見徹, “銀ナノインクを用いたパッシブ型圧力センサの人体貼付用途における設計手法, ” 電子情報通信学会総合大会, B-18-17, March 2016.

[P61] 笹谷拓也, 成末義哲, 川原圭博, 浅見徹, “送電共振器アレイを用いた無線電力伝送における給電効率向上のための受電共振器アレイ形状の検討, ” 電子情報通信学会ソサイエティ大会, B-21-6, Sept. 2015.

Patent

[P62] 特開 2020-145821, 国立大学法人東京大学, “無線電力伝送シート, ” 川原圭博, 成末義哲, 高橋亮, 笹谷拓也, 奥谷文徳, 2020 年 9 月 10 日公開.

Awards

[A1] 第 11 回日本学術振興会育志賞, 日本学術振興会, March 2021（内定）.

- 笹谷拓也, 生活空間をカバーするユビキタスな無線電力伝送の研究.

[A2] 2020 年度山下記念研究賞, 情報処理学会, March 2021（内定）.

- 笹谷拓也, 川原圭博, “部屋全域への無線電力伝送に向けたマルチモード準静空洞共振器,” 研究報告ユビキタスコンピューティングシステム（UBI）, 2019-UBI-62, pp. 1–8, June 2019.

[A3] Distinguished paper award, Proceedings of the ACM on Interactive, Mobile, Wearable and Ubiquitous Technologies (IMWUT), Sept. 2020.

- K. Sumiya, T. Sasatani, Y. Nishizawa, K. Tsushio, Y. Narusue, and Y. Kawahara, “Alvus: A Reconfigurable 2-D Wireless Charging System,” *Proceedings of the ACM on Interactive, Mobile, Wearable and Ubiquitous Technologies (ACM IMWUT)*, Vol. 3, No. 2, Article No. 68, June 2019.

[A4] 優秀論文賞, 第 62 回ユビキタスコンピューティングシステム（UBI）研究発表会, 情報処理学会, June 2019.

- 笹谷拓也, 川原圭博, “部屋全域への無線電力伝送に向けたマルチモード準静空洞共振器,” 研究報告ユビキタスコンピューティングシステム（UBI）, 2019-UBI-62, pp. 1–8, June 2019.

[A5] Best student paper finalist, IEEE Wireless Power Transfer Conference (WPTC) 2018, June 2018.

- T. Sasatani, Y. Narusue, and Y. Kawahara, “Dynamic Complex Impedance Tuning Method Using a Multiple-Input DC/DC Converter for Wireless Power Transfer,” *Proceedings of the IEEE Wireless Power Transfer Conference (WPTC) 2018*, pp. 1–4, Montreal, Canada, June 2018.

[A6] 研究科長賞, 東京大学大学院情報理工学系研究科, March 2018.

- T. Sasatani, “Multimode Quasistatic Cavity Resonators and DC-Controlled Complex Impedance Conversion Techniques for Wireless Power Transfer,” Department of Information and Communication Engineering, Graduate School of Information Science and Technology, The University of Tokyo, March 2018.

[A7] Bronze Medalist, 2016 TECO Green Tech Contest, Aug. 2016.

- Y. Narusue, A. Hashizume, T. Sasatani, X. Shi, Y. Mizutani, Y. Kawahara, and T. Asami, “Indoor Wireless Power Transfer, ” *TECO Green Tech Contest 2016*, Taipei, Taiwan, Aug. 2016.

[A8] 電気学術奨励賞, 電気学会東京支部, March 2016.

- 笹谷拓也, “磁界共振結合型無線電力伝送における遺伝的アルゴリズムを用いた受電共振器アレイの設計手法,” 東京大学工学部電気電子工学科, March 2016.

[A9] 優秀卒業論文賞, 東京大学工学部電気電子工学科, March 2016.

- 笹谷拓也, “磁界共振結合型無線電力伝送における遺伝的アルゴリズムを用いた受電共振器アレイの設計手法,” 東京大学工学部電気電子工学科, March 2016.

[A10] 最優秀論文賞 & 優秀プレゼンテーション賞, DICOMO 2016, July 2016.

- 橋爪崇弘, 笹谷拓也, 成末義哲, 川原圭博, 浅見徹, “銀ナノインクを用いた非接触読み取り可能なパッシブ型静電容量式圧力センサと着圧測定への応用, ” マルチメディア, 分散, 協調とモバイル (DICOMO2016) シンポジウム, 4G-1, pp. 840–845, July 2016.